Neural Substrates for Pattern Separation and Completion in the Dorsal Pallium of a Weakly Electric Fish

Stephen Benjamin Elliott

Thesis submitted in partial fulfillment of the requirements

of the Ph.D. program in Neuroscience

May 27, 2016

Department of Cellular and Molecular Medicine

Faculty of Medicine

University of Ottawa

ABSTRACT

The dorsodorsal division (DD) of the teleost telencephalon has been implicated in memory processes similar to those associated with the mammalian hippocampus. The network connectivity and neural activity underlying this involvement have remained unclear. This thesis attempts to elucidate both. Attempts have been made to record the neural activity of DD neurons, but none have succeeded in correlating the recorded firing with any meaningful stimuli. In this thesis, I present single-unit electrophysiological recordings of DD neurons that reveal persistent activity in the form of up-states which are evoked by two modalities of naturalistic sensory stimuli – visual and electrosensory. The anatomy of DD was a little better understood than the neural activity. Recent anatomical work has shown that DD is strongly inter-connected with the cortical-like dorsolateral division (DL) of the pallium, re-inforcing its similarity to mammalian hippocampal structures. This same work has also revealed much of DD's extrinsic connectivity. It was not, however, of a resolution fine enough to disambiguate the connections of the various DD subregions, nor to clarify the existence and structure of intrinsic DD connectivity. In this thesis, I further elucidate the connectivity of DD, by isolating its subregions. This was done by means of very small and precise neurotracer injections. These injections revealed strong recurrent connectivity within individual DD subregions, multiple pathways between DD and DL, and striking similarities between the connectivities of DL and DD and those of the mammalian dentate gyrus and CA3 respectively. From the results of these investigations I propose a model of homology between the teleost DD-DL loop and the putative pattern separation and completion networks contained in the mammalian cortico-hippocampal circuitry,

as well as a role for the observed persistent activity in DD within this model. I further propose the dorsal teleost telencephalon as an excellent model system for the further study of the network mechanisms of pattern separation and completion.

ABSTRACT (FRENCH)

La division dorsale (DD) du télencéphale des téléostéens a été impliquée dans plusieurs processus mémoriels comme ceux associés à l'hippocampe des mammifères. La connectivité du réseau neural et l'activité des neurones sous-jacente demeurent inconnues. Cette thèse tente de mieux comprendre les deux problèmes. Des tentatives ont été faites pour enregistrer l'activité des neurones de DD, mais aucune n'a réussi à corréler les décharges enregistrées avec des stimuli sensoriels significatifs. Dans cette thèse, je présente des enregistrements électrophysiologiques des neurones de DD qui montrent l'activité persistante sous la forme de « Up states » qui sont évoqués par deux modalités de signaux sensoriels naturels – visuels et électrosensoriels. L'anatomie de DD a été mieux comprise que l'activité neuronale. Des travaux anatomiques récents ont montré que DD est fortement inter-connecté avec une région semblable au cortex, la division dorsolatérale du pallium (DL), renforçant sa similarité avec l'architecture de l'hippocampe des mammifères. Ces mêmes travaux ont dévoilé la connectivité extrinsèque de DD. Cependant, la résolution n'était pas suffisamment fine pour éliminer les ambiguïtés de connexion de plusieurs sous-régions de DD ou de clarifier l'existence et la structure de la connectivité intrinsèque de DD. Dans cette thèse, j'ai permis de mieux comprendre la connectivité de DD en isolant ses sous-régions grâce à des injections précises et microscopiques de neurotraceurs. Ces injections révèlent une forte connectivité récurrente à l'intérieur des sous-régions de DD, des voies anatomiques multiples entre DL et DD, et des similarités surprenantes de la connectivité de DD et DL avec celle du gyrus denté et la région CA3 de l'hippocampe respectivement. À partir de ces résultats expérimentaux, je propose un modèle de l'homologie entre la boucle DD-DL et les réseaux impliqués dans la séparation et la complétion de patrons

contenus dans le circuit hippocampique des mammifères, de même qu'un rôle pour l'activité persistante observée dans DD dans ce modèle. De plus, je propose que le télencéphale dorsal des téléostéens soit un excellent système modèle pour explorer plus en détails les mécanismes des réseaux neuronaux de séparation et de complétion de patrons.

TABLE OF CONTENTS

LIST OF TABLES

LIST OF FIGURES

LIST OF ABBREVIATIONS

AC	Anterior Commission
AFR	Abrupt frequency rise
AptCx35	Apteronotus connexin 35 protein
AM	Amplitude modulation
c	Caudal
CA1	Cornu ammonis region 1 of hippocampus
CA2	Cornu ammonis region 2 of hippocampus
CA3	Cornu ammonis region 3 of hippocampus
col	Columnar
Comm	Commissural
Cx36	Connexin 36 protein
d	Dorsal
DC	Central division of dorsal telencephalon
DCc	Core subdivision of dorsocentral telencephalon
DCs	Shell subdivision of dorsocentral telencephalon
DD	Dorsal division of dorsal telencephalon
DDi	Intermediate subdivision of dorsodorsal telencephalon
DDmg	Magnocellular subdivision of dorsodorsal telencephalon
DDs	Superficial subdivision of dorsodorsal telencephalon
DG	Dentate Gyrus
DGgl	Granule cell layer of the dentate gyrus
DGml	Molecular layer of the dentate gyrus
DGpl	Polymorphic layer of the dentate gyrus
DIG	Digoxigenin
DL	Dorsal subdivision of dorsolateral telencephalon
DLc	Caudal subdivision of dorsolateral telencephalon
DLp	Posterior subdivision of dorsolateral telencephalon
DLv	Ventral subdivision of dorsolateral telencephalon
DM	Medial division of dorsal telencephalon
DM2	Subdivision 2 of the dorsomedial telencephalon
DM2c	Caudal part of the subdivision 2 of the dorsomedial telencephalon
DM2d	Dorsal part of the subdivision 2 of the dorsomedial telencephalon
DM2v	Ventral part of the subdivision 2 of the dorsomedial telencephalon
DP	Posterior division of dorsal telencephalon
EC	Entorhinal cortex
Ec	Caudal entopeduncular nucleus

EGR-1	Early growth response protein 1
Er	Rostral endopeduncular nucleus
FoxP2	Forkhead box protein P2
GABA	Gamma-aminobutyric acid
GRN	Global recurrent network
H_int	Hilar interneurons
Ha	Anterior Hypothalamus
i	Intermediate labeling
Inf Coll	Inferior colliculus
JAR	Jamming avoidance response
l	Lateral
lam	Laminar
LRN	Local recurrent network
m	Medial
MC	Mossy cells
nAPv	Anterior periventricular nucleus
OT	Optic tectum
Otx1	Orthodenticle homebox 1 gene
pcl	Pyramidal cell layer
PCR	Polymerase chain reaction
PG	Preglomerular complex
PKA	Protein kinase A
PPa	Anterior subdivision of the preoptic area
r	Rostral
s	Strong labeling
sl-m	Stratum lancunosum-moleculare
Sml	Molecular layer of the subiculum
so	Stratum oriens
sr	Stratum radium
SS	Somatostatin
st	Strong labeling
Sup Coll	Superior colliculus
TS	Taurus semicircularis
v	Ventral
Vc	Central subdivision of ventral telencephalon
Vd	Dorsal subdivision of ventral telencephalon
Vi	Intermediate subdivision of ventral telencephalon
Vl	Lateral subdivision of ventral telencephalon
Vp	Posterior subdivision of ventral telencephalon
Vs	Supracommissural subdivision of the ventral telencephalon
vta	Ventral tegmental area
w	Weak labeling
WTA	Winner take all network

Chapter 1 INTRODUCTION

In this introduction I summarize concepts related to electric fish and their electrosensory capabilities, persistent neural activity and neuronal up-states, mammalian hippocampal structure and function, as well and the structure and function of the teleost dorsal pallium, and some of the theoretical models which attempt to relate this structure to function.

ELECTROSENSE

All animals require sensory input to interact with one another and with their environment. Specialized organs have evolved which transduce light, sound, heat, pressure, movement, and chemical traces into neural signals that the brain uses to understand the organism's environment. Some, primarily aquatic, organisms have similarly evolved specialized organs to transduce electrical fields into neural codes and use the electrical characteristics of their environment to navigate, capture prey and even to communicate.

Two types of electrosenses have evolved: the passive electrosense transduced by ampullary receptors and the active electrosense transduced by tuberous receptors. Ampullary receptors have evolved from the water movement sensing lateral line receptors (Modrell et al., 2011). While it is suspected that tuberous receptors evolved from the ampullary type, there is no direct evidence for this notion.

In the case of passive electrosense, ampullary receptors detect low frequency (< 50Hz) electric fields from the environment. This serves primarily for detection and distinction of other organisms. For example, the low frequency electric potentials produced by the movements of crustaceans and the respiration of fish (Collin and Whitehead, 2004) can serve as signals for ampullary receptors and trigger predatory strikes in teleost fish. In some species, ampullary

receptors also play a role in encoding the low frequency components of electrocommunication signals (ex. Metzner and Heiligenberg, 1991).

Tuberous receptors are sensitive to the electric field produced by the fish's own electric organ discharge (EOD). They detect amplitude modulations of this EOD caused by perturbations of the EOD field induced by objects more or less conductive than the ambient water – this is the basis of electrolocation. Tuberous receptors also detect the EOD of conspecifics – this is the basis of electrocommunication. Many teleost fish are able to modulate the frequency of their EOD pulses. This can serve to increase environmental sampling (Jun et al., 2016), avoid interference from the EODs of other animals (Heiligenberg, 1991), and to allow communication with other electrosensing animals (Hupe and Lewis, 2008; Perrone et al., 2009.

ELECTRIC FISH

The fish that make use of an active electrosense are part of a larger group of electric fish which are all able to produce electricity. This is accomplished by means of a specialized electric organ consisting of a series of electrocytes. Strongly electric fish, such as the African catfish (*Malapterurus electricus*) or the electric eel (*Electrophorus electricus*), make use of this electrical production for defense and predation and are able to produce brief discharges up to 600 V (Catania, 2014). Weakly electric fish, by contrast, produce relatively constant, low voltage (< 1 V), discharges which are used for navigation, prey localization, and communication (Heiligenberg and Bastian, 1984). Since, in this work we are concerned primarily with memory and its sensory components, rather than predation and defense, we will consider only weakly electric fish.

There are two main categories of EOD production among weakly electric fish, pulse-type and wave-type. Pulse-type species intermittently emit stereotyped brief pulses; the pulse waveform shape is species (Hopkins, 1981) and sometimes sex (Zakon and Dunlap, 1999) specific. The rate of pulse emission can often be modulated. Increasing emission rate can help with sampling resolution (Jun et al, 2016) and decreasing emission rate, or stopping it all together, can serve as a communication signal (Perrone et al., 2009). Wave-type species produce a continuous waveform-like EOD, with a characteristic frequency. Both the frequency and the amplitude of this EOD signal can be modulated. This modulation is used to produce communication signals (Zakon et al., 2002), as well as to avoid electrical interference from other animals emitting at a similar frequency (Heiligenberg, 1991). It has been shown that tuberous receptors of wave type gymnotiform fish are precisely tuned to the fish's EOD frequency (Hopkins, 1976; Zakon and Meyer, 1983). For these fish, including the wave species used in my studies (*Apteronotus leptorhynchus*), the EOD/tuberous receptor combination serves as a species-specific sensory channel and thus reduces interference by the EODs of other electric fish.

Two principal branches of weakly electric fish have evolved independently, the African mormyroid fish, and the South American gymnotiform fish. Passive electroreception (ampullary receptors) is believed to be a primitive vertebrate sense since it is present in lampreys as well as elasmobranchs and primitive fish. Ampullary receptors were lost in the ancestors of teleost fish but regained independently in at least two genera: catfish and notopteroid fish. Mormyroid fish evolved from African notopteroid fish that already had ampullary receptors. In parallel fashion, gymnotiform fish evolved from catfish which are known to all have a passive electroreception (ampullary receptors) (New, 1997).

The mormyriformes are primarily pulse-type fish with the single known exception of *Gymnarchus niloticus* which is a wave-type species producing a continuous quasi-sinusoidal EOD at a frequency close to 500 Hz. Gymnotiformes are a mixed group with many pulse and wave-type species.

ELECTROLOCATION

One of the most significant uses of an EOD is electrolocation. Like the bat's sonar, our saccadic eye movements or a rodent's whisking, electrosense is an active sense. Weakly electric fish monitor distortions in the field produced by their EOD. Conductive objects (conductivity greater than the ambient water) cause a higher current density (and correspondingly larger voltage) across subjacent electroreceptors. Resistive objects (conductivity lower than surrounding water) produce the opposite effect. The region of skin with altered transcutaneous voltage is called the electric image; the affected and responding receptors are those within this area. Fish are able to discriminate object location with great acuity based on the pattern of receptors that are affected. To improve sensory acuity, fish will often 'scan' objects by moving their body back and forth parallel to the object (Jun et al., 2016). Other parameters such as the phase delay caused by a given electric image (effect of an object's capacitance) are used by some gymnotiform fish to gather more information about the nature of an object (Von der Emde, 1999).

Two types of tuberous receptors, T-type and P-type, are present in wave-type gymnotiform fish, each specialized to encode different aspects of the modulated EOD field. T-type receptors (T-units) fire single phase locked spikes at each cycle of the EOD. The latency of

the T-unit spike following the production of an EOD cycle is dependent on the EOD amplitude – it decreases with increasing amplitude. T-units are believed to be predominantly associated with electrocommunication and have their own distinct pathway from periphery to midbrain. There are relatively few T-units in *Apteronotus* and so they will not be further discussed.

P-type receptors probabilistically encode the amplitude of the detected EOD in their firing rate. These receptors capture the various amplitude fluctuations, produced both by the fish's own modulation of the EOD and by environmental modulation as previously mentioned. Pulse-type gymnotiform and mormyroid fish each employ different coding strategies, but as our present work is concerned with wave-type gymnotiformes, these will not be discussed here.

ELECTROSENSORY COMMUNICATION

Electrocommunication became possible with an active electrosense. At a most basic level, the production of an EOD allows detection and localization by other electrosensing organism. This process works differently in pulse-type and wave-type species. Pulse-type species generally do not modulate the structure of the stereotyped EOD pulse, but rather the frequency of these discharges. Studies on groups of mormyriforms have shown that this modulation of pulse frequency is used to coordinate the EOD pulse trains of interacting fish in ways that depend on the nature of the social interaction. Neighboring fish produced 'echo responses' which consisted of one fish timing its discharges to follow immediately (within 30 ms) that of a nearby fish. Transient synchronicity (temporal correlation) between the EODs of grouped fish was also observed (Gebhardt et al., 2012). Mormyrids also have a separation of receptor types which deal with endogenous and exogenous electric fields independently. This is further assisted by a

corollary discharge, or internal signal, letting the fish know the exact timing of its own discharges, allowing them to be better discriminated from any exogenous pulses.

Pulse-type gymnotiforms have been shown, both in a laboratory and natural setting, to produce at least 3 types of characteristic communication signals, chirps, accelerations, and interruptions. These are carefully explained by Perrone et al. (2009) in their examination of *Brachyhypopomus pinnicaudatus*. Chirps consist of brief (20-400 ms duration) modulations of both amplitude (significant reduction) and frequency (significant increase). In this species, four distinct patterns of chirp have been characterized. Interruptions represent a cessation of EOD production, in this species lasting from 100 ms to 14 s. Accelerations represent a brief increase in EOD production rate accompanied by a reduction in amplitude, but both being significantly less dramatic than those seen with chirp production. These communication signals have been associated with male-female interactions linked to courtship and with male-male aggressive behaviors.

I will concentrate, from this point forward on wave-type gymnotiform species as the current work focuses primarily on a wave-type species, *Apteronotus leptorhynchus*. With wave-type species, different species emit different waveforms centered at different frequencies which allows their detection and discrimination from one another (Fugère and Krahe, 2010). Even within the same species, differentiation of conspecifics is possible with small differences in EOD shape or frequency between males versus females (reviewed by Gonçalves and Oliveira, 2010). In close proximity the electric fields of two EODs interact and modulate one another. The production of an amplitude modulation (AM) has been observed with frequency equal to the

frequency difference between the interacting EODs (Figure 1-1). Weakly electric fish have been shown to be highly sensitive to these AMs and to be able to identify and remember specific frequencies of EOD with remarkable acuity (Harvey-Girard, 2010). For example, individual *Apteronotus leptorhynchus* can produce a quasi-sinusoidal EOD at a fixed frequency. EODs of mature females typically range between 600-800 Hz, while those of mature males usually between 800-1000 Hz. Each individual fish typically emits at a relatively fixed frequency with little variation over short time scales (Moortgat et al., 1998). This frequency can change if the distribution of other conspecifics in its immediate environment changes. EOD frequency can also be affected by temperature, increasing with heating and decreasing with cooling.

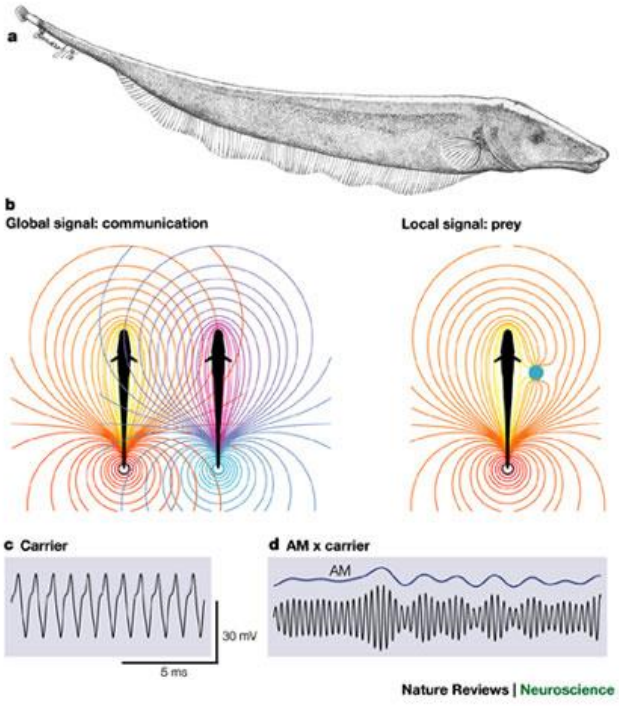

Figure 1-1: Electrolocation and electrocommunication (from Krahe and Gabbiani, 2004)

A) Drawing of *A. leptorhynchus*. B) How the electric fields produced by the EODs of adjacent fish overlap and how the presence of a nearby object affects this electric field. C) An example of an

A. leptorhynchus EOD waveform. Signal is shown as voltage over time. D) The AM created as an EOD is modulated by other EODs and environmental objects.

Most weakly electric fish are able to modulate their EOD production. This allows for the jamming avoidance responses (JAR), which prevents interference from other EODs transmitting at, or very near a fish's own frequency. The introduction of another EOD within 10 Hz of a fish's current EOD frequency will prompt a JAR whereby the higher frequency emitting fish will increase its EOD frequency to increase the frequency separation of the two EODs (Heiligenberg, 1980). EOD modulation also greatly enriches this method of communication. Electrocommunication signals include chirps and abrupt frequency rises (AFR) and consist of transient modulations of both the EOD amplitude and frequency (Figure 1-2; Zupanc, 2002). These signals have been associated with courting and aggressive behaviors in fish (Hupe and Lewis, 2008; Hagedorn and Heiligenberg, 1985).

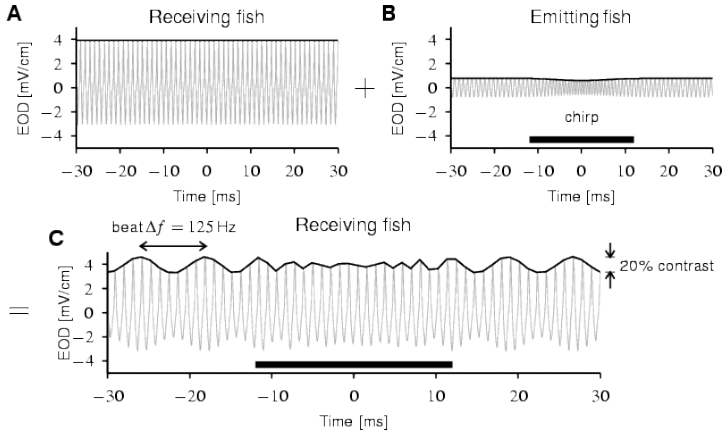

Figure 1-2: Chirps (From Benda et al., 2006)

A) An individual fish experiences its own EOD (gray line) with constant amplitude (black line). B) The EOD of a distant fish has a smaller amplitude (here 20%) at the location of the receiving fish. This distant fish emits a large chirp (thick horizontal bar) that reduces the amplitude by

25% and increases the frequency by 600 Hz during 24 ms. Shown is an artificially designed chirp signal that we used as a stimulus for the electrophysiological recordings.
C) The superposition of the two wave forms of the receiving fish (A) and the emitting fish (B) is the effective electric field that stimulates the electroreceptors of the receiving fish. A beat is created (here with frequency Δf = 125 Hz) that is disrupted during the large chirp (thick horizontal bar); this amplitude modulation (black line) is what we refer to as the "stimulus" in this paper and is shown in the remaining figures as "EOD AM." Note that the AM fades away during the large chirp.

PERSISTENT NEURAL ACTIVITY

An interesting phenomenon is occasionally observed in the mammalian cortex in which the neural response seemingly elicited by a given stimulus will outlast the stimulus presentation. This has significant implications to both the neural circuitry required to produce such a response, e.g. simple feed-forward processing no longer is sufficient, and the processing that such activity might allow, e.g., such as the integration of temporally dissociated stimuli. Colombo and Gross (1994) found that the spiking activity of neurons in both the inferior temporal cortex and hippocampal formation of macaques, although evoked by the presentation of a brief (1 s) visual stimulus, persisted into the delay period leading up to the presentation of a comparison stimulus. Similar activity has been noted elsewhere for similar tasks, often for those considered to involve short-duration working memory.

Theoreticians have proposed models to explain how such activity might be produced and maintained. These mostly involve the network dynamics produced by highly recurrent connectivity (eg., Wang, 2008). I will discuss these theories in my Discussion.

UP AND DOWN STATES

In addition to classical neuronal membrane potential fluctuations caused by action potentials and synaptic events, recordings in some neurons in cortex, striatum, and in the hippocampal formation have revealed bimodality in membrane potential, sometimes related to the behavioral state of the animal. Some neurons show a clear preference for two distinct voltage levels or states, one that is depolarized and generally exhibiting a higher variance and more frequent spiking activity, and a second that is hyperpolarized, relatively quiescent. These preferred levels or states have come to be known as up-states and down-states respectively and have been, in several instances, associated with persistent activity (eg., MacLean et al., 2005).

IN-VIVO EVIDENCES FOR UP-STATES

Up-states have been observed frequently in the mammalian cortex. They have been associated with behavioral states such as sleep. They are also common under anesthesia. An example of such a recording, taken from a rat visual cortex neuron is shown in figure 1-3. The left most panel shows the normal up-state down-state spontaneous transition commonly seen in sleep or, in this case, under urethane anesthesia. The right panel shows a longer, here termed, 'persistent' up state. The authors (Li et al., 2009) demonstrate that inducing burst firing in a single cortical neuron can trigger persistent up-state activity in a larger area of cortex up to 6 mm away.

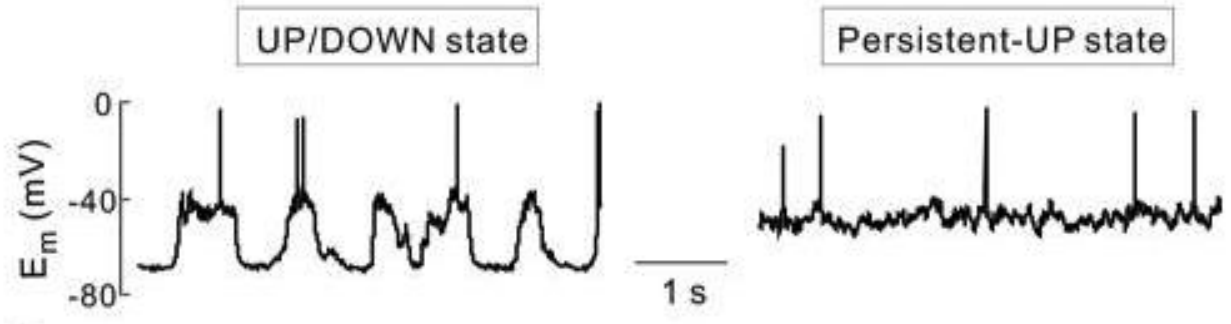

Figure 1-3: Up-states (adapted from Li et al., 2009)

Recordings from the visual cortex of an anaesthetized rat reveal spontaneous short (left panel) and long (right panel) up-states.

Wilson and Kawaguchi (1996) suggest that up-states seen in rat striatal spiny neurons (again under urethane anesthesia) are caused by a maintained synaptic barrage working in concert with dendritic potassium channels to maintain the stable depolarized state.

IN-VITRO EVIDENCES FOR UP-STATES

Up-states have also been successfully recorded from brain slices. Slices of ferret prefrontal cortex produce spontaneous periods of elevated membrane potential and increase spiking propensity which last several seconds when maintained in a solution close to the natural cerebrospinal fluid (McCormick et al., 2003). Figure 1-4 shows an example of one such up-state.

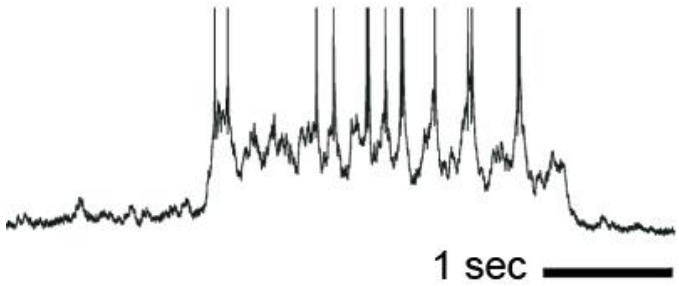

Figure 1-4: Up-state in-vitro (Adapted from McCormick et al., 2003)

Example of an up-state recorded from a slice of ferret prefrontal cortex.

This study found that the up-states depended on both NMDA and non-NMDA glutamatergic receptors. They also concluded that the origin of the up-states was from recurrent network excitatory activity in nearby pyramidal cells, carefully balanced by inhibitory

interneurons to provide the stable up-state. Injection of current was not able to induce up-state activity. Larimer and Strowbridge (2010) found that they could evoke up-states in the hilar neurons of the rat dentate gyrus though perforant path stimulation *in-vitro*. These up-states were caused by prolonged discharges of the dentate's semilunar granule cells. McLean et al. (2005) used calcium imaging to observe that stimulation of thalamic inputs was able to evoke up-state activity and corresponding firing activity in ensembles of layer 4 somatosensory cortical cells in rat brain slices. Instead of being caused by the thalamic input, it appears that the thalamic input recruited the activity of cortical ensembles which were responsible for the production of the up-state behavior. Although often evoked by stimulus, in all cases considered the activity outlasted the presentation of the stimulus.

CONNECTING THE EVIDENCE

Although persistent activity has been connected directly to behavior, up-states, and recurrent connectivity, these latter three have not been well connected to each other. Two important questions then arise: do up-states play a role in behavioral processing and are they produced, as theorized, in recurrent networks under naturalistic conditions? We will attempt to tie these loose ends together by showing evidence in this work of up-state mediated persistent activity, evoked by naturalistic stimuli in a recurrent network implicated in memory.

THE MAMMALIAN HIPPOCAMPUS

LOCALIZATION OF MEMORY FUNCTIONALITY

Much of the early evidence for what memory functionality is located in the hippocampal formation and its constituent fields has come from localized damage in the human and rodent hippocampus leading to measurable impairments memory acquisition or recall (eg., Stark and Squire, 2000; Spiers et al., 2001; Fortin et al., 2002). More recently, this has been greatly supplemented by more elegant techniques such as temporary or rescuable inactivation of specific brain areas, improved in-vivo neuronal recording in a behaving animal, and functional imaging. Since neither parallels in the anatomical structures, nor the types of memory present have been perfectly established across vertebrates, I will survey the findings related to this topic as observed in four model organisms.

HUMAN EVIDENCE

Scoville and Milner (1957) studied ten patients with medial temporal lobe (MTL) resection and noted significant retrograde impairment to memory acquired within a limited timeframe, and significant, although specific, anterograde memory impairment. This was subsequently elaborated on to suggest that the medial temporal lobe is important for the acquisition of semantic (or fact-based) and episodic (event-based) memory (declarative memory), but not generally necessary for working memory, or non-declarative (implicit) memory. Further data from patients with more localized damage, restricted to the hippocampus, have shown that despite severe impairments in explicit memory, no impairment in related implicit tasks is apparent. As an example, a patient with near complete hippocampal loss showed normal priming, or bias toward previously viewed words, while unable to recall that the words had been viewed (Stark and Squire, 2000).

Such investigations have also demonstrated severe impairment in patients with damage to the hippocampus while performing spatial memory tasks (eg., Spiers et al., 2001). Some studies have gone further to suggesting that damage to the right hippocampal formation causes more severe impairment to spatial memory than similar damage to the left hippocampal formation (Abrahams et al., 1997). To further confirm the human hippocampus' involvement in spatial memory, place cells have been identified in patients with implanted diagnostic electrodes (Ekstrom et al., 2003).

Investigations of humans rely on incidental damage (rarely perfectly contained), incidental electrode placement, and often subjects with irregular brain function (eg. Epilepsy), leading to low numbers of well-suited subjects. The data, nonetheless, seem to strongly indicate that the human hippocampus is directly involved in spatial, episodic, and semantic memory (although there remains some indication that this is less significant than episodic impairment), and that it is not generally involved in implicit memory. Retrograde amnesia is also commonly reported with hippocampal damage, but the range and specificity varies widely.

Non-human primate Evidence

Mishkin (1978) was one of the first researchers to attempt a replication of the results seen in patients like H.M. (Scoville and Milner, 1957) in a non-human primate. A lesion in the MTL of a monkey produced memory impairment similar to that seen in humans with similar lesions. The advantages of a non-human model for studying the effects of MTL lesions are obvious. Firstly, as the lesions are deliberate, they can be targeted to a specific area and the extent and precise location of the lesion can be verified immediately by histological examination. Secondly, the

subjects are presumably healthy and the numbers involved in a study can be much higher that when depending on incidental damage in human patients. Lastly, the number of techniques available increases dramatically in a non-human model.

Many of the early primate studies using lesioning techniques damaged not only the hippocampus, but also adjacent tissue. This was in part because researchers were attempting to replicate the incidental lesions seen in human subjects, and in part because of the location of the hippocampus which inhibited direct surgical access. There was also a preference for general evaluation of memory ability using the same tests and preferring the use of the delay non-match to sample test (DNMS) (see Squire, 1992 for review). This test involves the subject examining a sample object and then after some delay having to choose between this object and a novel object with choosing the novel object rewarded. Monkeys with MTL damage showed impairment on DNMS testing after long delays, although not always after shorter delays. Later, more specific lesions showed that damage to perirhinal cortex alone was sufficient to produce the impairment, whereas, in most cases, damage to the hippocampus or EC alone did not (see Zola et al., 2000 for exception). Other tests were also used to evaluate declarative memory with MTL damage (eg., reviewed by Squire and Zola-Morgan, 1991). These similarly showed deficits with damage, but under more careful testing have been shown to implicate non-hippocampal structures in many cases. Additionally, some of the results were problematic as very similar memory tasks showed differing results. For example, a concurrent discrimination task with 8 pairs shown multiple times per day in training was shown to be impaired by MTL lesion (Squire, 1992). A 20-pair version where pairs were shown only once per day in training showed no impairment with similar lesions (Malamut et al., 1984). Thus, although early primate work does establish that workable animal

models of amnesiac patients are possible and do show signs of severe memory impairment with damage to the MTL, it did not establish clearly the role of the hippocampus, and significant ambiguity remained. More recent and more specific lesions (eg., excitotoxic lesions) allowed for containment of the lesion to the target area without affecting adjacent areas or fibers of passage. This has allowed some disambiguation, but the results are still contested. Murray and Mishkin (1998) showed expansively that selective excitotoxic hippocampal lesions do not cause DNMS deficits. Zola et al. (2000) show however that they do.

Lesions to the amygdala and perirhinal cortex produced deficits in a cross-modal transfer task where monkeys examined objects in the dark (by touch) and then had to distinguish this object from another in the light. Hippocampal and parahippocampal cortex lesions produced no deficit on the same task (Murray and Mishkin, 1985). Similar lesions led to opposite results on a task where monkeys had to choose between objects based solely on place, or based on the object-place association (Parkinson et al., 1988). Again neither of these lesions was restricted to the target area, and both proved to implicate the damaged adjacent cortices more significantly than the target are, but a functional distinction between the strategies required to solve these different problems has proved informative. Researchers have suggested that these experiments suggest a distinct localization for intrinsic or familiarity based strategies used to solve a problem compared with a more explicit or recollective strategy.

Non-human primate work has been able to reproduce many studies very similar to those done in human subjects with remarkable similarity. It has also informed important distinctions in the localization of functionality. However, it has not proved definitive in clarifying the roles of

some MTL nuclei in specific memory types. We will proceed to rodent studies, which although more dissimilar to the human case, have has some more success in functional dissociation.

RODENT EVIDENCE

Arguably one of the largest specific advances from the rodent work on hippocampal function is the case for spatial memory. Lesion studies have demonstrated impairment on a variety of spatial tasks in the rodent, but perhaps the most compelling evidences are the results of electrophysiological recordings performed in the behaving animal. These studies have revealed the presence of so called "place cells" in the CA3 and CA1 fields of the hippocampus which exhibit selective firing related to the animal passing through certain, usually feature-related, areas of its environment (O'Keefe, 1976). Not only do they appear to encode the animal's current position in the environment, but it has been suggested that they also encode intended future position (Muller and Kubie, 1989) and that they replay sequences of places associated with learned, experienced (Skaggs and McNaughton, 1996), and expected trajectories (Diba and Buzsaki, 2007). These fields are associated with both external landmarks and internal proprioceptive information (O'Keefe, 1976). They are formed using combinations of different sensory modalities and will still form in the absence of individual or combinations of these modalities (eg., Hill and Best, 1981). Similar place cells have been since identified in the primate hippocampus as well (eg., Hori et al., 2005).

Although declarative memory is not something humans can presently evaluate in rodents, there is increasing suggestion in the literature that rodents do exhibit aspects of episodic memory, with which human hippocampal function has been implicated (ex. Fortin et al., 2002).

This remains a controversial proposition with many insisting that non-humans animals show no evidence of so-called “autonoesis” necessary to true episodic memory, but mounting evidence suggests that non-human animals do employ mechanisms and strategies that would operate under the title of episodic memory were the subject human. As with the work done in humans, this operational episodic memory is highly hippocampus dependent. Thus an examination of these evidences is highly relevant to my efforts to identify the hippocampus’ role in memory.

I will now examine the rodent experiments which worked to further clarify the idea of familiarity versus recollective strategies employed in solving memory tasks in our discussion of primate studies. Fortin et al. (2002) demonstrated that rats with selective hippocampal lesions are able to recognize odors previously experienced, but are unable to demonstrate recollection of their order of presentation (when required to select the odor having appeared earlier in the sequence from a pair). Eichenbaum et al. (2012) developed a rather clever way to perform Receiver Operating Characteristic (ROC) analysis with rats and pair this with selective hippocampal lesions. Similar to what was expected from ROC analysis with humans, this group found that rats with hippocampal lesions employed familiarity-based strategies to solve problems which normally biased recollection-based strategies. This is important for two reasons. Firstly, it provides a great potential tool for discriminating the relative contributions of parallel strategies for solving memory tasks in a way that parallels investigations on humans. Secondly, it provides another possible explanation for some of the discrepancies between similar tests performed on humans and other primates in the idea of preferred and compensatory strategies applicable to the same task. For example, some organisms might use similar strategies to solve a problem, but one might not be dependent on this strategy if it is not available (because of

damage or lesion) due to the availability of a compensatory strategy. Thus, even if a brain area performs a very similar function in each of the different organisms, its lesioning might only result in significant impairment in one and not in the other organism.

There have also been experiments directed to demonstrating the location of putative memory processes such as pattern completion and pattern separation. Pattern completion is the putative process by which an animal who encounters a partial representation of a memory (eg., a street where the occupants and weather are different), and is able to recognize the street and thereby access the complete memory of its significance. Pattern separation is in some ways the opposite process. It refers to the putative process by which an animal encountering a representation of a memory which shares many common elements with other memories (eg., this same street which is in some ways very similar to all streets), but is able to identify this unique memory by emphasizing salient aspects which render it unique. These have proved more difficult to design tests for than the other, more behaviorally defined, memory types, but some promising results have been seen. Theoretical models have suggested that pattern separation takes place in the mammalian dentate gyrus and some experimental evidence supports this proposal (for review, Kesner, 2007). Some of the most compelling evidence for pattern completion in the hippocampus comes from studies such as that completed by Nakazawa et al. (2002). CA3-restricted knockout of NMDA receptors in mice produced a very specific impairment in CA1 place cell firing when the animal was re-exposed to a partial-cue version of a familiar environment. Although the place cells fired normally in the complete environment,the animal had difficulty recalling the full environment from a partial cue suggesting a deficit in pattern completion.

Overall, rodent experiments provide compelling evidence that the hippocampus is important to spatial, sequence, and the functional equivalent of episodic memory. It also supports the theory that the hippocampus performs its functions by making use of processes such as pattern completion in CA3 and pattern separation in the dentate gyrus.

Evidence from the Teleost Fish

Although fish do not have a formally defined hippocampus, following the pattern set out in our discussion of rodent episodic memory we will discuss evidences related to similar functionality and where in the fish brain this functionality appears to be localized. Early studies, as in other organisms, involved large lesions of the telencephalon and produced memory impairment (ex. Salas et al., 1996). However, as this represents the removal of a significant portion of the brain we will begin our discussion with more recent and more precise work.

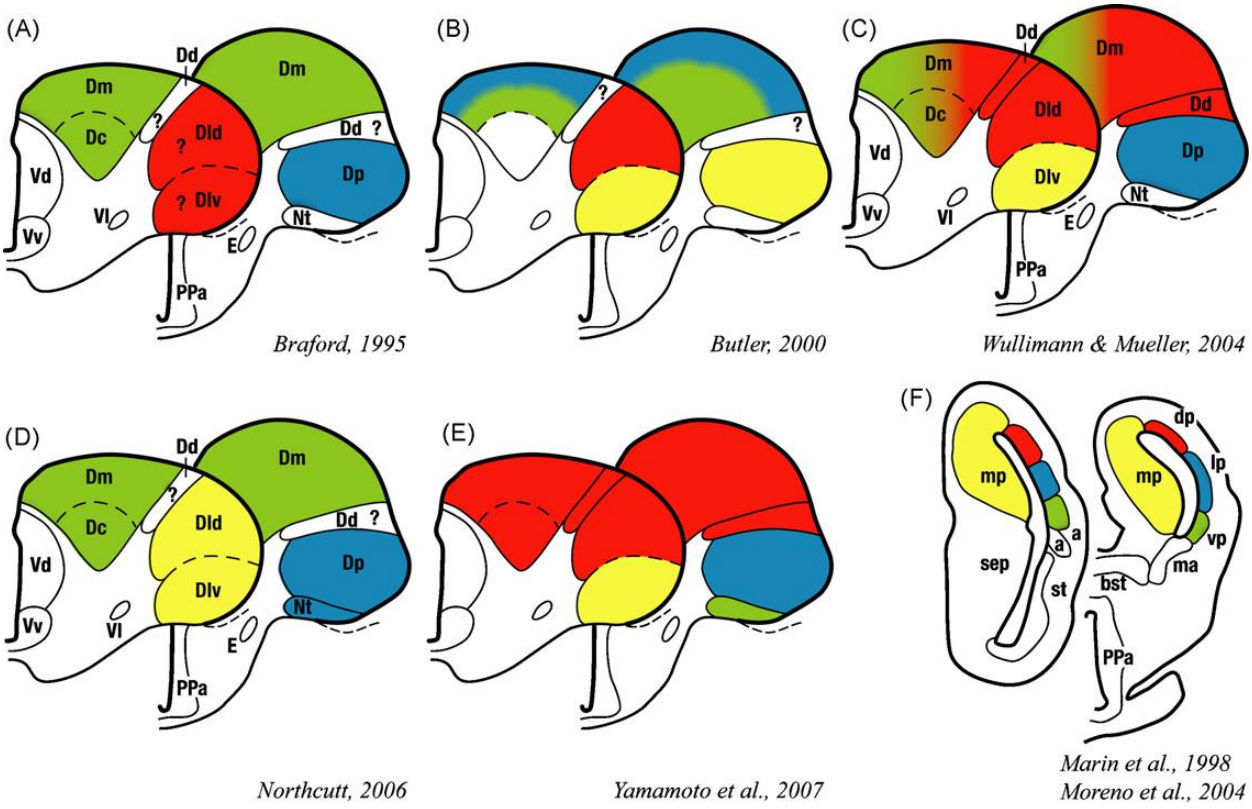

Figure 1-5: Five recent hypotheses (A-E) regarding pallial homologies between teleosts (A-E) and amphibians (F) (from Northcutt, 2008)

Each hypothesis is illustrated by a pair of rostral and caudal sections of the right cerebral hemisphere of *Carassius* color coded to the suspected pallial homologues of an amphibian represented by *Rana* (F). Question marks indicate uncertainty regarding a specific homologue by the authors. aa, anterior amygdaloid area; bst, bed nucleus of the stria medullaris; Dc, central subdivision of area dorsalis; Dd, dorsal subdivision of area dorsalis; Dld, dorsal part of lateral subdivision of area dorsalis; Dlv, ventral part of lateral subdivision of area dorsalis; Dm, medial subdivision of area dorsalis; dp, dorsal pallium; Dp, posterior subdivision of area dorsalis; E, entopeduncular nucleus; lp, lateral pallium; ma, medial amygdala; mp, medial pallium; Nt, nucleus taeniae; PPa, anterior parvocellular preoptic nucleus; sep, septum; st, striatum; Vd, dorsal nucleus of area ventralis; vp, ventral pallium (lateral amygdala); Vv, ventral nucleus of area ventralis.

Localized telencephalic lesion studies demonstrated a functional separation between lateral pallium (LP), consisting primarily of the ventral (DLv) and dorsal (DLd) subregions of dorsolateral telencephalon (DL) and medial pallium (MP) consisting primarily of the dorsal (DMd) and ventral (DMv) subdivisions of dorsomedial telencephalon (DM). Rodriguez at al. (2002) lesioned DP (DLv and DLd) in goldfish and reported a significant impairment in choosing the correct arm of a maze when navigation depended on external visual cues. Specifically, fish had to choose between the right and left arm of a “plus” maze where the start location was alternated randomly. This required use of external environmental cues to decide whether the baited (goal) arm was to the right or left, depending on which start box was used for that particular trial. The same test was repeated with lesions in MP (DMd and DMv), as well as in DP (primarily dorsodorsal telencephalon (DD)). Neither of these lesions produced a significant impairment. The same DL lesion was used in a simple cue association test where the fish had to choose between 2 exit doors to escape a box. One was obstructed transparently and did not allow escape, the other was

clear and marked with a visual cue. The location of both the unobstructed exit and the associated cue was alternated randomly. In this task the DL lesion had no impact on performance, presumably as no spatial memory was required.

Vargas et al. (2009) summarize a series of experiments performed in goldfish where specific pallial areas were lesioned in the context of a cued aversive stimulus avoidance task. Fish were shown a colored light and had to move to another location within a set time frame to avoid a mild electric shock. If the shock began while the light (cue) was still active (delay conditioning), performance was affected by DM lesions, but not DD or DL lesions. If there was a time interval in between removal of the cue and presentation of the shock (trace conditioning), then DD or DL lesions produced significant impairment.

Thus we may conclude that the DL region is integral to spatial memory and both DL and DD to trace conditioning, where DM is associated with aversive stimulus avoidance. Further evidence for the dissociation of the involvement of DL versus DM in different memory tasks is outlined by Broglio et al. (2005) and is shown in figure 1-5. In this figure, impairment on the task listed in the left column is indicated by a "+", whereas no impairment is shown by a "-" for lesions in DL, DM, mammalian hippocampus (H) or mammalian amygdala (A) respectively. These results suggest a functional analogy between the hippocampus and DL (LP) and between the amygdala and DM (MP).

	Teleosts		Mammals	
	LP	MP	H	A
Spatial memory	+	-	+	-
Cue learning	-	-	-	-
Reversal learning	+	-	+	-
Trace motor classical conditioning	+	-	+	-
Delay motor classical conditioning	-	-	-	-
Heart rate conditioning	-	+	-	+
Delay avoidance conditioning	-	+	-	+
Trace avoidance conditioning	+	+	+	+

Figure 1-6: Results of Lesions in Teleost Versus Mammals (adapted from Broglio, 2005)

Involvement of the mammal hippocampus and amygdala, and the teleost fish lateral and medial pallia, in different learning and memory processes. This represents a summary of results obtained by several groups and in several species. The sign "+" indicates the involvement in a given function. The sign "–" denotes no involvement. A, corresponds to amygdala; H, hippocampus; LP, lateral pallium; MP, medial pallium.

An important advance was made based on the expression of early growth response protein 1 (Egr-1), an immediate early gene associated with memory consolidation. Jones et al. (2001) showed that an EGR-1 knockout mice lacked late phase long-term potentiation (LTP). Tetanus was able to induce early LTP in the dentate gyrus, but late LTP was absent after 24 hrs. These mice also showed impairment in tests requiring long-term, but not short-term memory. Mice were able to overcome the deficits, but only with extended and distributed training. In-situ hybridization studies in weakly electric fish have shown a dramatic increase in expression of a homolog of Egr-1 (AptEGR-1), in DD following presentation of a novel electrical signal mimicking another weakly electric fish. The expression of AptEgr-1 was associated with the fish learning and remembering the frequency of an EOD mimic. This response was observed if either the frequency

of the signal (identity of the fish) or the origin of the signal (relative position of the fish) was novel (Harvery-Girard et al., 2010). A recent study by Aoki et al. (2013) used calcium imaging in a zebrafish to demonstrate activity localized to an area of DD (although they do not identify it clearly as such) in response to an aversive stimulus avoidance task where a fish learned to avoid a shock by changing location in response to the activation of a light. This localized activity was seen 24 hours, but not 30 minutes following training. Ablation of this area resulted in a performance deficit again 24 hours, but not 30 minutes, after training on the same task. If the ablation was performed after training, a similar deficit also appeared. The authors conclude that this region is integral to the long-term recall of memory associated with such a task.

Across different species of teleost fish the evidence is compelling that much of the spatial and other memory function of the mammalian hippocampus is localized in the teleost DD and that of the mammalian amygdala, including aversive memory, in the teleost DM. The teleost DL has also been implicated in memory functionality associated with hippocampal-cortical interaction in the mammal.

Development of the Mammalian Hippocampal Formation

The hippocampal formation develops in the wall of the rostral neural tube which has differentiated from the adjacent diencephalon by embryonic day 36 in the human. The outermost telencephalic division, the dorsal pallium, will differentiate into the neocortex, while the hippocampal formation originates in the adjacent medial pallium. It is phylogenetically related to cortex, and represents an old form of cortex known as the archicortex. It develops in the medial temporal lobe along the lateral ventrical (Anderson et al., 2007).

The hippocampal formation is highly interconnected with the neocortex. A summary of these connections is provided in the figure 1-6 (figure 1, Rolls, 2013). A more detailed description of the inputs to the entorhinal cortex, and by extension to the hippocampal formation, is given in figure 1-7 (figure 2, Lavanex and Amaral, 2000). These are followed by a more detailed description of the specific connectivity of each field and nucleus contained within this formation.

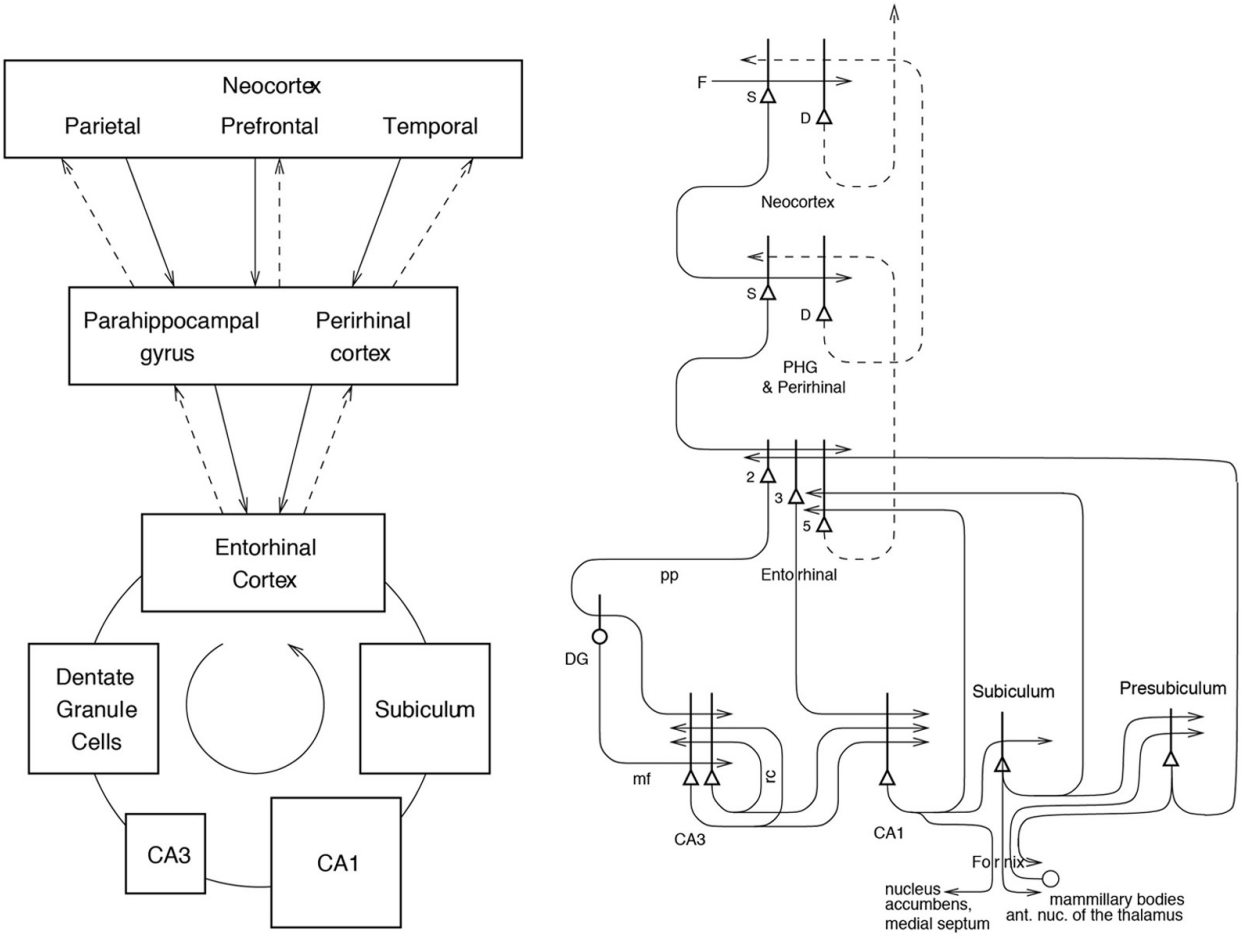

Figure 1-7: Inputs to and Interconnections between Fields of the Hippocampal Complex (from Rolls, 2013)

Forward connections (solid lines) from areas of cerebral association neocortex via the parahippocampal gyrus and perirhinal cortex, and entorhinal cortex, to the hippocampus; and backprojections (dashed lines) via the hippocampal CA1 pyramidal cells, subiculum, and parahippocampal gyrus to the neocortex. There is great convergence in the forward connections down to the single network implemented in the CA3 pyramidal cells; and great divergence again in the backprojections. Left: block diagram. Right: more detailed representation of some of the principal excitatory neurons in the pathways. Abbreviations: D, deep pyramidal cells; DG, dentate granule cells; F, forward inputs to areas of the association cortex from preceding cortical areas in the hierarchy; mf, mossy fibres; PHG, parahippocampal gyrus and perirhinal cortex; pp, perforant path; rc, recurrent collateral of the CA3 hippocampal pyramidal cells; S, superficial pyramidal cells; 2, pyramidal cells in layer 2 of the entorhinal cortex; 3, pyramidal cells in layer 3 of the entorhinal cortex. The thick lines above the cell bodies represent the dendrites.

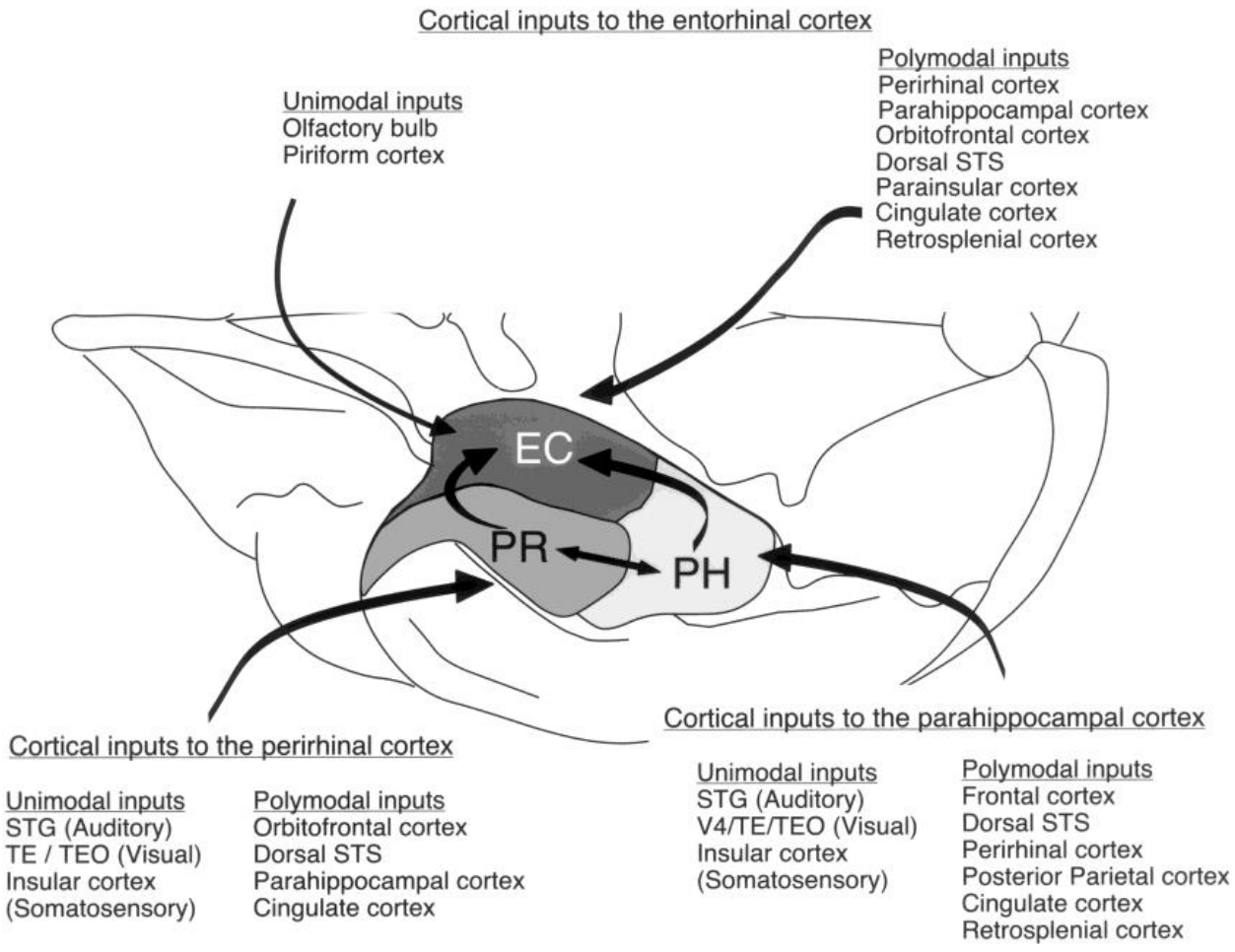

Figure 1-8: Cortical Inputs to the Entorhinal Cortex (from Lavenex and Amaral, 2000)

Summary diagram showing the ventral surface of the macaque monkey brain. The major connections of the entorhinal and perirhinal and parahippocampal cortices are indicated.

NEUROANATOMY OF THE MAMMALIAN HIPPOCAMPAL FORMATION

ENTORHINAL CORTEX

The entorhinal cortex (EC) serves in many ways as both the primary input and one of the primary outputs of the hippocampal formation. The EC is organized in a laminar formation consisting of six layers (according to Ramón Y Cajal, 1901-1902). Alternative layering schemes have been proposed which are similar, but delineate the layers at slightly different points. The outer-most layer, layer I, contains stellate cells and GABAergic horizontal cells which project both to EC layer II and to the DG. Layer II contains stellate and pyramidal cells which project to CA3 and again to DG, as well as to other areas of EC layer II. Layer III is principally populated by pyramidal cells projecting to CA1 and subiculum with local connections to EC layers I and III. Many other neuron types are found in layer III, most believed to contribute to the perforant path projections. Layer IV does contain some cell bodies of varied types but is generally thought of as being cell-free. Layer V contains three primary classes of neuron, pyramidal, spherical, and fusiform. These cells send projections to the white matter, but also back to different layers of EC. Diverse other neuron types are found in Layer V, but none as numerous as the three aforementioned. Known targets of Layer V cells include projections to the amygdala, striatum, septum. Layer VI neurons send three different types of projection, each originating from a different group of cells, one locally to layers V and VI, a second columnar projection to layers I – III, and a third group of projection neurons to the white matter. Some of those in this third group project to DG and the hippocampus.

Significant commissural projections originate in the EC and terminate in the contralateral EC as well as the contralateral DG, hippocampus, and subiculum. The commissural EC connections originate in all layers of the EC, while that to the other fields of the hippocampal formation originate in layer III.

Major inputs to the EC vary greatly with species, but include significant projections from: piriform, frontal, insular, temporal, cingulate, parietal, and occipital cortices. Subcortical inputs include those from the amygdala and claustrum. The septum provides the main cholinergic innervation to the EC. Dopaminergic innervation originates in the ventral tegmental area and serotonergic innervation from the raphe nuclei. Different areas of thalamus send major or minor projections to the EC (reviewed in Anderson et al., 2007).

DENTATE GYRUS

The dentate gyrus (DG) is a semi-lunar structure consisting of three layers. The outer layer, or molecular layer (DGml), contains very few cell bodies, apart a few interneurons, and is primarily occupied by the dendritic arbors of the dentate granule cells. It is therefore also the primary input layer from the EC. The second layer, or granule cell layer (DGgcl), contains the densely packed granule cell bodies. Axons from these, the principal cells of the DG, extend through the third layer, the polymorphic layer (DGpl) on their way to the stratum lucidum, just above the pyramidal cell layer of the CA3 region. Although the CA3 pyramidal cells remain the primary recipients of the DG granule cell output, these axons, called mossy fibers, also send recurrent collaterals through the polymorphic layer which contact other cell types within the DG which extend dendrites into this layer, notably the mossy cells and the pyramidal basket cells.

These mossy fibers are believed to be primarily glutamatergic, but also show evidence of both GABA and dynorphin expression (Walker et al., 2002).

The pyramidal basket cells have bodies located between the DGml and the DGgcl. Single apical dendrites extend into the DGml and a basal arbor into the DGpl. These cells send GABAergic projections onto the cell bodies and proximal dendrites of the DG granule cells. These connections spread across a large number of cells and it is estimated that a single basket cells may project to as much as 1% of the total number of granule cells in the DG (Amaral et al., 2011).

The third major cell type found in the DG is the mossy cell whose bodies are located in the DGpl. The dendrites of the mossy cells are primarily restricted to the DGpl. The mossy cells send glutamatergic projections to the dendrites of the DG granule cells. These projections are both ipsilateral and commissural in the rat, but not primate, where only the ipsilateral connections are seen. Numerous additional interneurons, mostly inhibitory, are found throughout the DG, including some in the DGml. Most of these project back to the granule cells. One such connection of some note in this work is the hilar performant path-associated (HIPP) cell which stains positive for both GABA and somatostatin. These cells are located in the DGpl and provide a local recurrent feedback connection to the DG granule cells.

Although major input to the DG is from EC via the perforant path, there are other minor projections worth noting. A projection of unknown type arrives from the presubiculum and parasubiculum (Kohler, 1985). Cholinergic and GABAergic fibers arrive from the septal nuclei, with the cholinergic projection terminating mainly on DG granule cells with some innervation of the mossy cells. The GABAergic projections terminate mainly on the DGpl interneurons.

Hypothalamic projections to the DG are glutamatergic, but also often carry calretinin or less often substance P. The DGpl also receives noradrenergic input from the nucleus locus coeruleus, dopaminergic input from the ventral tegmental area (vta), and serotonergic projections from the raphe nuclei (reviewed in Anderson et al., 2007).

HIPPOCAMPUS

The hippocampus itself is a laminar "V" or "U" shaped structure which abuts the DG at one end and the subicular complex at the other. It is divided into three fields CA3, CA2, and CA1 listed in order as proceeding along the length of the structure from DG to subiculum. The outermost layer, the stratum oriens (so), also called the infrapyramidal layer, contains the basal dendrites of the pyramidal cells. The pyramidal cells are the principal neurons of the hippocampus and they are located in the aptly named pyramidal cell layer (pcl) which is the second layer after the so. A thin layer containing principally the mossy fibers originating from the DG is located just above the pcl and this is succeeded by the much thicker stratum radium (sr), or suprapyramidal layer. The sr contains the Schaffer collateral connections which run from CA3 to CA1 as well as many of the local intra-CA3 connections. A small portion of these connections is also located in the so. The inner-most layer is called the stratum lacunosum-moleculare (sl-m) and is where afferent fibers originating in the EC terminate. The apical dendritic trees of the pyramidal cells spread throughout the sr and sl-m. Numerous interneurons are located in all layers of the hippocampus and a description of the laminar distribution of the principal classes is shown in figure 3-28 of "The Hippocampus Book" (Anderson et al., 2007).

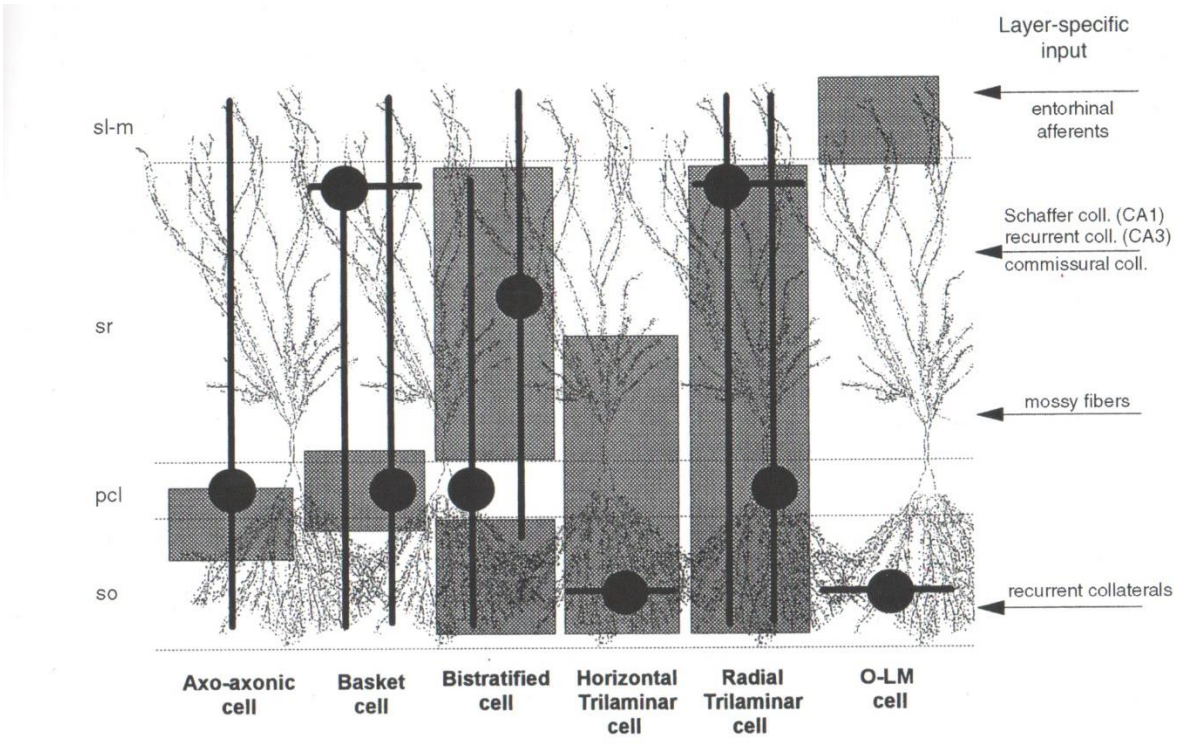

Figure 1-9: CA3 Interneuron Projections (from Anderson et al., 2007)

Morphological classification of the interneurons in the hippocampus proper. Filled circles indicate the location of the cell bodies, and thick lines indicate the predominant orientation and laminar distribution of the dendritic tree. The pyramidal cells (principal neurons) are illustrated in the background, providing an indication of which domain is innervated by the various interneuron groups. The laminar distribution of the inputs, which often show correspondence with the interneuron type or axon distribution, is also indicated. pcl, pyramidal cell layer; sl-m, stratum lacunosum-moleculare; so, stratum oriens; sr, stratum radiatum. (*Source:* adapted from Freund and Buzsaki, 1996)

Connectivity in the hippocampus is highly recurrent, both locally and globally. The pyramidal cells of the CA3 and CA2 fields are each massively innervated by local (from ipsilateral CA3 and CA2) and commissural (from contralateral CA3 and CA2) recurrent connections. It should be noted however that these commissural connections are mostly found in the rat, less so in the monkey, and are not believed to exist in the human. The primary input to CA1 pyramidal cells is not from other CA1 cells, but from CA3 pyramidal cells. In fact, all CA3 and CA2 pyramidal cells

project to CA3, CA2, and CA1. CA2 pyramidal cells also project to the DG. The CA3 to CA3 recurrent connections are known as the associational connections, while the CA3 to CA1 projections are known as the Schaffer collaterals. Some associational, or local recurrent connection, is present in CA1, although far less than in CA3 and most of this appears to be multi-synaptic recurrence via inhibitory interneurons.

Although, as mentioned earlier, the EC projections terminate throughout the length of the sl-m in all three hippocampal fields, these connections do not all originate in the same part of the EC. EC projections to CA3 and CA2, like those to the DG, originate in EC layer II, whereas those to CA1 originate in EC layer III. CA1 also appears to be the only field which projects back to the EC and to the subiculum. Similarly, CA1 is the only field to directly project to and receive input from the neocortex, where the major target of such communication is the perirhinal and postrhinal cortices (Anderson et al., 2007).

Although both CA3 and CA1 receive amygdalar input, it appears that only CA1 projects back to the amygdala. Both CA3 and CA1 show reciprocal projections with the septum. The CA3 projection to septum is bilateral however, compared with the ipsilateral CA1 projection. Only CA2 receives a significant input from the posterior hypothalamus. The thalamus projects to the hippocampus generally as well as noradrenergic and serotonergic fibers from the brain stem. CA1 also receives input from the nucleus reniens (reviewed in Anderson et al., 2007).

SUBICULUM

By its location, the subiculum appears as an extension of the CA1 region. It has a similar laminar structure to CA1 but with a wider pcl, and the sr being replaced with the much wider

molecular layer (Sml). This Sml is where projections from CA1 and EC terminate. Similar to the fields of the hippocampus, the principal cells of the subiculum are large pyramidal cells located in the pyramidal cell layer (pcl). These cells appear to occupy two distinct classes, regularly firing cells and bursting cells. The bursting cells project recurrently in a local, columnar fashion to other pyramidal cells, while the regularly firing cells also project recurrently, but in a more diffuse manner, distributed throughout the subiculum's pcl. There are numerous interneurons distributed throughout the subiculum, but little is known about their connectivity.

The subiculum is one of the major output structures of the hippocampal formation sending major projections to: diencephalon, brain stem, neocortex, amygdala, and mammillary nuclei, with minor connections to thalamus and presubiculum. The subiculum also receives input from: EC, supramamillary region, thalamus, and brain stem (reviewed in Anderson et al., 2007).

TELEOST PALLIAL CONNECTIVITY

The teleost telencephalon is divided into two main divisions, pallium and subpallium. The pallium is further sub-divided into the Dorsolateral (DL), Dorsocentral (DC), Dorsodorsal (DD), Dorsomedial (DM), and dorsoposterior (DP) subdivisions. As the development of the teleost brain differs significantly from the mammalian brain (eversion versus inversion) comparison by location to areas of the mammalian brain is difficult. Some functional comparison is possible and has already been alluded to. Comparison on the basis of marker expression and by similarities in connectivity is also possible. In Chapter 3 we will present evidence that homologous connectivity

to parts of the mammalian cortico-hippocampal circuitry is located in the DD and DL regions of the teleost pallium.

THEORETICAL MODELS OF HIPPOCAMPAL FUNCTION

Research into the neural basis of learning and memory has inspired many theoreticians to attempt the development of computational models of simulated neurons capable of storing, processing, and retrieving information.

Hopfield (1982) proposed a model wherein reciprocal local connectivity within a group of neurons was capable of storing so-called "content addressable memory." He extended Marr's (1971) proposal that the entirety of a memory should be retrievable by even a flawed partial representation, or cue. This process has been elaborated into what has become known as pattern completion. In his model, networks of highly interconnected nodes (or neurons) effectively store information in the malleable strength of the interconnections. Memories are represented as stable states (or configurations of active vs. inactive nodes) which can be read as output. Input configurations place the network of nodes into a state (usually not stable), and by means of reverberatory activity via recurrent collateral connections, the state will self-adjust incrementally until settling into a stable state representing a memory. This general structure has been called an attractor network as the encoded memories act as local minima or sinks in the state space and "attract" the state of the nodes into that particular configuration of activity.

The hippocampus, and specifically CA3, was, and is, considered the most likely candidate for an implementation of such a network, both due to its being linked to associative memory, and to

its highly recurrent circuitry. This led Marr (1971) and those who followed him to base their models in the known neuroanatomy of this structure. As specific mechanisms for Hebb's (1949) ideas of coincident activity leading to the establishment or enhancement of neural interconnections were discovered in the form of the various types of synaptic plasticity, these were incorporated into models providing insight into not only how stored memories might be recalled, but how these memories and associations might be encoded in the interconnections of the hippocampus' recurrent networks (eg., McNaughton and Morris 1987).

Early models also identified the advantage of non-overlapping or orthogonal input patterns in avoiding recall errors (eg., Marr, 1971; McNaughton and Morris 1987). McNaughton and Morris (1987) also point out how inclusion of hippocampal-associated networks such as the DG could help expand the capacity of the CA3 memory system. The subsequent combination of these two ideas has led to the theory that the DG would be well suited to contribute to the CA3 network by orthogonalizing its inputs through a process now known as pattern separation (Amaral et al., 1990). Several models have since been developed showing how this might be accomplished (See Rolls, 2013 for review).

As available anatomical information has increased, this has been incorporated into newer, more elaborate models which include additional features such as unique functionality provided by cortical or temporal lobe nuclei (Hasselmo and McClelland, 1999) and adult neurogenesis as a means of improving pattern separation (Aimone et al., 2011).

Another, perhaps incidental, byproduct of the models which developed for recurrent, Hebbian memory networks, was a mechanism for persistent activity. This has become more

important with the discovery of up states (eg., Larimer and Strowbridge, 2010) to help explain how neural responses might outlast the presentation of stimuli and help to reconcile the immediate neural responses seen in single-unit electrophysiological recordings with the delayed responses seen using imaging techniques to visualize the activity of neural ensembles (eg., Aoki et al., 2013).

Although theoretical models have been informed and advanced by progress in anatomical work done in the hippocampus and cortex, the biological investigations have also profited greatly from the predictions made by theoretical models. Their results have informed interpretation of anatomical data and highlighted important directions for further or more careful investigation. Thus in our current endeavor we will refer both to experimental and theoretical models to inform our functional conclusions and comparisons.

Chapter 2

STIMULUS INDUCED UP STATES IN THE DORSAL PALLIUM OF A WEAKLY ELECTRIC FISH

S. B. Elliott, L. Maler

Published Manuscript
The Journal of Neurophysiology, 2015, 114(3): 2071-2076

CONTRIBUTION OF CO-AUTHORS

S. Benjamin Elliott: Performed all in-vivo recordings, data analysis, and interpretation of the results, as well as writing of the manuscript.

Len Maler: Contributed to the analysis, interpretation of results, and writing of the manuscript.

ABSTRACT

We investigated the response of putative novelty-detecting neurons in the pallium of an electric fish to electrosensory and acoustic stimuli. Extracellular and whole-cell patch recordings were made from neurons in the dorsal pallial nucleus (DD) of *Apteronotus leptorhynchus*. DD neurons were typically quiescent and exhibited hyperpolarized resting membrane potentials. Stimulation induced, with a variable long latency, rapid though transient depolarization and spike discharge. The transition between resting and depolarized/spiking states resembled the transition to Up states seen in mammalian telencephalic neurons.

INTRODUCTION

Electrophysiological recordings from mammalian cortex and striatum have revealed the existence of Up states: the normally quiescent and hyperpolarized membrane potential is interrupted by a brief period of depolarization, increased MP variance, and spike discharge. Up states have been observed both in vivo (Wilson & Kawaguchi, 1996; Li et al., 2009) and in vitro (McCormick et al., 2003) and typically occur spontaneously. Up states in cortical pyramidal cells are due to intrinsic cortical dynamics but can be triggered by thalamic input (Maclean et al., 2005), and are controlled in a complex manner by GABAergic inhibition (Mann et al., 2009). It has been difficult to establish a clear link between Up states and external triggering events, and their function remains unknown.

Our work focused on *Apteronotus leptorhynchus*, a weakly electric fish that utilizes its sinusoidal electric organ discharge (EOD) and electroreceptors to communicate, navigate, and

locate prey (Chacron et al., 2011; Marsat et al., 2012; Krahe & Maler, 2014). The *Apteronotus* EOD is a constant high frequency sinusoid and when two fish are in proximity, their EODs interfere to generate an amplitude modulation (AM) or beat with a frequency equal to the difference of their EOD frequencies. *Apteronotus* is very sensitive to such AMs and can remember specific beat frequencies for at least three days (Harvey-Girard et al. 2010).

We recorded from neurons in the dorsal pallium (DD). Neurons in DD have been shown to respond to initial electrosensory beat stimuli and acoustic stimuli with dramatic delayed increases in immediate early gene expression (Egr-1, Harvey-Girard et al., 2010). Egr-1 expression also increases in other pallial regions, but to a lesser extent. Egr-1 expression in DD declines to undetectable levels as the fish habituates to a repeatedly presented beat frequency, and expression again increases when novel beat frequencies are presented. This led us to hypothesize that DD was involved in detecting novel stimuli and initiating long-term memory storage of the beat frequency in the large dorsolateral pallium (DL). DD receives glutamergic input from DL which, in turn, receives a sparsely encoded representation of electrosensory features, including AM (beat) stimuli, as well as acoustic input from a thalamic analogue, the preglomerular nucleus (PG) (Giassi, Duarte, et al., 2012). DD then projects back to DL via glutamatergic synapses. Both DD and DL contain densely connected recurrent networks of both glutamatergic and GABAergic neurons (Giassi, Harvey-Girard, et al., 2012).

We performed *in vivo* recordings from the DD region of restrained fish while presenting the animal with mimics of natural electrosensory or acoustic stimuli. The electrosensory stimuli consisted of sine waves (20 s on, 20 s off, modified from our behavioural protocol, Harvey-Girard

et al., 2010) delivered across the fish's body at 20% of its EOD amplitude and with frequencies in the species EOD range; the beat frequencies generated were therefore within the natural species range (Engler & Zupanc, 2001, Krahe & Maler, 2014; Marsat et al., 2012). The acoustic stimuli consisted of low frequency (600 Hz) tones similar to those emitted by electric fish predators (Stabentheiner, 1988). Gymnotiform fish belong to the otophysian superorder and have Weberian ossicles; 600 Hz is likely in the middle of their sensitivity range (Popper & Fay, 1973).

MATERIALS & METHODS

ANIMAL MODEL

All experiments were performed on *Apteronotus leptorhynchus*, a weakly electric fish native to South America. Fish were kept at 28°C. All procedures were approved by the University of Ottawa Animal Care and follow guidelines established by the Society for Neuroscience.

SURGERY AND ELECTROPHYSIOLOGY

Fish of either sex were anesthetized with 0.2% 3-aminobenzoic ethyl ester (MS-222; Sigma) in water just before surgery. Anesthetized fish were transferred to a holder with a breathing tube providing oxygenated water containing MS-222. The top of the skull was removed, exposing both lobes of the forebrain. The fish were revived and then immobilized by means of an intramuscular injection of 2mg/ml tubocurarine pentahydrate (curare; Sigma) in saline. The fish's body was submerged with the exception of the surgical opening in a plexiglass

experimental tank (40 x 45 x 20 cm) containing water held between 27-29°C with conductivity around 200 µS.

In vivo recordings were performed using either metal filled microelectrodes for extracellular recordings, or borosilicate micropipettes filled with intracellular solution (130mM K-Gluconate, 10 mM KCl, 10 mM HEPES, 4 mM NaCl, 4 mM Mg-ATP, 10 mM Disodium-Phosphocreatine, 0.3 mM Na-GTP in water) for whole-cell patch recordings. Electrode tip was positioned using a micropositioner (David Kopf Instruments model 2662).

The procedure for obtaining whole-cell recordings was as follows. Resistance of the electrode tip was monitored by means of a repetitive test pulse while the electrode was advanced through the tissue. Rapid increase in tip resistance signalled tip occlusion and suction was applied in an attempt to achieve a gigaohm seal. If successful, the test pulse was replaced by a small hyperpolarizing holding current and brief intense suction was applied. A sudden drop in tip resistance accompanied by a sudden drop in observed voltage at the tip indicated successful opening of the membrane.

Cells in the DD region were located using mediolateral measurements from the medial and caudal edges of the forebrain lobe. Dorsal-ventral measurements were measured from the brain's surface at the point of penetration. The number of all single cell recordings (N) is reported.

The temporal dynamics of Up states, specifically rise and fall kinetics, were highly variable and it often required multiple exponentials to approximate a fit. We therefore instead used 10-90% rise and fall times instead of time-constants for this analysis. For consistency, we also used this analysis for the rise and fall times of current induced membrane depolarizations.

HISTOLOGY

To identify recorded cells, patch pipettes were filled with 1% Lucifer Yellow (Lucifer Yellow CH dilithium salt; Sigma) in intracellular solution. Lucifer Yellow was ejected from the pipette during and following recording by application of hyperpolarizing current. Fish were perfused under anesthesia with 4% para-formaldehyde, 0.1% gluteraldehyde, 0.2% picric acid in 0.1M PBS pH=7.4. The brains were removed, placed in 4% para-formaldehyde, 0.2% picric acid, 15% sucrose in 0.1M PBS pH=7.4 and stored at 4°C. Fixed brains were cryoprotected in 30% sucrose in PBS, sectioned (25µm transverse sections cut in cryostat) and sections were mounted on Superfrost slides. Slide-affixed sections were washed in 0.1M PBS for 10 min at room temperature and then counterstained with green fluorescent Nissl reagent 1:300 (Molecular Probes, NeuroTrace® 500/525 green-fluorescent Nissl Stain #N21480) in PBS for 20 minutes at room temperature.

Sections were visualized on a Zeiss LSM5 Axiovert 200M. Microscope control and image capture was accomplished using Axiovision software (Zeiss) on a Windows 7 PC.

STIMULATION

All stimulation signals consisted of sinusoidal waves generated in Spike2 (Cambridge Electronic Design Limited, Cambridge, England).

Electrosensory signals were attenuated (PA4, Tucker-Davis Technologies, Alachua, FL), isolated (Model No. 2200; A-M Systems, Carlsborg, WA) and delivered to the fish by means of two carbon electrodes affixed to either side of the experimental tank and oriented parallel to the fish's longitudinal axis. Sinusoidal stimuli were given at a specific frequency difference (relative

to the individual fish's characteristic EOD frequency). These frequency differences ranged from -40Hz to +40Hz.

Ampullary receptor stimulation was attempted by means of a fixed frequency 5Hz sinusoid delivered in a manner identical to that described above for electrosensory stimuli.

Acoustic signals were delivered by means of two amplified speakers (Logitech X-260) positioned outside of the experimental enclosure beside the tank.

Manipulations of the electrode position required light and we therefore did not use light stimuli.

RESULTS

We first performed extracellular recordings from DD (N = 16) using Woods metal filled glass electrodes (Dowben & Rose, 1953). We typically recorded from one to four neurons and used Spike 2 software (Cambridge Electronic Devices) to sort spikes. DD consists of superficial (DDs), intermediate (DDi) and magnocellular (DDmg) divisions (Giassi, Harvey-Girard, et al., 2012). In DDs (< 200 µm from the surface, Maler et al., 1991), neurons were encountered that discharged spontaneously at a low rate. The spiking activity did not appear to be modulated by acoustic or electrosensory stimulation in any reproducible way and we did not further explore this region. In the DDi/DDmg region (200 to 600 µm from the surface), initial penetration mechanically provoked a few spikes, but the cells immediately stopped discharging and remained quiescent in the absence of sensory input. Filled cells following intracellular recording (see below)

suggested that we were recording primarily from DDi cells although we cannot exclude the possibility that some recordings were from nearby DDmg cells (Fig. 3F, Giassi, Harvey-Girard, et al., 2012).

We initially waited for 300 – 864 seconds (Figure 1A) before commencing stimulation. Stimulation with the electrosensory signals was associated with sustained discharge after a long and variable latency (onset latency: 592.7±232.8 s, range = 137-1170 s) after which the neurons returned to their quiescent state. The responses themselves were highly variable (number of spikes: 6-1135: duration of spiking response: 10-2428 seconds; peak instantaneous firing rate: ranged 0.25-78Hz). Spiking was not directly linked to the stimulus since it could commence during (7/16) a stimulus presentation or between (9/16) presentations. In many cases (N = 10) spiking was initiated during stimulus presentation but continued after stimulation ceased.

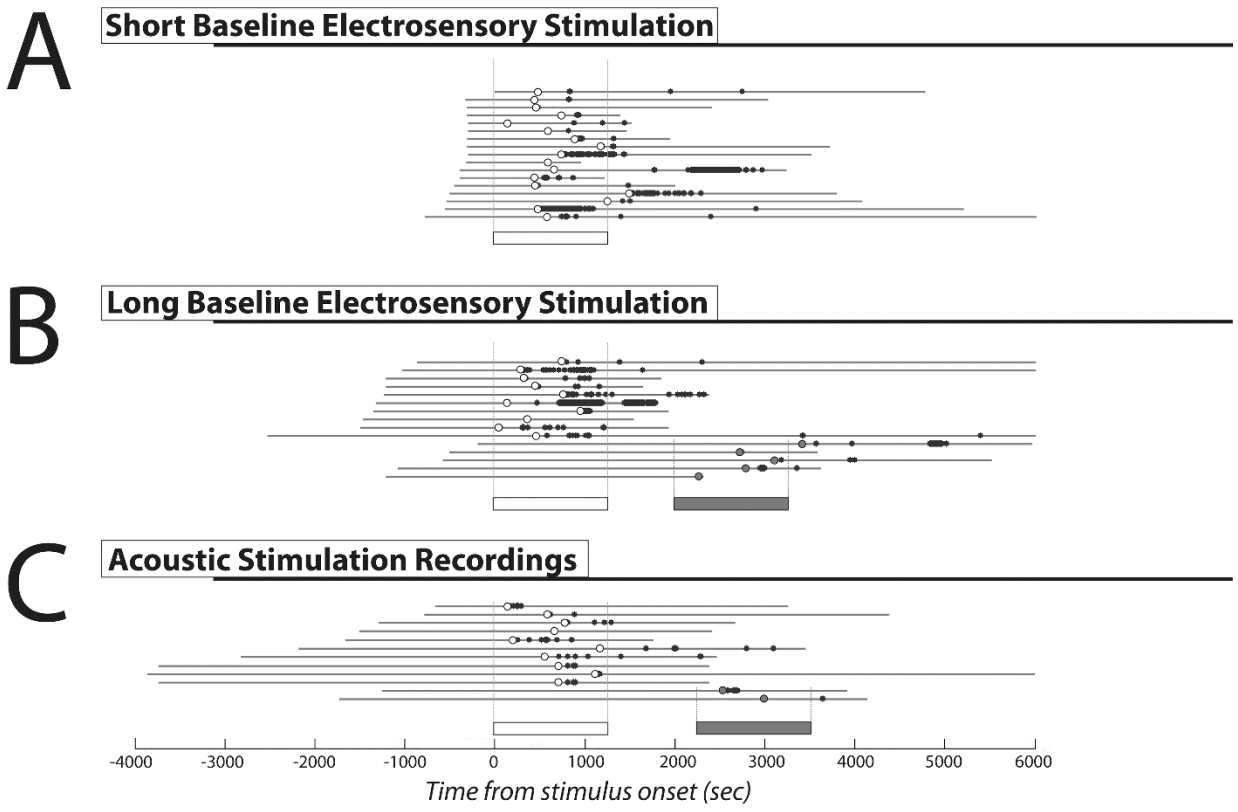

Figure 2-1: Extracellular Recordings

Results of extracellular recordings from DD cells with **(A)** short pre-stimulus baseline electrosensory stimulus, **(B)** long pre-stimulus baseline electrosensory stimulus, and **(C)** long pre-stimulus baseline acoustic stimulus respectively. Gray lines indicate the total length of recording. The 0 s time point indicates the onset of the first stimulus presentation. Negative time values therefore allow measurement of the quiescent baseline recorded prior to stimulus presentation. The hollow bars represent the duration of the first stimulus set presented in a given recording. Gray-filled bars represent a subsequent stimulus set presentation. Dots represent recorded spikes. Highlighted dots indicate the first spike seen during recording. Hollow dots indicate that the first spike occurred during or following the first stimulus presentation. Gray-filled dots indicate that the first spike was seen during or following a subsequent stimulus set presentation. Recordings have been ordered with respect to length of recorded pre-stimulus baseline with recordings containing multiple stimulus presentations following those containing only the presentation of a single set. Vertical dashed lines framing the stimulus bars indicate in which recordings that stimulus set was presented.

As we had only recorded over a brief baseline period, the variability in latency and relation to the stimulus made it uncertain as to whether the spiking activity was induced by stimulation or had occurred spontaneously, since the distributions of latencies from either recording or stimulus onset were similar (Figure 2A). We reasoned that, if the spiking activity was spontaneous, then we should observe it during longer baseline recordings. We therefore performed additional recordings (N = 15) with longer and varying lengths of pre-stimulus baseline recording (306 – 2521 s). We never observed discharge during the baseline period. The distribution of latencies from recording onset versus stimulus onset were now nearly completely disjunct. The first spike response was clearly correlated with stimulus, but not recording, onset (Figure 1B). Although still varying over the wide range of 1-20 minutes post stimulus onset, the first recorded action potential always occurred following the onset of stimulus presentation and was strictly confined to this observed range (onset latency: 581.2±383.9 s, range = 40-1409 s; response duration: 953.4±873.7 s, range = 10.7-2428.1 s).

We next repeated these experiments using acoustic stimulation (N = 12) and found the same results (onset latency: 641.0±325.7 s, range = 138.5-1173.1 s; response duration: 528.7±649.9 s, range = 0.77-1919.6 s, Figure 1C). Individual cells could respond to stimulation with either modality; in five cases we found neurons that responded to both acoustic and electrosensory stimulation and within the same latency range.

We were not able to elicit a spiking response with a 5 Hz sinusoidal stimulus that will activate the fish's ampullary electroreceptors (Carr & Maler, 1986); this stimuli was attempted on five fish and with five attempts per fish and the lack of any response suggests that DD cells do not respond to ampullary receptor stimulation.

Although the stimulus (electrosensory or acoustic) induced firing response was always restricted to the 1-20 minute temporal range, it should be noted that not every neuron responded to every stimulus presentation. We observed instances where a neuron would not respond to the first presentation of a stimulus but would respond to a subsequent electrosensory signal, be it the identical stimulus or one with a different beat frequency (N = 8). While most cells which responded to a first presentation remained silent during subsequent stimulation (N = 11), a few neurons (N = 7) responded to both an initial and a subsequent stimulus presentation. The second response occurred with the same latency as the first but was typically diminished with respect to the number of spikes fired (Figure 1B,C).

To increase confidence that the spiking responses were indeed being induced by the applied stimulus, we generated histograms of the latencies to the first observed spike from the onset of stimulus presentation and, for comparison, from the beginning of recording. The

resulting distributions are shown in Figure 2 for our initial, short baseline electrosensory stimulus, recordings (A), longer baseline electrosensory stimulus recordings (B), acoustic stimulus recordings (C), and the pooled data of all three groups (D). If DD cell discharge were spontaneous and random, then the response latency would be independent of stimulus onset and we would expect that the histograms on the left and right (Fig. 2D) would be similar. In this case we would see first spikes occurring both before stimulus onset and throughout the length of recording. However, when measured relative to stimulus onset, we do not see any first spikes with either time < 0 s (preceding stimulus onset) or with time > 1500 s. When measured relative to the commencement of recording however, the latencies are arbitrarily spread out and not clearly related to the reference time (Fig. 2B,C,D) and we do see first spikes occurring >3000 s in the recording. In order to better quantify these impressions we fit normal distributions to the pooled histograms of latency to stimulus onset and latency to recording onset. We compared the goodness of fit (Chi-square test) of the normal distribution for each pooled set. For the histogram of latencies from the beginning of recording (Fig. 2D right) the null hypothesis that the data was normally distributed was rejected ($p = 0.04$). For the histogram of latencies from stimulus onset (Fig. 2D left; fit: red line), the null hypothesis could not be rejected ($p = 0.48$). We conclude that the stimulus does alter the time of spike occurrence and therefore does indeed influence DDi cell spiking.

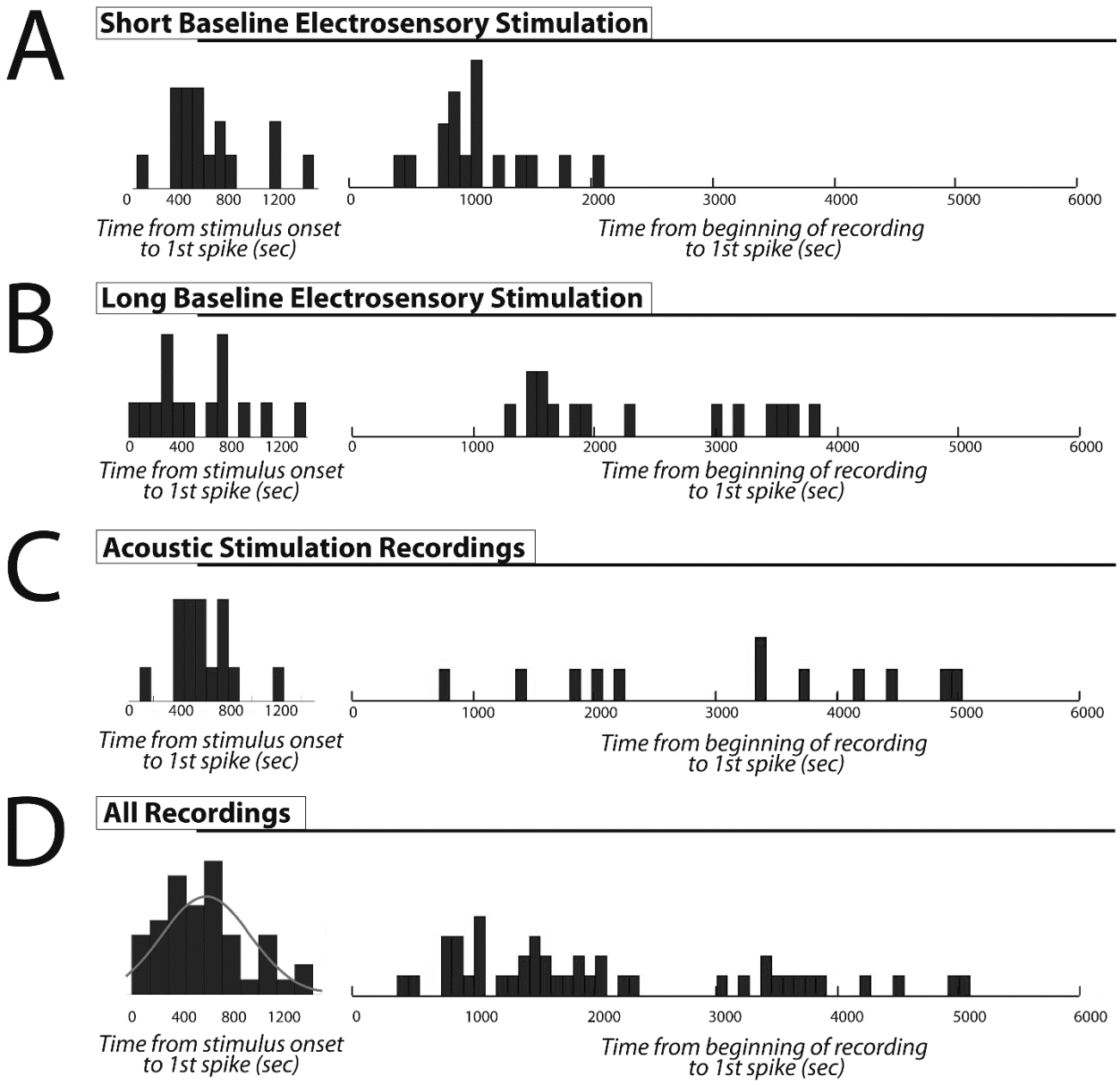

Figure 2-2: Response Onset Latency

This figure displays histograms of the latency to first spike generated from the extracellular recordings shown in Figure 1. For each category, the distribution on the left shows latency to first spike relative to the onset of stimulus presentation. The distribution on the right shows the latency to first spike relative to beginning of recording (including any recorded pre-stimulus baseline). Bin widths are 90 s. **(A)** Short Baseline Electrosensory Stimulation. The pre-stimulus baseline varied very little and we see similar, though slightly time-shifted distribution for both choices of the time point for latency measurements. **(B)** Long varied pre-stimulus baseline lengths. Here we found that the distributions based on the beginning of the recording becoming more flat and arbitrary. **(C)** Acoustic stimulation. A similar result is seen with acoustic stimulation

(D) Histogram of pooled data from all recordings. The left histogram show that the latency to first spike mostly occurs within 800 s and is loosely associated with the stimulus onset; the gray line is the Gaussian density fit to the histogram. The right histogram clearly shows that there is no preferred latency range to recording onset. The longer latencies (>3000 s) in this histogram are the ones with long and variable pre-stimulus baselines. These cases make clear that these cells did not discharge spontaneously.

We next performed *in-vivo* whole-cell recordings of DDi/DDmg neurons in order to investigate the cellular basis of their apparent stimulus induced spiking response. DD neurons' resting membrane potential during Down state baseline recordings was -70.8±6.0 mV. Similar to extra-cellular recordings, spontaneous spiking was never observed pre-stimulus. Although we did not observe spontaneous spiking, we were able to induce spiking by positive current injection. Induced spike heights measured 61.6±14.9 mV with half widths of 3.2±0.9 ms (N = 7). Hyperpolarizing after potentials (AHP) measured 4.9±2.0 mV. Spike rates driven by current injection showed rapid adaptation, beginning with doublets or triplets reaching instantaneous rates up to 77 Hz and then rapidly slowing to rates of up to 15 Hz. Overall rate was largely dependent on the magnitude of current injection with rates seen as slow as 1.4 Hz with depolarizations just above spike threshold. We estimated action potential thresholds in six cells where we had both current-evoked spiking as well as spiking during Up states. Positive current injections evoked spiking at -45.3± 5.8 mV while Up state spikes had a threshold of -49.9±2.4 mV. These values were not significantly different ($p = 0.5581$, paired t-test).

We again used the same stimulus protocol with acoustic or electrosensory signals. Note that in whole-cell recordings pre-stimulus baseline (344.5±123.5 s) was abbreviated to reduce cell washout. Stimulus presentation (N = 13) induced a strong depolarizing response (Up state) after a variable delay period (555.8±335.6 s, N = 13) and with a variable duration (201.5±332.6 s; range:

1.5 to 1023 s; N = 13) and spike rate (mean = 2.1±0.9 Hz, peak = 19.8±24.2 Hz, N = 13; number of spikes: 1-1099; peak instantaneous firing rate: 2.5-62.1Hz); again, the response could occur during (N = 6) or between (N = 7) stimulus presentations.

The dynamics of Up state onset and termination were highly variable (see Fig. 3). The response consisted of a rapid (t_{rise} = 15.8±24.6 s, range: 0.08 to 78.2 s; N = 13) shift in membrane potential from -70.8±6.0 mV to a significantly more depolarized level, -44.6±8.0 mV, for a net shift of V_m Shift = 26.8±5.6 mV, N = 13. The membrane potential was therefore bimodal with no overlap between Up and Down states. This period of sustained depolarization was followed by a typically longer relaxation (t_{fall} = 50.5±119.0 s; range: 0.35 to 417 s; N = 12,) back to the baseline potential; in 1 case the time course of relaxation was too variable to confidently set a start and end point so it was not considered. Occasionally the response would consist of multiple occurrences of such events (Fig. 3).

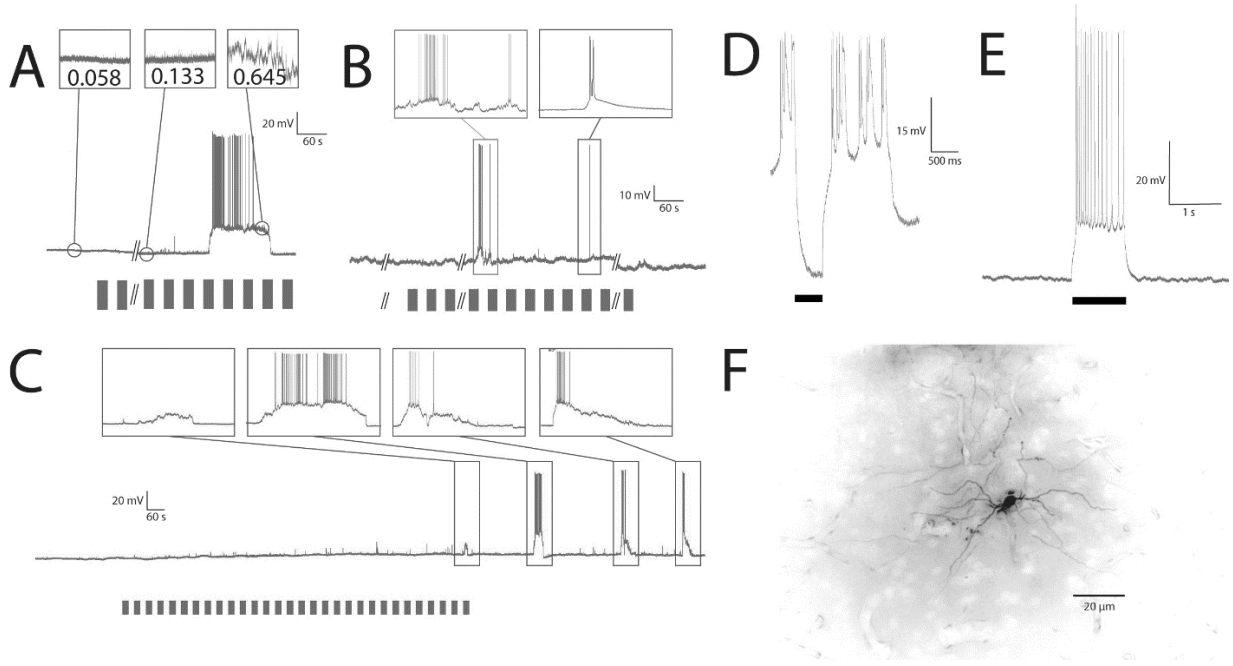

Figure 2-3: Up States

Bars below voltage traces represent stimulus presentations. (**A**) Induction of an Up state and variance measurements before, during, and following an Up state. (**B**) Examples of Up states showing the variety of Up states which we observed even within the same recording. The first of the two Up states indicated shows how variable the MP can be during an Up state, making it difficult to be certain if we are observing a single, highly variable state, or multiple states without an extended Down state separating them. (**C**) Example of a non-spiking Up state and of multiple Up states resulting from one stimulus set presentation. We observe here that a non-spiking Up state of smaller MP deviation is followed by a series of larger, spiking Up states. All appear to result from a single stimulus set presentation. This likely accounts for the clustered firing observed in extracellular recordings shown in Fig. 1. (**D**) Hyperpolarizing current injection (black bar) was able to repress Up state while applied, but not to arrest it following cessation. (**E**) Depolarizing current injection was able to produce firing (in the example shown we saw 14 spikes over 1 s depolarization), but not initiate persistent activity or Up state. (**F**) Cell filled with Lucifer yellow following intracellular recording. This cell can be identified as a DDi cell by its location and the orientation of its dendritic processes (Giassi, Harvey-Girard, et al., 2012).

The Up states were characterized by significantly increased membrane variance (Up state = 1.9±2.3 mV^2, pre-Up state = 0.5±1.0 mV^2, post-Up state = 0.5±1.0 mV^2, N = 8). In some cases (Fig. 3A, C) it appeared that membrane variance increased gradually following stimulation and in the 100s of seconds leading to the Up state. This provoked a more detailed analysis of all the recordings. We found that this effect was not consistent and there was no significant increasing trend in variance leading to an Up state. As no significant difference existed between pre-Up state and post-Up state values ($p = 0.9164$, Kruskal-Wallis test) they were pooled for the reminder of the analysis. Up-state variance was significantly different than the pooled non-Up-state variance ($p = 0.00002$, Kruskal-Wallis test). In most cases (N = 9), the depolarized state was associated with spike discharge, at rates similar to those seen with extracellular recordings. In the remaining responses (N = 4) only a single spike was produced. Although depolarized states

were associated with periods of spiking, the spiking could slow or cease altogether while the depolarization persisted (Fig. 3A); duration of the spiking response during an Up state was 3-710 s. The shape, duration, spike rate, and other characteristics of individual Up states were highly variable, even within the same recording (Fig. 3), but all represented clear and significant switches to a state of depolarization with dramatically increased propensity for spiking. In a few cases (N = 5), we observed smaller depolarizations (V_m Shift = 14.9±4.5mV; duration = 96.5±165.9 s) which did not evoke spiking (Figure 3C). We refer to these periods of stimulus-induced depolarization as Up states based on their clear resemblance to the Up states observed in some cortical neurons (Maclean et al., 2005; Lewis & O'Donnell, 2000). Other, smaller depolarizing events are also visible (Figure 3C). These were highly variable in size, shape, and duration and were not analyzed in detail. Although no spiking occurs outside of Up states or pre-stimulus, the membrane is still active with such small events.

Similarly to what was seen with extra-cellular spiking responses, we were not able to elicit an Up state response with a 5Hz ampullary receptor stimulus.

We wondered whether Up/Down state transitions might be triggered by strong depolarization or whether hyperpolarization could revert an Up to a Down state. We were not able to evoke Up states with intra-cellular current injection (N = 24, Figure 3E) even when sufficient current was injected to depolarize the cell membrane well beyond that reached in an Up state and sufficient to drive a strong spiking response for over 4 s; immediately upon cessation of current injection, the membrane returned to its quiescent hyperpolarized state. The kinetics of the neuron's responses to depolarizing pulses were not at all variable and vastly faster than

those associated with Up states: t_{rise} times were 0.22±0.10 and t_{fall} times were 0.16±0.09– these are two orders of magnitude smaller than those associated with Up states. We then investigated whether a hyperpolarizing current injection could pre-maturely revert an UP state to a Down state. We found (N = 5) that even the injection of a large (500 pA , 500 ms pulse) hyperpolarizing current was not able to return a cell to baseline quiescence once an Up state had been initiated. Spiking activity was suspended during application of the hyperpolarizing current, but resumed immediately following cessation of injection (Figure 3D).

DISCUSSION

Neurons in DDi/DDmg, although quiescent under rest conditions, can be induced to strong though transient depolarized states and spiking activity by naturalistic electrosensory or acoustic stimulation. These Up states are highly variable with respect to onset latency, spike rate, and duration, but always begin within a fixed delay window following stimulus presentation. However, response onset was not more likely to occur during versus between stimulus presentations. Further, the Up to Down state transition simply leads to the resting MP and is not associated with an obvious hyperpolarizing event. We conclude DDi cell Up states are not directly evoked or terminated by sensory input consistent with the lack of direct sensory input from PG.

The differences in the histograms of Fig. 2B-D demonstrate that the Up states do not occur spontaneously but are linked to the stimulus. We hypothesize that Up states are induced by complex and variable pallial network activity that intervenes between sensory input and DD

cells. Periods of spiking activity are associated with sustained increases in the mean and variance of membrane potential and resemble Up states seen in mammalian cortical cells.

Up states could neither be induced nor terminated by manipulations of the membrane potential. We therefore hypothesize that the observed Up states are not the result of intrinsic, voltage-gated bistability. We propose, rather, that Up states are directly the result of synaptic input from neurons in the DL recurrent network that have been induced to a maintained, though variable duration, state of reverbatory activity. This is further supported by two observations. First, the greatly increased membrane noise during Up states strongly suggests that there is greatly increased synaptic input to the DD cells. Secondly, the variable and often lengthy rise and decay times of Up states (compared to current evoked depolarizations) also strongly suggest that Up states are the result of network activity rather than intrinsic cell properties.

DL and DD form a feedback loop and both structures consist of intrinsic recurrent networks (Giassi, Ellis, & Maler, 2012) and this complex circuitry presumably underlies the variability of Up state induction and maintenance. Alternatively, it is therefore also possible that the Up states are caused by DD recurrent network activity that is first initiated by DL input, or even by some combination of DL and DD recurrent network activity.

Based on previous results (Harvey-Girard et al., 2010; Giassi, Ellis, & Maler, 2012) we further propose that Up state activity is an important factor in the consolidation of memories in the DD/DL/DC network. This conclusion is consistent with the importance of DD for trace conditioning in goldfish (Vargas, Lopez & Portavella, 2009). Interestingly, a recent study has shown that a similarly located and connected pallial region in zebrafish becomes active (Ca^{2+}

imaging) when stimulated 24 hours (but not 30 minutes) after the fish has undergone reinforcement learning (Aoki et al. 2013). The relation between the Up states we observed and the intracellular Ca^{2+} increases observed by these authors is not clear. Both results, as well our earlier data on learning-associated induction of Egr-1 expression, indicate that the activity of DD cells is not clearly and immediately linked to sensory input, but is modulated by such input over very long time scales. DD is the highest level of the gymnotiform brain in the sense that, unlike other pallial regions, it does not receive direct sensory input from PG, nor project to brainstem motor regions, e.g. tectum (Giassi, Duarte, et al., 2012; Giassi, Ellis, & Maler, 2012). Instead, DD interconnects various pallial and subpallial regions (Giassi, Ellis, & Maler, 2012) suggesting that its activity is indicative of cognitive processes. DD and the pallial regions with which it interconnects (Giassi, Ellis, & Maler, 2012) may therefore prove to be a useful model system for the study of the long time scale neural processes associated with cognition, learning and memory formation.

Chapter 3

HIPPOCAMPAL-LIKE CIRCUITRY IN THE PALLIUM OF AN ELECTRIC FISH: POSSIBLE SUBSTRATES FOR RECURSIVE PATTERN SEPARATION AND COMPLETION

S. B. Elliott, E. Harvey-Girard, A. C. Giassi, L. Maler

Manuscript in Press
The Journal of Comparative Neurology

CONTRIBUTION OF CO-AUTHORS

S. Benjamin Elliott: Performed all in-vivo experiments. Analyzed all connectivity data and connected in-vivo to in-vitro results. Wrote the manuscript and prepared figures.

Erik Harvey-Girard: Performed in-situ, and in-vitro experiments, and numerical analysis, prepared figures, and contributed to writing of the manuscript.

Ana C. C. Giassi: Contributed to analysis and interpretation of tracer results, advised on technical issues, and contributed previously published material which formed the context of the discussion and conclusions of this paper.

Len Maler: Contributed to the analysis and interpretation of tracer results, and contributed significantly to the interpretation of the results presented in the discussion of this paper and to the writing of the manuscript.

ACKNOWLEDGEMENTS:

This work was supported by the Canadian Institutes for Health Research Grants #6027 and #49510. We would like to thank William Ellis for assistance with the histology. We would like to thank Avner Wallach for helpful discussions. LM would like to thank Harvey Karten for pointing out the importance of the Prox1 gene as a possible marker of dentate gyrus granule cells and for detailed and very informative discussions on homology of brain nuclei that guided the formulation of our Discussion.

ABSTRACT

Teleost fish are capable of complex behaviours including social and spatial learning; lesion studies show that these abilities require dorsal telencephalon (pallium). The teleost telencephalon has subpallial and pallial components. The subpallium is well described and highly conserved. In contrast, the teleost pallium is not well understood and its relation to that of other vertebrates remains controversial. Here we analyze the connectivity of the subdivisions of dorsal pallium (DD) of an electric gymnotiform fish, *Apteronotus leptorhynchus*: superficial (DDs), intermediate (DDi) and magnocellular (DDmg) components. The major pathways are recursive: the dorsolateral pallium (DL) projects strongly to DDi with lesser inputs to DDs and DDmg. DDi in turn projects strongly to DDmg which then feeds back diffusely to DL. Our quantitative analysis of DDi connectivity demonstrates that it is a global recurrent network. In addition, we show that the DD subnuclei have complex reciprocal connections with subpallial regions. Specifically, both DDi and DDmg are reciprocally connected to pallial interneurons within the misnamed rostral

entopeduncular nucleus (Er). Based on DD connectivity, we illustrate the close similarity, and possible homology, between hippocampal and DD/DL circuitry. We hypothesize that DD/DL circuitry can implement the same pattern separation and completion computations ascribed to the hippocampal dentate gyrus and CA3 fields. We further contend that the DL to DDi to DDmg to DL feedback loop makes the pattern separation/completion operations recursive. We discuss our results with respect to recent studies on fear avoidance conditioning in zebrafish and attention and spatial learning in a pulse gymnotiform fish.

INTRODUCTION

Early comparative studies hypothesized that the six-layered mammalian cortex was essential for learning and adaptive cognitive functions while the non-layered telencephalon of birds, reptiles and fish could only support stereotyped instinctive behavior. This view has long since been discredited for birds (Clayton et al., 2003; Gentner et al., 2006; Jeanne et al., 2011; Blaser et al., 2013; Clayton, 2015; Roth, 2015). More recently, many behavioral studies have clearly demonstrated that teleost fish, including weakly electric fish, are also capable of very sophisticated behavior and learning (Graff et al., 2004; Siebeck et al., 2009; Sovrano and Bisazza, 2009; von der Emde et al., 2010; Darmaillacq et al., 2011; Schluessel et al., 2012; Bshary and Brown, 2014; Bshary et al., 2014). In some instances, these capabilities can be attributed to the dorsal telencephalon (pallium). In particular, spatial and emotional learning have been clearly associated with specific pallial subdivisions (Broglio et al., 2005), and there is also anatomical differentiation related to the type of conditioning procedure, i.e. delay versus trace conditioning (Vargas et al., 2009). The association of specific forms of learning with particular pallial subdivisions has naturally led to the hypothesis that these subdivisions are homologous to the mammalian pallial regions associated with equivalent forms of learning. There is, however, very little detailed knowledge of the structure of the teleost pallium. This deficiency is further exacerbated by the enormous variability in the structure of the telencephalon of different teleost species.

The teleost telencephalon is generally recognized to be composed of pallial and subpallial divisions. The organization of the subpallium is now reasonably well understood and strong evidence for homology of teleost and amniote subpallial subdivisions have been presented (Ganz

et al., 2012; Harvey-Girard et al., 2013); even here, however, there still remain important discrepancies in the literature that we attempt to clarify (see Discussion). The teleost pallium is thought to be composed of dorso-lateral (DL), dorso-medial (DM), dorsal-posterior (DP), dorso-central (DC) and dorsal-dorsal (DD) subdivisions (Giassi et al., 2012d). The putative developmental trajectory that results in the adult teleost pallium - eversion, rotation, and differential growth patterns (Yamamoto et al., 2007; Folgueira et al., 2012) - is so different from that of the mammalian pallium that direct comparisons are difficult. Instead, behavior and the expression of a small number of genes are often used to infer homology despite the lack of direct fate mapping data or accurate knowledge of connectivity. This is most evident for the DD subdivision. The appearance of the putative DD varies across teleosts and even its existence as separate from DC has been questioned (Mueller et al., 2011). Our earlier studies clearly showed that DD was a very distinct component of the gymnotiform pallium (Giassi et al., 2012b; Giassi et al., 2012d). In this paper, we analyze the connectivity of the gymnotiform DD in great detail. This allows us to suggest a very direct homology to a similarly situated region in the goldfish, cichlid and zebrafish pallium and some unexpected potential homologies to mammalian hippocampus. These putative homologies, in turn, directly lead to new hypotheses as to the function of both DD and DL, in particular in spatial learning and memory.

MATERIALS AND METHODS

Apteronotus leptorhynchus fish were kept at 28°C in community tanks. Before tracer injection or other processing, fish were deeply anesthetized with 0.2% 3-aminobenzoic ethyl ester (MS-222; Sigma-Aldrich, RRID: SCR_008988) in water just before surgery or tissue

preparation. All procedures were approved by the University of Ottawa Animal Care and follow guidelines established by the Society for Neuroscience.

NORMAL MATERIAL.

Paraffin sections in the transverse and parasagittal plane were available from standard Nissl stained series prepared (Harvey-Girard and Maler, 2013) and photographed as previously described (Trinh et al., 2015). Sections were 10 µm thick.

***IN VIVO* TRACER INJECTION.**

The number of fish used in *in vivo* experiments was thirteen.

This protocol was adapted from Giassi et al. (2012a; 2012b). Anesthetized fish were transferred to a holder with a breathing tube providing oxygenated water containing MS-222. The bone over DD was removed. Neurobiotin (2%, Vector Labs, RRID: SCR_000821) in 0.1 M Potassium Methylsulphate, or Dextran-Tetramethylrhodamine (BDA, Mini-Ruby or Alexa-647) 10,000 MW (Life Technologies, RRID: SCR_008817) in 0.1 M PBS pH 7.2, was injected by iontophoresis using a glass pipette, broken back to provide a 5 µm or 10 µm diameter tip respectively, attached to a DC current source (Midgard CS3 High Voltage Precision Current Source). A 4-5 µA current was applied for 4-18 sec. Electrode tip was positioned using a micropositioner (David Kopf Instruments model 2662). A cap was placed over the skull and oxygenated water was substituted for that containing MS-222 until the fish revived from anesthesia. Survival times from 4-24 h proved sufficient for tracing pathways entirely confined to the telencephalon, based on a few longer survival times.

Fish were deeply anesthetized, packed in ice and perfused with 4% paraformaldehyde, 0.1% glutaraldehyde, and 0.2% picric acid in 0.1M PBS pH 7.4. The brains were removed, placed in 4% paraformaldehyde, 0.2% picric acid and 15% sucrose in 0.1M PBS pH 7.4 and stored at 4°C until brains sunk in the solution indicating that the sucrose had permeated the tissue. Fixed brains were cryoprotected in 30% sucrose in PBS, sectioned (25 µm transverse cryostat sections) and the sections mounted on Superfrost slides (Fisher Scientific, RRID: SCR_008452). Slide-affixed sections were incubated with 3% Triton-X and 0.1M PBS for 3 hrs at room temperature. Neurobiotin injected sections were incubated in streptavidin Cy3 1:100 in 1% normal goat serum, 1% BSA, 0.3% Triton-X and PBS for 48 hrs at 4°C. All sections were counterstained with green fluorescent Nissl reagent 1:300 (Molecular Probes, NeuroTrace® 500/525 green-fluorescent Nissl Stain #N21480, RRID: SCR_013318) in PBS for 20 minutes at room temperature.

Sections were visualized on a Zeiss AxioObserver.Z1 Microscope with an X-Cite lamp, using A-Plan 0.25 Ph1 objectives, or using an upright Zeiss LSM 510/AxioImager M1 Confocal Microscope using a HeNe laser. Microscope control and image capture was accomplished using Axiovision software (Zeiss) or Zen software (Zeiss) on a Windows 7 PC.

Both neurobiotin and BDA were used for *in-vivo* tracer injections. Neurobiotin yielded better labeling and had better transport rates over short distances. However, over longer survival times it is known to metabolize quickly (Lanciego et al., 2011) and was replaced with BDA for injections with longer survival times. 10,000 MW BDA was selected over the more quickly moving 3,000 MW as it has more flurofore binding sites and therefore provides stronger fluorescence. Reiner et al. (2000) also suggest the labeling with 10,000 MW BDA was superior to that with a

3,000 MW. This was thought desirable given that the volume of our injections was extremely restricted by the size of the target regions. Transport rates for 10,000 MW BDA were measured by Fritzsch (1993) in tadpoles at 22 °C to be 1 mm/h. Other references cite differing values, but most of these measurements were taken uniquely in rodents (eg. Reiner et al, 2000) and the estimation methodology is not always clear. Both Fritzsh's measured rates and his conditions corresponded more closely with what we saw in our injections. Our own preliminary measurements suggested that cells 200 µm from the injection site were filled after 15-30 mins.

IN VITRO TRACER INJECTION.

In vitro experiments allowed better control of the precise location of an injection site into small structures (e.g. DDmg). There was also better control of the injection volume since injections of fluorescent tracers were terminated under direct visual control. Finally, initial measurements of distance between injection site and labeled cells were easy to determine by direct observation.

The number of fish used in *in vitro* experiments was eight.

Slice preparation. We followed the protocol previously described (Trinh et al., 2015). Anesthetized fish were quickly installed on a dissection rig, a breathing tube providing oxygenated water containing MS-222. Ice-cold oxygenated (95% O_2 and 5% CO_2) artificial CSF (aCSF) solution was continuously dripped on the brain as the skull was opened and the telencephalon separated from the diencephalon. The telencephalon was removed and transferred to a plate containing ice-cold oxygenated aCSF solution. This aCSF solution had the

following composition (in mM): 130 NaCl, 3 KCl, 0.75 KH_2PO_4, 2 $CaCl_2$, 4.5 $MgSO_4$, 24 $NaHCO_3$, 10 D-glucose (Sigma-Aldrich, RRID: SCR_008988).

For slices through the longitudinal DD plane, the meninges and chorioid tela were removed and the dorsal pallium split to slightly separate the two pallium hemispheres. In the *Apteronotus* telencephalon, DD has a nearly vertical orientation in the transverse plane along a medio-rostral to latero-caudal axis. To extract DD from the rest of the telencephalon, most of the lateral division of dorsal telencephalon (DL) was removed by cutting a 400-500 µm thick DL slab in the vertical plane following the expected lateral edge of DD (Maler et al., 1991). The true longitudinal DD slices were made by cutting the telencephalon 600 µm more medially at the same angle. This DD slice preparation contained most of DD including DDs (superficial division), DDi (intermediate division) and DDmg (Giassi et al., 2012c).

The slice was then transferred to the recording chamber, perfused with oxygenated aCSF and incubated 15 minutes for recovery at room temperature. Dextran-conjugated fluorescent dyes, Dextran-Tetramethylrhodamine (Mini-Ruby) and Dextran-Alexa Fluor 647, 10 000MW (Life Technologies, RRID: SCR_008817) were injected by iontophoresis in DDs, DDi, or DDmg (true longitudinal DD slice) using a glass electrode connected to a direct current stimulation unit which was driven by a TTL pulse delivered by a Digidata 1440A controlled by a Multiclamp 200B (Molecular Devices) and pClamp 10.3 on a Windows 7 PC. The stimulation unit generated five to ten 400 msec pulses of -92.8V via an 11±2M□ electrode (I= -8.3±1.2 µA) to deliver the dextran-conjugated fluorescent dyes. The electrode tip was positioned using a micromanipulator (Scientifica, UK) and injections were monitored visually. Injections were made 200-300 µm deep

in the slice. Slices were then incubated overnight at room temperature with continuous perfusion of oxygenated aCSF to allow retrograde and anterograde transport of the neurotracers. Finally, they were transferred in 4% paraformaldehyde in 0.1 M PBS pH=7.2 for fixation and stored at 4°C.

The slices were rendered transparent using the SeeDB procedure (Ke et al., 2013). In brief, slices were incubated in ascending concentrations of fructose (20, 40, 60, 80% w/v for half a day; and 100 and 115% w/v for a day) in 0.01 M PBS pH=7.2 containing 0.5% □-thioglycerol. The slices were imaged immediately after the 5-day tissue clearing procedure using an upright Zeiss LSM 510/AxioImager M1 Confocal Microscope using 543 nm and 633 nm HeNe lasers depending on the fluorophore used during injections. Z-stacks were imaged using a 10x Plan-NeoFluar 0.3 Ph1 objectives with a working distance of 550 µm (Zeiss) controlled by Zen software (Zeiss) on a Windows 7 PC. We were unable to use a higher power objective due to the thickness of our slices and, because of this, there is some pixelization in some of the magnified images we present. This does not, however, detract from identification of fluorescently labeled cells and fibers. Image maximum intensity was carefully adjusted during data acquisition (confocal microscope) to ensure a full range for resolving labeling intensity; as a result, labeled cell intensity was normalized to a maximum of 255 for each injection allowing us to pool data from different injection sets. This is an 8 bit scale with 256 values (0 to 255) and with arbitrary units since we normalized over injections with differing absolute intensities.

Data analysis for volume and distances was made using the 3D imaging software Imaris (Bitplane). Data binning and curve fitting were determined using Igor Pro 6.37 (WaveMetrics). All

error values are expressed in standard deviation. Graphs were initially made in Excel and incorporated into Figures using Adobe Illustrator.

Quantitative analysis of connection probability in DDi was done as previously described (Trinh et al., 2015) except that we now used spherical shells around the injection site. We divided the images into multiple spherical shells around the injection site. The volume around the injection site was divided into an initial shell which had a radius of 10 µm and subsequent shells had an increasing radius by steps of 10 µm until all the labeled cells were incorporated into a shell. We then calculated the total number of cells found within the volume of each hollow sphere formed by the shells. The connectivity probability is found by dividing the total number of labeled cells in a shell by the number of cells estimated in the shell from our previous cell density estimates (Trinh et al., 2015). There is a serious and unavoidable artifact when using this procedure for radii > ~250 µm. DDi is a much smaller structure than DL and we cannot be certain that, for some of our injections, larger radii did not incorporate adjacent structures, e.g. DDs, DDmg or even DL or DM. In this case, the denominator (volume) would have been overestimated and the connection probability for distances > ~250 µm was therefore underestimated. We could not calculate an error bound since it was not possible to accurately estimate the amount of infringement of the shells into non-DDi structures.

THE NATURE OF THE LABELED ELEMENTS IN OUR TRACER EXPERIMENTS

The *A. leptorhynchus* telencephalon is a small structure (<2 mm in width) and all the tracers we used resulted in both strong anterograde and retrograde labeling across different regions after less than 24 hours survival times; we used survival times ranging from 4 to 24 hours but, for similar injection sites, found no differences in the amount or intensity of the staining with

any of our tracers. This is abundantly illustrated in Figures 8 to 13. For example, Figure 12D shows uniquely anterograde staining within DL from an injection in DDmg with a survival time of 7 hrs. Figure 13A shows anterograde staining in DM2v following injection in DDi with a survival time of 7 hrs. Figure 12B shows retrograde staining within DL from an injection in DDi with a survival time of 24 hrs. Figure 10B shows some anterograde staining, but also retrograde labeling in two cells with a survival time of 7 hrs.

When we analyze the connectivity within the DD subdivisions, the question arises as to whether the neuronal somata are labeled via retrograde transport or direct uptake into their dendrites. Here we present the three reasons we believe we are analyzing predominantly true retrograde transport at least at distances greater than 30 µm from an injection site.

In our experience, retrograde transport and dendritic uptake produce very different patterns of neuron labeling. This is well illustrated in a study of the electrosensory hindbrain of *A. leptorhynchus* (Maler and Mugnaini, 1994). Figure 12A of this paper illustrates strictly retrograde transport (a commissural connection): the somata and, in some cases, a small length of proximal dendrite, are labeled. Figure 12B illustrates the deliberate injection into a small part of the dendritic trees of neurons (same structure as in Fig. 12 A): this results in extensive filling of the entire dendritic arborisation, including very fine branches. This differential effect of retrograde vs dendritic filling has been seen after numerous injections of low-level electrosensory structures (LM, unpub. obs.).

We clearly illustrate the same distinction in our material. Injections of two fluorescent tracers were made, separated by 70 µm (Fig. 7A). Figure 7B shows a section between the two

sites: 20 µm from one injection site (BDA, mini-ruby: magenta), and 70 µm from the other (BDA, Alexa-647: blue). We see cells labeled from both injections. The cell labeled from the more distant injection shows strong labeling (cyan) restricted to the soma. In contrast, cells labeled by the closer injection show both somatic labeling and extensive labeling of dendritic arborisations but only for cells close to the injection site. The injection site is located to the bottom left and the injection edge is marked with an '*'. Small white arrows mark cells showing clear evidence of dendritic filling; the dendritic arborization is stained with almost the same intensity as the soma and for some distance extending from the cell. Numerous labeled dendrites are seen between the two cells indicated. The majority of cells with labeled dendrites lie within our 30 µm exclusion zone and so would not be used for quantitative analyses. In contrast, the intensely labeled blue cell (top right corner) which was labeled by the other injection (~70 µm away) shows no dendritic filling; we interpret this label as due to retrograde transport from axons terminals.

The appearance of the labeled cells in DDs (Fig. 3), DDmg (Fig. 4) and DDi (Figs. 5, 7) is therefore consistent with retrograde transport and not with filling via dendritic uptake. In all these cases, anterograde filling of fine preterminal axons and boutons is also observed.

Dendritic uptake would be expected to preferentially label neurons closest to the injection site because their dendrites would be more likely to strongly intrude onto the injection site. We would not expect to see unlabeled neurons intervening between the injection site and labeled neurons. The latter result is, however, what we commonly observe (e.g. Fig. 3). This is especially salient in the DDmg injection (Fig. 4) where two unlabeled cells (indicated by small white arrows) intervene between the site of injection and a more distal, labeled cell;

anterogradely labeled boutons are in close proximity to the unlabeled cells demonstrating that the cells at the injection site project to these cells, but do not receive input from them.

This argument can be made more precise and rigorous with respect to Figure 5B. First, imagine a sphere centered at the injection center and with a radius that encompasses the two strongly labeled cells ("s"). This sphere has a volume of 4.19 x 10^6 μm^3. We exclude a spherical volume with radius of 30 µm also centered at the injection site, leaving a volume of 4.08 x 10^6 μm^3 in the remaining shell. Based on the DDi cell density estimates of Trinh et al (2015), we would expect approximately 856 cells in this volume. Instead, we count 17 stained cells (~2%), a far lower number than expected; the majority of the labeled cells >30 µm from the injection site edge lack the dendritic filling that we believe is characteristic of dendritic uptake of tracer. To be certain that no stained cells were obscured by the fluorescence of the injection itself, this count was confirmed by direct observation of the entire confocal stack (not shown). The more numerous unlabeled cells between the injection site and the strong cells should have dendrites that intrude more strongly on the injection site than these labeled ("s") cells and yet are not labeled. Further, we note that a weakly labeled cell ("w") is seen between the lower "s" cell and the injection site; this cell is closer to the injection site; again, this cell might be more likely to have dendrites within the injection site and yet is far less strongly labeled than its more distant neighbour.

This, of course, is true for all the cases we used for analysis given the low probability of encountering labeled cells at all distances from the injection site > than the 30 µm exclusion zone. We conclude that these results strongly support our contention that the vast majority of locally

labeled neurons in DDs, DDmg and DDi (>30 µm from the injection site) represent true retrograde labeling and not labeling via dendritic filling.

GABA IMMUNOHISTOCHEMISTRY.

Immunohistochemical localization of GABA utilized sections from a previous publication (Giassi et al., 2012c). Briefly, fish were perfused and then post-fixed using 4% paraformaldehyde, 0.5% glutaraldehyde, and 1% metabisulphite in 0.1 M PB (pH 7.4), then cryoprotected in 4% paraformaldehyde, 30% sucrose 1% sodium metabisulphite, and 0.01% thimerasol at 4°C. After cutting on a cryostat, sections were processed using a tyramide signal amplification kit (TSA, Invitrogen/Molecular Probes, Carlesbad, CA; RRID: SCR_008410) and pre-incubated in 80% methanol and 0.6% H_2O_2 in 0.9% saline and incubated in 1% blocking solution (TSA kit) in 0.9% saline. After washing, sections were incubated in horseradish peroxidase-conjugated goat anti-rabbit IgG (1:2000) in 1% blocking solution (TSA kit), and then in Alexa fluor 488-conjugated tyramide (1:1000) and 0.0015% H_2O_2 in amplification buffer (TSA kit) and counter-stained with red fluorescent Nissl reagent (Molecular Probes, #N-21482, RRID: SCR_013318; 1:3000) in saline. The antibody used was Immunostar (RRID: SCR_013473), rabbit polyclonal, #20094 (Immunostar acquired DiaSorin, formerly known as IncStar)

CLONING AND *IN SITU* HYBRIDIZATION OF *APTERONOTUS* CONNEXIN 35.

An *A. leptorhynchus* adult fish was anesthetized with water containing tricaine methanesulfonate (Finquel, Redmond, WA) and sacrified. Its brain was quickly removed and homogenized in Trizol (Sigma-Aldrich, RRID: SCR_008988) to purify total RNA. First-strand cDNAs

were synthetized using the RevertAid H Minus First Strand cDNA Synthesis Kit (Thermos). A PCR was performed using the DreamTaq Green Polymerase Kit (Thermos) and degenerate forward (5'-ATG GGN GAY TGG ACN ATC CT-3': MGEWTIL) and reverse (5'-C ACT NGA CTG NGT NCG NCC C -3': GRTQSS) primers. The 899 bp long PCR product was inserted in the pGemT-easy vector (Promega, Madison, WI, RRID: SCR_006724). Eight plasmid DNA clones were purified with the PureYield DNA purification kit (Promega, RRID: SCR_006724) and digested with Nde I and Sac II for verification. Three clones were sent out for sequencing to the University of Ottawa core sequencing facility (CAREG).

We deduced the putative protein sequence from the AptCx35 cDNA PCR product and connexin amino acid sequences of other vertebrates obtained from GenBank (Bethesda, MD) using the Clustal W method in the software Jellyfish (Labvelocity, Lewisburg, PA). The sequences were resampled by bootstrapping 1,000 times in SEQBOOT of Phylogeny Inference Package (PHYLIP; Felsenstein, 1989; RRID:SCR_006244). Calculations of phylogenetic distances using the maximum likelihood estimates based on the Dayhoff PAM matrix were performed in the PROTDIST. The tree was determined by the UPGMA method using the NEIGHBOR program. A consensus tree was determined in CONSENSE: values on top of each branch show its level of confidence.

AptCx35 cDNA clone was linearized by digesting with restriction endonucleases PspOM I (antisense probe) and Spe I (sense probe). The nucleotide sequence corresponding to the entire amino acid sequence of AptCx35 (Fig. 14, A) was used to make the probe. Then, digoxigenin (DIG)-labeled RNA probes were synthetized using the DIG RNA Labeling Kit (Sp6/T7; Roche Applied

Science, RRID: SCR_001326) as recommended by the manufacturer. RNA probes were ethanol-precipitated and conserved at -80°C.

In brief, we performed *in situ* hybridization on five adult fish brains as previously described (Harvey-Girard et al., 2007; 2012; 2013). Preincubation and hybridization were performed at 60°C. After hybridization slides were washed with gentle agitation twice in 2x SSC (NaCl and Na citrate solution) for 10 minutes, twice in 1x SSC containing 50% formamide for 20 minutes, and twice in 0.2x SSC for 20 minutes at 60°C.

After immunodetection, all images of *in situ* hybridization labeling were photographed on a Zeiss AxioObserver.Z1 Microscope with an X-Cite lamp, using A-Plan 0.25 Ph1 objectives controlled by the Axiovision software (Zeiss).

RESULTS

CYTOARCHITECTURE

The teleost telencephalon, as in all vertebrates, is divided into dorsal (pallium) and ventral (subpallium) telencephalon. As previously described (Giassi et al., 2012c), the gymnotiform pallium is readily segmented into the five classic teleost pallial subdivisions: dorsolateral (DL), dorsocentral (DC), dorsodorsal (DD), dorsomedial (DM), and dorsoposterior (DP) pallium (Fig. 1, Fig.2 A, C, E). DD spans the central third of the dorsal pallium (rostro-caudal) (Fig. 1 A-D) and is located from 300 µm to 900 µm lateral to the midline along its dorsal surface (Fig. 2 A-B). This region sits wedged between DL on its lateral side and DM on its medial side; a small sulcus also marks the boundary between DD and DM. DD forms a wedge into the deeper DC. The cytoarchitectonics of DL, DC and DM that differentiate them from DD have been previously

described (Giassi et al., 2012d). These differences are even more apparent in the thinner paraffin sections and better microscopy used in this study. Cells in DD are mostly larger and more loosely packed than those in DL (Figs. 1, 2) and DM (Fig. 2). Differentiation of DD from DC is accomplished by means of the sparser distribution of larger cells in DC (Figs. 1, 2).

We previously divided DD into superficial (DDs), intermediate (DDi) and magnocellular (DDmg) regions but noted that the boundary between DDi and DDs was difficult to discern (Giassi et al., 2012c). In our new Nissl stained thin paraffin sections the demarcation between all three subdivisions is very apparent (Figs. 1, 2). DDmg is oriented so as to tilt both lateral and caudal from its dorsal to ventral aspect (Figs. 1A-B; 2C-D). Rostrally, DDmg is only separated from the pallial surface by a thin layer of DDs cells (Figs. 1A-B; 2C-D). Caudally, DDmg moves laterally as it extends ventrally, passing under DL and its caudal subdivision, DLc (Figs. 1A-B; 2C-D) (Trinh et al., 2015). DDi effectively surrounds DDmg so that a few DDi cells separate DDmg from the overlying DL and DLc. Rostrally, DDi replaces DDmg and is still overlain by DDs. DDmg, as previously described (Giassi et al., 2012c), consists of large, densely packed neurons, interspersed with smaller interneurons (Figs. 1A-B; 2C-D).

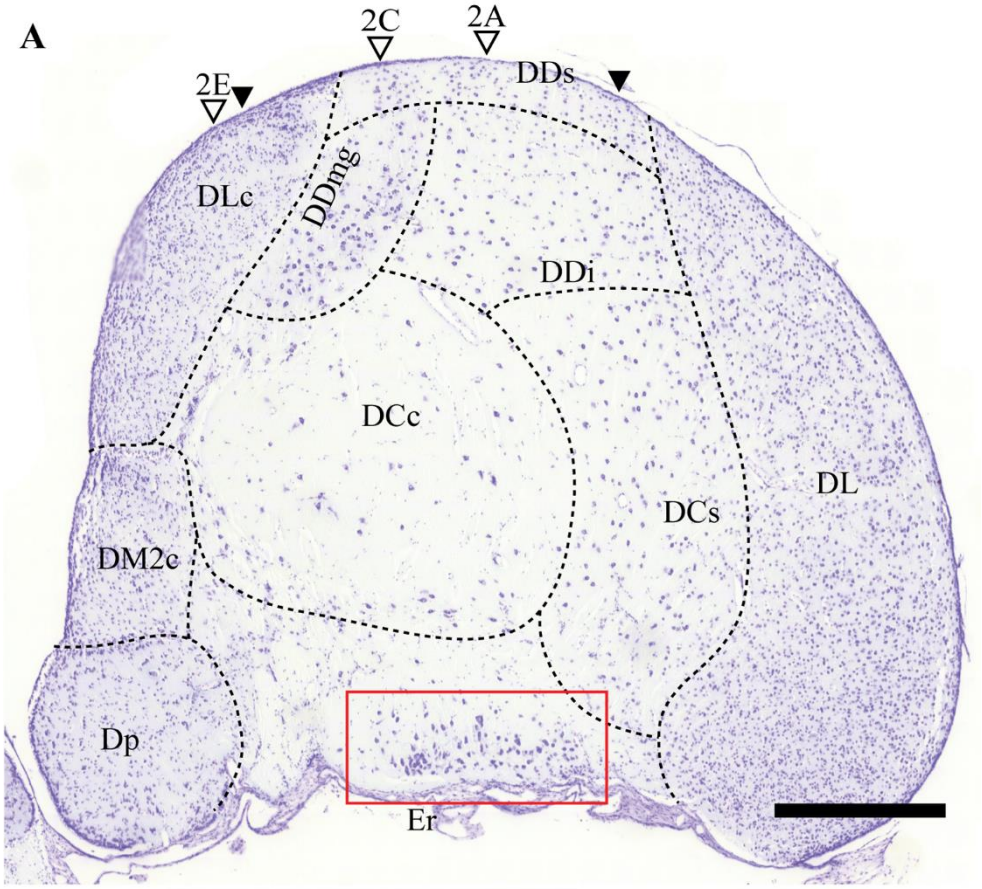
A
2C
2A
2E
DDs
DLc
DDmg
DDi
DCc
DL
DCs
DM2c
Dp
Er

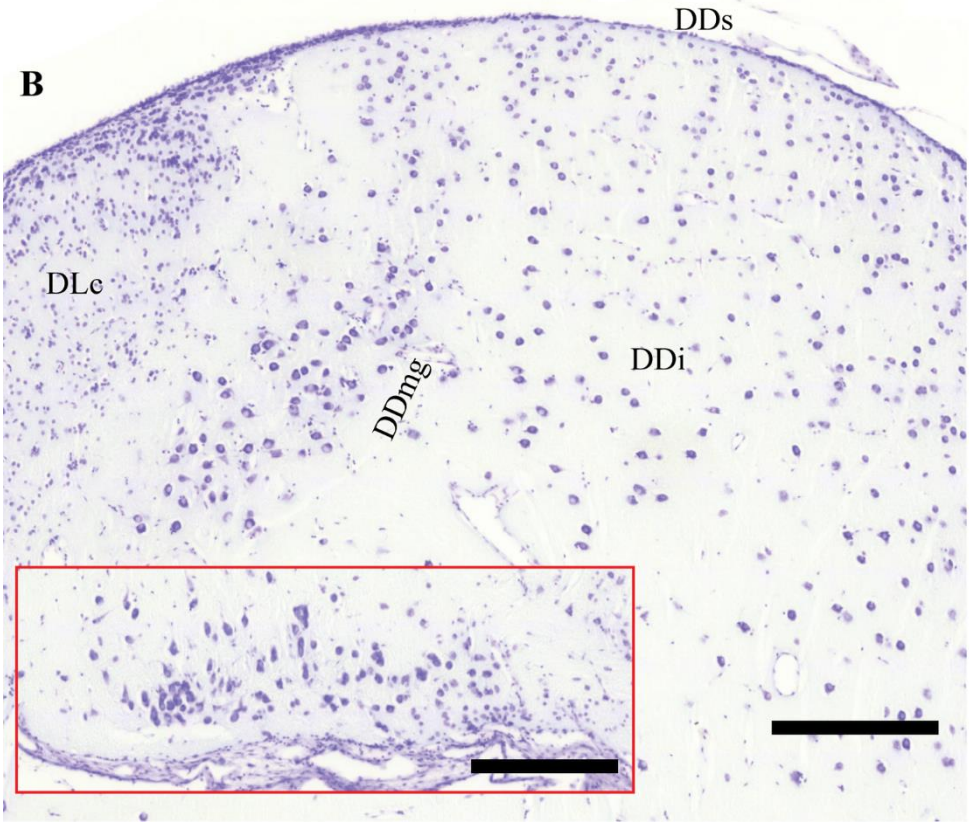
B
DDs
DLc
DDi
DDmg

Figure 3-1: Telencephalic anatomy in the sagittal plane

A: Cresyl-violet stained parasagittal section cut roughly midway (approx. 850 µm from midline) through one lobe of the telencephalon showing relative locations of pallial and subpallial structures. Black arrows indicate the boundaries of the higher magnification panel B. Bounding box indicates the location of a high magnification insert showing Er included in panel B. White arrows show the relative locations of transverse sections shown in Figure 2. **B:** High magnification showing relative positions of DD regions. The three regions are most easily distinguishable from one another by different cell size and orientation. Insert shows a high magnification of Er. Scale bar for A is 500 µm; scale bar for B and the insert is 200 µm.

In our new Nissl material the distinction between DDs and DDi is clear. DDs is characterized by smaller, flatter cells (Figs. 1A, B; 2B) with processes aligned parallel to the brain's dorsal surface (Giassi et al., 2012c). This region extends ventrally to a depth of approximately 200 µm (Fig.1B and D & Fig.2A-B). Ventral to DDs is located the wedge-shaped intermediate subdivision of DD (DDi), characterized by relatively round and sparse neurons (Figs. 1B, 2B) which have processes oriented along the dorsal-ventral axis (Giassi et al., 2012c). This wedge of cells follows the medial surface of DL (Fig. 2), extending to a depth of approximately 800 µm, spanning from the rostral boundary of DD, for approximately 600 µm (Fig.1 A-D & Fig.2 A-B). At this point we see the beginnings of the magnocellular subdivision (DDmg) which, as previously described, interposes itself inside DDi and continues in this manner throughout the caudal aspect of DDi.

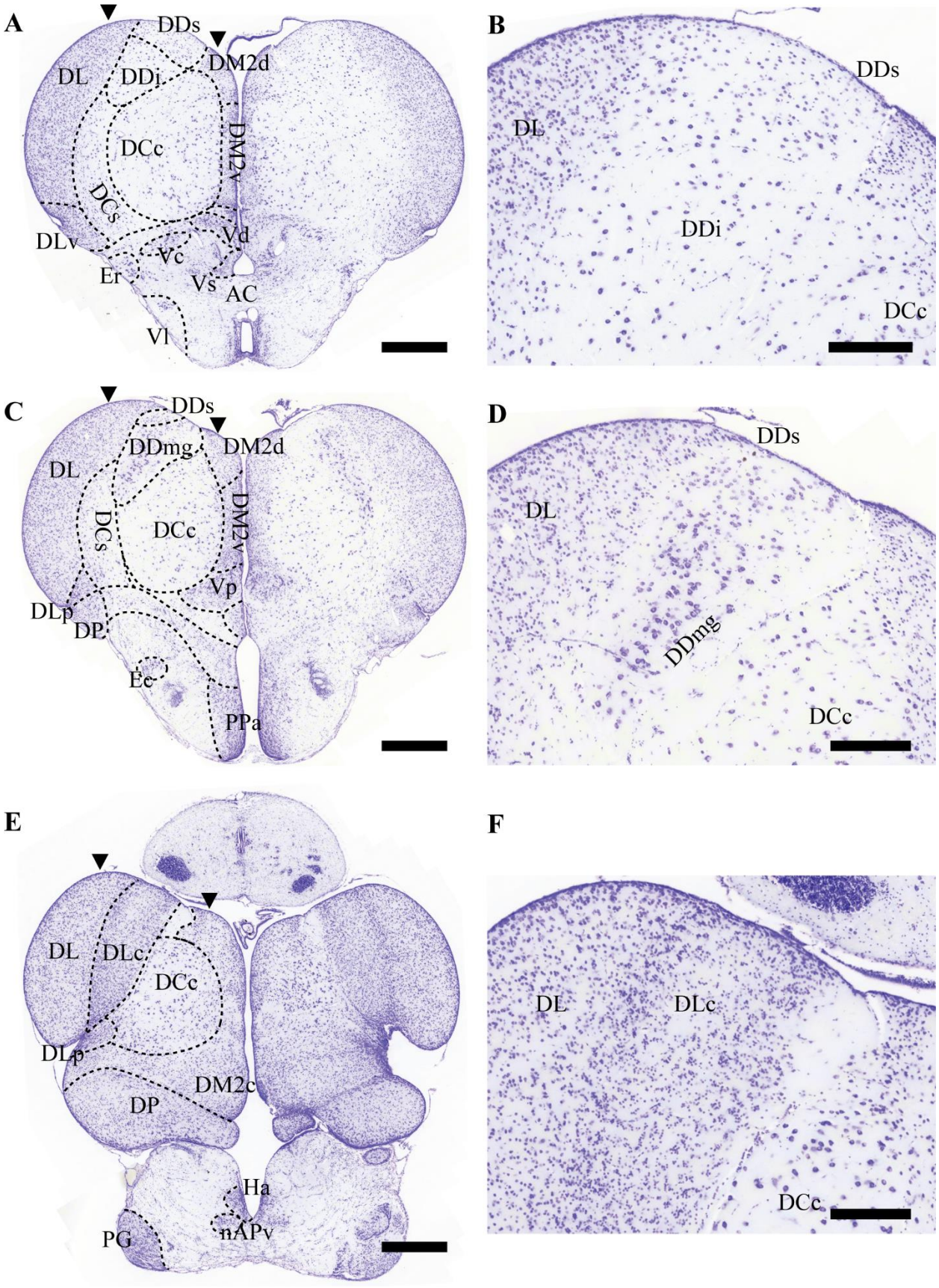
A
DDs
DM2d
DL
DDi
DCc
DM2v
DCs
DLv
Vd
Vc
Er
Vs
AC
Vl
B
DDs
DL
DDi
DCc
C
DDs
DDmg
DM2d
DL
DCs
DCc
DM2v
Vp
DLp
DP
Ec
PPa
D
DDs
DL
DDmg
DCc
E
DL
DLc
DCc
DLp
DM2c
DP
Ha
PG
nAPv
F
DL
DLc
DCc

Figure 3-2: Telencephalic anatomy in the transverse plane

Cresyl-violet stained transverse sections cut at locations indicated by white arrows in Fig. 1, panel A. Black arrows in left column panels show the medio-lateral boundaries of the higher magnification images in the adjacent right column panel. **A:** Relative positions of pallial and sub-pallial regions at the level of DDi. **B:** High magnification showing DDi and DDs bounded by small sulci on the dorsal surface and distinguishable from one another by cell size and cell orientation. **C:** Relative positions of pallial and sub-pallial regions at the level of DDmg. **D:** DDmg and DDs bounded by sulci on the dorsal surface and a rarefication in cell density separating them from adjacent DL, DM2d, and DCc respectively. They are distinguishable from each other by cell size and cell orientation. **E:** Relative positions of pallial and sub-pallial regions at the level of DLc. **F:** High magnification showing DLc bounded medially and laterally by an increased density of cells. This difference in cell density allows distinction of DLc from DL. Distinction from medially located structures is further facilitated by differential cell size and a local rarefication of cell density. Scale bars for A, C and E are 500 µm. Scale bars for B, D and F are 200 µm.

In a previous paper (Giassi et al., 2012c) we described the cell distribution in DL as containing both isolated cells and clumps of 2-4 cells; subsequently, we demonstrated that the cell distribution was, in fact, random (Poisson) (Trinh et al., 2015). Simple observation shows that cells in DDi have a far more regular spatial distribution that those of DL (Figs. 1A, 2B, C) with entirely isolated cells. Unfortunately, the small size of DDi made it impossible to get a large enough sample to quantitatively prove this point. DDmg and DDs are too small to make even a qualitative assessment of this kind.

Some subpallial nuclei are of critical importance for the comparative and functional interpretation of our results and are therefore briefly described. The rostral entopeduncular nucleus (Er) consists of a group of large cells located in the lateral subpallium dorsal to the anterior commissure (AC; Figs.1A; 2A). As previously described (Sas and Maler, 1991) Er also contains a cluster of more densely packed small cells (Fig. 1B, insert). The lateral subdivision of

ventral telencephalon (Vl) lies ventral to Er and AC (Fig. 2A). Finally, two groups of large and densely packed neurons are located dorsal to the AC forming the central subdivision (Vc) and the dorsal subdivision (Vd) of subpallium (Fig. 2A).

INTRINSIC CONNECTIVITY WITHIN DD SUBDIVISIONS

DDs. Because of the narrow depth of DDs and the difficulty of seeing the DDs/DDi boundary in thick slices, we were only able to achieve a small number of *in vivo* tracer injections completely confined to DDs (N=2). Small injections confined to DDs (depth < 50 µm, Fig.3A-B) resulted in retrogradely labeled cells roughly symmetrically located medial and lateral to the injection site (Fig. 3B) and up to distances greater than 100 µm from it. The labeled cells were sparse and there were clearly unlabeled cells intervening between the injection site and the distant labeled cells (Trinh et al., 2015). Given that the medio-lateral extent of DDs is ~600 µm at the surface, this implies that a DDs cell will likely receive input from a small random subset of cells located at distances >100 µm from it, or more than 15% of its medio-lateral extent.

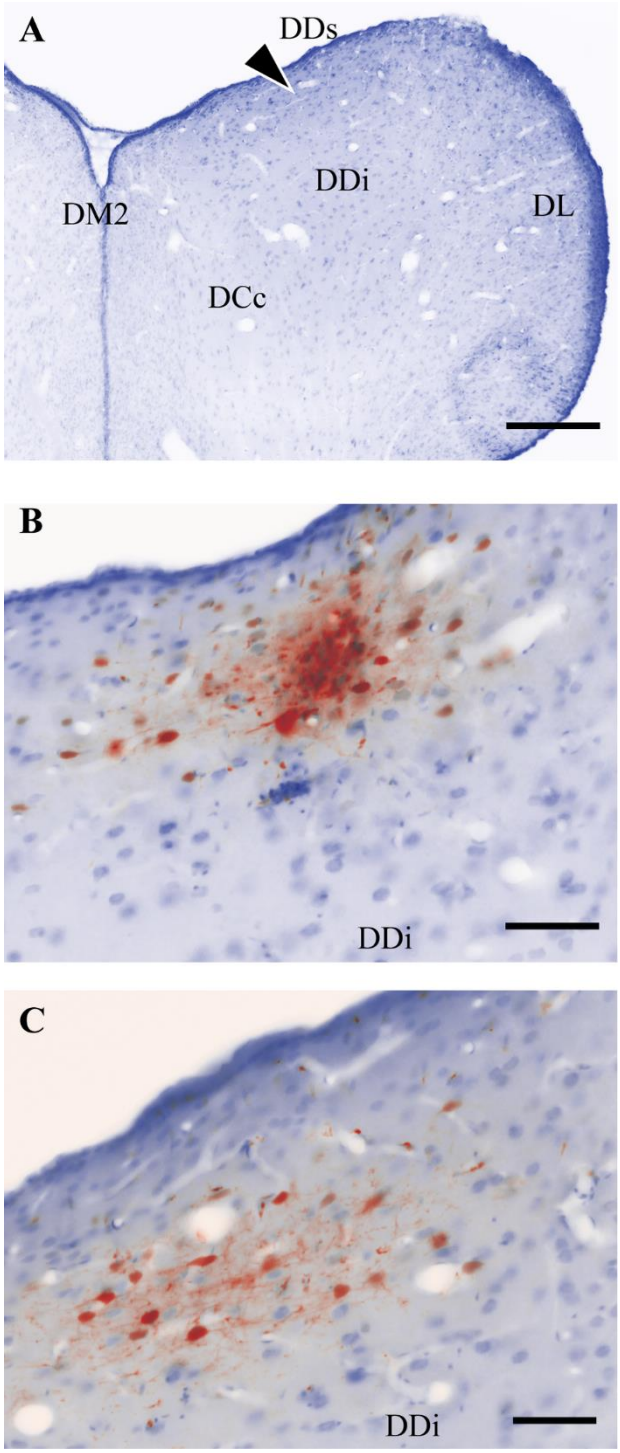

Figure 3-3: Intrinsic connectivity in DDs

A: Nissl staining of a transverse section illustrating the pallial organization at the injection site. Black arrow shows location of injection in Panel B. **B:** high magnification of the injection is shown along with retrograde labeling in immediately adjacent cells (medio-lateral). **C:** Retrograde

labeling is shown in cells caudal (~30µm) to the injection site. Scale bar A is 500 µm; Scale bar B-C is 50 µm.

As illustrated in Fig. 3C, DDs cells also receive intrinsic input from more rostrally and caudally located cells. The retrogradely labeled cells are still centered at the medio-lateral location of the injection site, but are now far more dispersed (>200 µm in this case). Again, not all cells are labeled. In the case illustrated in Fig. 3, retrogradely labeled cells were found up to 225 µm rostral and caudal to the injection site and this represents approximately 30% of the full rostro-caudal extent of DDs.

We conclude that, although the DDs-intrinsic input to a DDs cell is spatially confined, the spread of these cells and their dendrites within the small extent of the entire nucleus implies that DDs is a globally connected recurrent random neural network. By "globally connected" we mean that any DDs cell is only a few synapses (<4 in the rostro-caudal dimension) away from any other cell. By "random" we mean that we could not discern any pattern in the location of labeled versus unlabeled cells. We suspect that the intrinsic DDs connections result in a strongly connected network but, given our limited sample, we are unable to make the exact calculations to support this hypothesis.

DDMG. We were able to achieve N=1 *in vivo* and N=4 *in vitro* injections confined completely to DDmg. We found similar results for both types of injections and therefore did not distinguish between them in our analyses. In the *in vitro* case illustrated in Fig. 4 (a flattened confocal image) a very small injection made in the middle of DDmg resulted in a total of six completely filled DDmg neurons. These are easily identified by their large ovoid somata, all oriented in the same direction

and presenting extended dendrites at both ends (Giassi et al., 2012b; Giassi et al., 2012c). The narrow rostro-caudal limits of DDmg are indicated by dashed arrows and illustrate two points. First, there are a small number of retrogradely labeled DDi cells caudal to DDmg in its intrinsic longitudinal plane; we will illustrate and analyze in depth the far more numerous retrogradely labeled DDi cells rostral to DDmg (see below). Secondly, dendrites of DDmg cells extend into DDi (Giassi et al., 2012c). We estimated this extension to be 144±54 µm (N = 7cells) and can therefore DDmg neurons can presumably receive any afferent input terminating in caudal DDi (see Discussion).

As is evident from Fig. 4 and from the DDmg cell density (Trinh et al., 2015), DDmg is only sparsely and randomly recurrently interconnected. Given our small sample size, we were unable to compute the connection probability; however, from the limited intrinsic connectivity, we doubt that DDmg will be a strongly connected network.

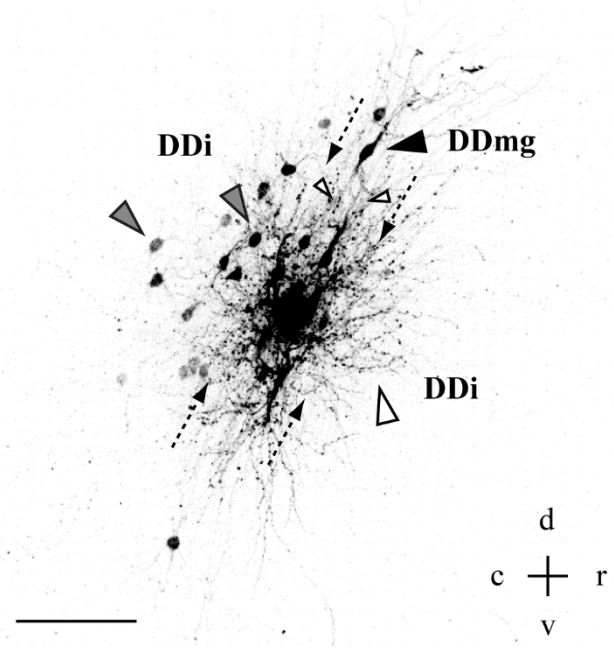

Figure 3-4: Intrinsic connectivity of DDmg

Intrinsic connectivity of DDmg (longitudinal slice). Dashed arrows display the boundaries between DDmg and DDi. Dendrites of directly labeled DDmg neurons extending 144±54 µm into DDi (large white arrow). A small number of DDmg neurons (black arrow) were retrogradely labeled as were DDi neurons (gray arrows) caudal to DDmg. This image could only be taken with a 10X objective (see Methods). We applied excess contrast enhancement to clearly visualize dendrites extending into DDi (large white arrow). Small white arrows indicate unlabeled cells intervening between the injection and labeled cells. Note anterogradely labeled boutons in close apposition to these unlabeled cells. Scale bar is 100 µm.

DDi. We used small *in vitro* injections confined to DDi (N=8, 508 neurons retrogradely labeled neurons) in order to quantify intrinsic DDi connectivity (Fig. 5). We had additional *in vivo* DDi injections (N=4); these showed the same qualitative results but the injections were too large and were therefore not suitable for a detailed quantitative analysis (these injections were used to study other connections of DDi, see below). In addition we had two double *in vivo* injections of tracer (4 injections altogether). These injections were of intermediate size and so not useful for the most quantitative analyses (graph theory); they were used to specifically study in greater detail the how DDi cells might form strongly connected intrinsic networks.

IN VITRO INJECTIONS: QUANTITATIVE ANALYSIS.

A small DDi injection sectioned in the DD longitudinal plane (see Methods) directly labels a small number of neurons and consistent with previous work (Giassi et al., 2012c) their axons and dendrites, are seen to sparsely radiate out to ~200 µm from the injection site (Fig. 5A, B). In the smallest injections it was clear that not all neurons <50 µm from the injection site were labeled (Fig. 5A, B) even though their dendrites would have traversed the injection site; this rules out uptake by dendrites as a major cause of labeling. In order to be even more stringent, we did not

include labeled neurons with 30 µm of the injection site in our statistical analyses in case their dendrites had taken up the tracer. Labeled cells form a nearly symmetric cloud surrounding the injection sites and extending out over 200 µm from it (Fig.5A); these neurons did not display any dendritic label and are assumed to be retrogradely labeled. We did not find any directional preference for the location of the labeled cells. In order to be certain we checked along the DDi intrinsic planes – longitudinal plane and perpendicular to this plane – and, in addition re-plotted the 3-D confocal stack in spherical coordinates; in no case did we find any preferential direction for labeled cells. We conclude that the labeled cells lie within a sphere surrounding the injection site (see Materials and Methods). Retrogradely labeled DDi neurons display different intensities of labeling. Fig.5B illustrates apparently randomly intermingled strongly (s), weakly (w) and intermediately (i) labeled DDi neurons. It is important to note that weakly and strongly labeled neurons can be located adjacent to one another (Fig. 5B). The choice of weak, intermediate and strong labels is based on a quantitative analysis presented in detail below.

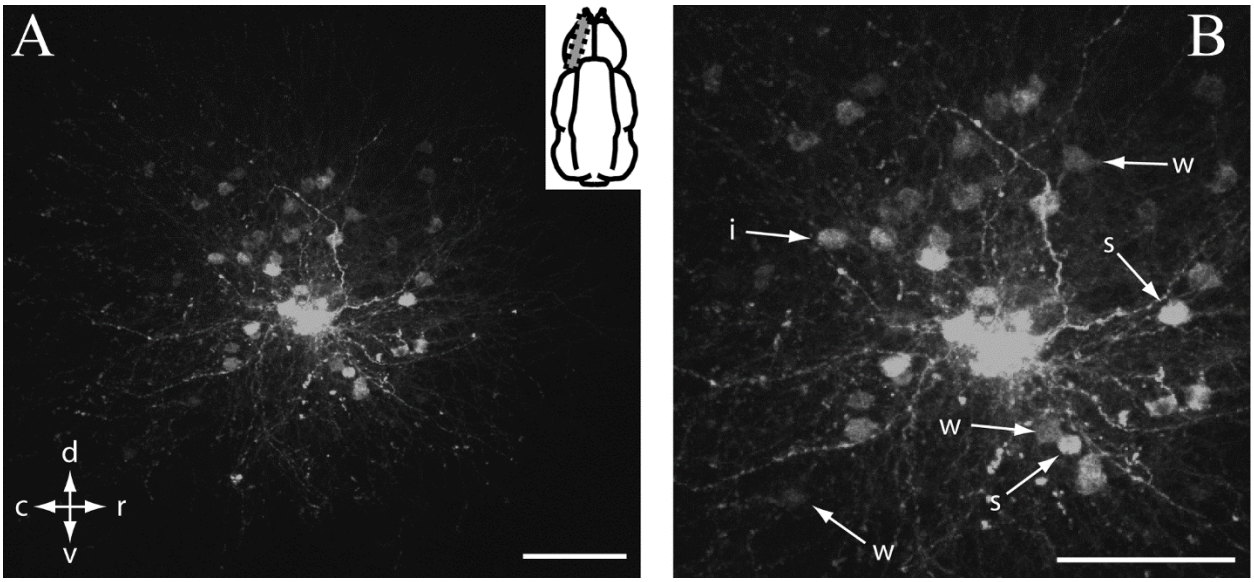

Figure 3-5: Intrinsic connectivity of DDi

Intrinsic connectivity of DDi (longitudinal slice). **A:** The DDi injection site with retrogradely labeled neurons and neurites. The insert shows the geometry of the slice preparation. Arrows in the left bottom display the slice orientation **B:** A higher magnification illustrates the fall off of labeled cells with distance from the injection site and differences in the intensity of retrogradely labeled DDi neurons: “i”: intermediately labeled; “s”: strongly labeled; “w”: weakly labeled. Scale bar A, B is 100 µm.

To quantitatively analyze the connectivity probability between any two DDi neurons, we plotted the overall probability of connection as a function of distance independent of the labeling intensity (Fig. 6A). We found that an exponential decay gave an excellent fit to the data (chi^2=0.00021): $f(x) = 0.09e^{-.025x}$. We note that this is not an exponential (continuous) distribution since it does not integrate to 1; it is an estimate of the probability of connectivity at discrete locations. After 90 µm, the connectivity probability estimate falls to less than 0.01.

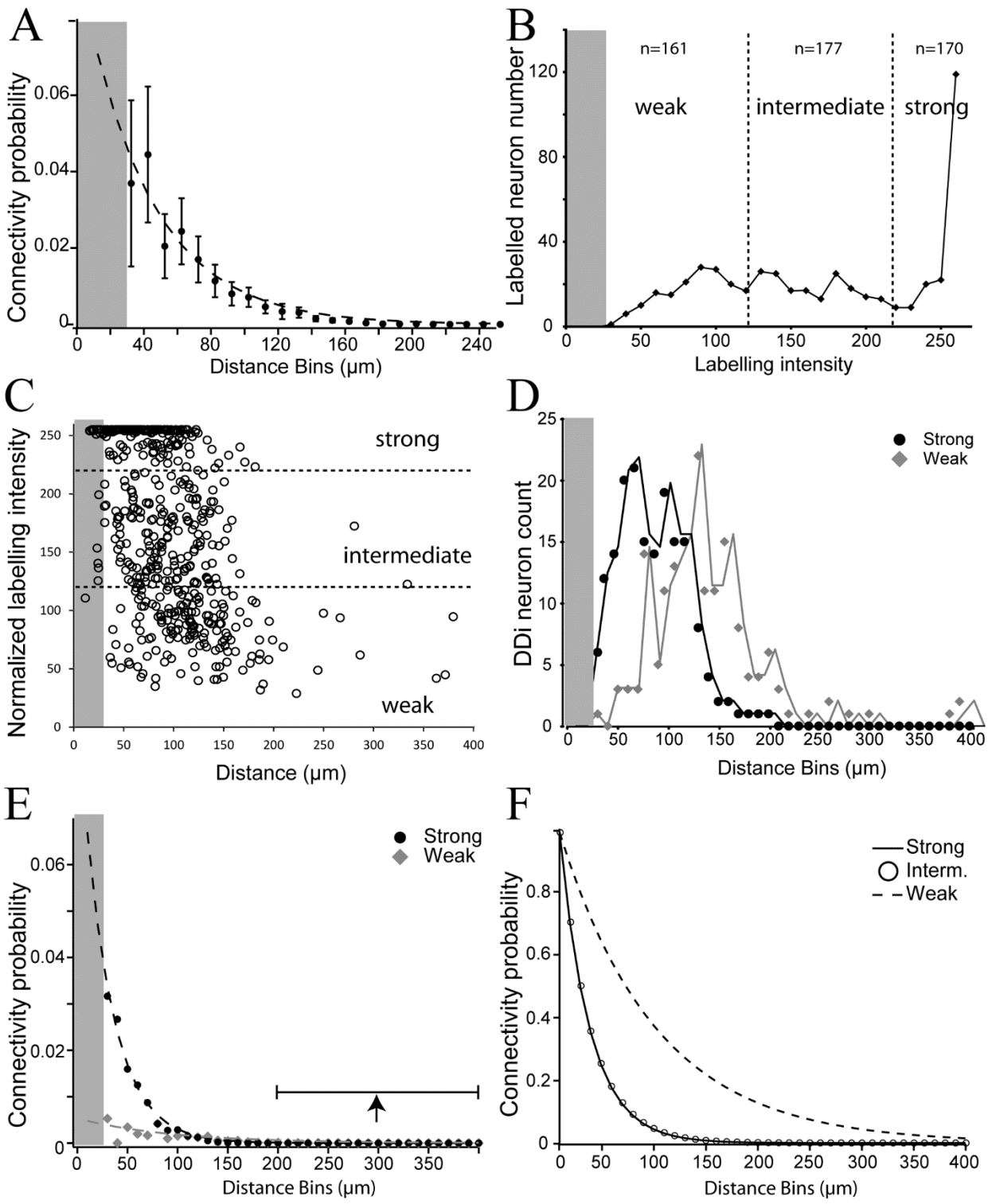

Figure 3-6: Analysis of intrinsic DDi connectivity

A: Connectivity probability of the entire retrogradely labeled DDi neuron population as a function of distance. The exponential curve fit is shown as a dashed line. **B:** Histogram of the labeled neurons' intensity of staining in a 256 level gray scale and classification of the staining of DDi neurons into weak, intermediate and strong categories; see Fig. 5 for an illustration of these categories. Boundaries between weak, intermediate and strong labeling were set at 120 and 220 gray scale units respectively. **C:** the population of individual labeled DDi neurons as a function of distance (μm) from the site of injection. The dashed lines display the boundaries set in B at 120 and 220 to distinguish weak, intermediate, and strong categories. It is clear that the weakly labeled cells are found at far greater distances from the injection site than the other categories. **D:** Distribution of strongly (black circles) and weakly (gray diamonds) labeled DDi neurons as a function of distance bins (μm) from the site of injection. Weakly labeled cells can be found up to 400 μm from the injection site while the strongly labeled neurons are mostly confined to within 150 μm. **E:** Connectivity probability for strongly (black circles) and weakly (gray diamonds) labeled DDi neurons as a function of distance bins (μm). The curve fits are shown in dashed lines. **F:** Normalized exponential curve fits made in E in order to better contrast the differences between the decay (with distance) of strongly/intermediately versus weakly labeled neurons. The curve fit for strongly labeled DDi neurons is shown with the a continuous line, that for the weakly labeled neurons is displayed with a dashed line, and the curve for DDi neurons with intermediate labeling is displayed as open circles. In all cases, the gray area displays the distance area were data were discarded because neurons were too close to the injection site.

In order to clarify whether the clearly strongly and weakly labeled neurons were distinct categories we made a histogram of the binned labeling intensities. There were clear local minima in the histogram and we chose the leftmost minimum as the cut-off defining the weakly labeled cells and the right most minimum as defining the strongly labeled cells. This gave three classes of labeling intensity with roughly equal numbers of neurons in each (Fig. 6B). Although there was an additional minimum within the "intermediate" class, we did not further subdivide at this point because the resulting classes would be too small for realistic statistical analyses. These categories are therefore: weak (<119.9); strong (>220); intermediate between 120 and 219.9. Plotting all labeled cells as a function of intensity and distance from the injection site reveals that all the

strong and intermediate cells are located within 150 µm of the injection site, while there are substantial numbers of weak cells at distances > 250 µm (Fig. 6C). Because strong and weak categories appear dissimilar, we plotted the raw connection count of strong and weak labeled cells versus distance in Fig. 6D. It is clear that the weak cells are mostly located further from the injection site than the strongly labeled cells and can be found at nearly 400 µm from it. Finally, we fit exponential distributions to the strongly and weakly labeled cell intensities (Fig. 6E). As might be expected, the decay exponent (with distance) for the strong intensities (0.034) was three-fold greater than that for the weak intensities (0.011). In order to better visualize this result, we plotted the normalized (peak=1) intensity decay curves (Fig. 6F). The much slower decay with distance of the weak intensities is clearly evident. Interestingly, the strong and intermediate decay with distance are identical so that the intermediate curve was only made distinguishable by superimposing circle markers. We conclude that there at least two very distinct categories of labeled cells: those that are weakly labeled and those that are labeled strongly or at an intermediate level; it remains to be seen whether the intermediate category is indeed a natural one. The strongly/intermediately labeled cells tend to connect to nearby cells while the weakly labeled cells to more distant cells. It might be argued that such a fall off of labeling intensity would be expected with increasing distance caused by a decreased accumulation in cells as they are further from the injection source. This however seems less likely due to a significant overlap in distance where we see both strong and weak labeling.

Our exponential fits were excellent but they were dominated by the very large number of labeled cells located near the injection site versus those >150 µm from it (Figs. 6C, D). We therefore checked whether this fit would account for the most distant labeled cells. Calculating

the estimated probability of these distant cells would entail summing the discrete estimates from the exponential fit taken at each distance where a cell is located. We used, as an approximation, the area (integral) under the exponential curve taken from 225 to 400 μm. This gave a value of ~0.01. In other words, we would expect roughly 0.01 x 500 = 5 cells labeled at these distances. In fact, we found 8 such cells. There are no exact statistical tests for these estimates that we are aware of. Furthermore, long-tailed densities are difficult to fit with small sample sizes because of the small numbers of cell in the tails. In addition, as described in the Methods, we were likely underestimating the connection probability for distances > ~250 μm from the injection site. Therefore, while we cannot exclude an exponential fit as being correct, we also cannot exclude that other types of long-tailed densities (e.g. Levy distribution) might be a more appropriate distribution. We return to this important point in the Discussion.

GRAPH THEORY ANALYSIS OF DDI CONNECTIVITY.

We found, using the graph theory calculations described in Trinh et al (Trinh et al., 2015) that, for spherical diameters of 130 μm and greater, DDi is strongly connected; the computed probability of being strongly connected at a diameter of 130 μm was 0.96. The mean path length at this diameter was 2.4 implying that, as in DL (Trinh et al., 2015), DDi neurons are likely to locally connect to other neurons via either one or two intervening cells. Therefore, DDi is, overall, a strongly connected network. Although the probability of connections is low for distances >100 μm, all neurons will always be synaptically "close" to each other.

A key point for the functional interpretation of DDi connectivity is a quantification of its connection loops, e.g., for cells A, B and C within DDi, how many loops of the form A -> B -> C->

A would we expect. Strong connectivity implies that loops must exist within spheres of diameter > 130 µm. The number of such loops of various sizes has important implications for the function of DDi (see Discussion). We can easily calculate the number of loops for any path length based on the standard assumption that the probability of connections is random and has a Binomial density. In a DDi sphere with a diameter of 130 µm there will be 241 cells (Trinh et al., 2015) and the mean probability of connections will be ~0.038. Any cell near the center of this sphere will, on average, receive input from 9 other cells. For the shortest loop, A -> B -> A, we then need the probability of 0, 1…9 cells in B will project to A. The mean of the binomial distribution is Np, where 'N' is the number of cells and 'p' the probability of connection; therefore there will be, on average, 0.3 cells for this loop, i.e., the shortest length loops are unlikely to occur.

For A -> B -> C-> A, each of the nine 'B'cells will in turn contact nine 'C' cells giving a total of 81 cells that might contact 'A' and complete the loop; here, as a first order approximation, we ignore overlap. The same calculation yields 2-4 (mean 3) likely loops with three synapses. The next loop, A -> B -> C-> D->A, will saturate the 241 cells. The calculation then yields 7-10 loops likely loops (mean 9) with a four synapse mean. We conclude that, on average, neurons in DDi will reconnect to themselves over 12 loops. Assuming a long delay (conduction plus time to EPSP peak) of 10 ms, this implies that spiking in one DDi neuron can feedback to itself within <50 ms; DDi is enriched in NMDA receptors and this duration is less than that of an NMDA receptor mediated EPSP (see Discussion). There will be even longer loops that include cells outside the 130 µm diameter sphere. We cannot compute their distribution in the same way because the assumption that the connection probability can be estimated by averaging becomes much less

realistic. Direct modeling of the DDi graph structure will be needed for this more sophisticated analysis.

IN VIVO DOUBLE INJECTIONS: QUALITATIVE ANALYSIS OF OVERLAPPING CONNECTIVITY.

We initially performed double tracer injections in DDi *in vitro* (N=2) spaced 200 µm apart. We found numerous adjacent neuron pairs with one neuron projecting to one injection site, and the other to the other site. In a few cases, one neuron extended its axon over the closer injection site to reach the further one (data not shown). This demonstrates that the random sparse connectivity in DDi extends over a large volume (>200 µm). However, we found only one instance of a double labeled cell. This is presumably due to the low probability of connections at 200 µm (Fig. 6A).

We therefore turned to *in vivo* double injections where we could have longer survival times. We injected two different dextran-biotinylated fluorophores (mini-Ruby and Alexa-647) in DDi separated by approximatively 100 µm (N=2 fish or 4 injections; Fig. 7 A; magenta and cyan dots). Both injections were placed very close to the center of DDi. Fig. 7 C, D and E display DDi 25 µm thick transverse sections taken at the rostral pole of DDi (C), between the injection sites (D), and caudal to the injection sites (E), respectively. We observed a total of 1454 cells labeled with either or both fluorophores in all the DDi sections. Labeled cells were again distributed randomly in DDi with no obvious pattern and not seeming to depend on the direction from the injection sites. The number of cells labeled with a tracer clearly decreased with distance from the injection site, but there was extensive overlap of cells labeled with either or both tracers. Most cells were labeled with only one dye (86%; mini-Ruby: 756 cells; Alexa-647: 488 cells) indicating that these

cells projected to only one injection site. However, 14% of the DDi labeled neurons (210 cells) were labeled with both tracers. In order to simplify the following analysis, we simplified our categories into “strong” labeling and “weak or intermediate” labeling; the latter category is now referred to as simply “weak”. This grouping was selected in this instance as the separation between the strong and intermediate peaks was much larger than the small dip between the intermediate and weak peaks in the histogram shown in Figure 6B. It therefore seemed more fitting that strong remain its own distinct category. We then classified the double-labeled cells into three groups, according to their intensity of labeling: strong labeling for both dyes (s/s); weak labeling for both dyes (w/w); and strong labeling with one dye and weak with the second dye (s/w; Fig. 7 G1-4). 13% of the double labeled cells were strongly connected to both injection sites (2% of the total labeled cells), 31% of the double labeled cells were weakly connected to both injection sites (5% of the total labeled cells) and 56% of the double labeled cells were strongly connected to one injection site and weakly to the other one (8% of the total labeled cells). Globally, these observations suggest the global network between DDi neurons may have additional complexity in terms of the patterns of connectivity strength (see Discussion).

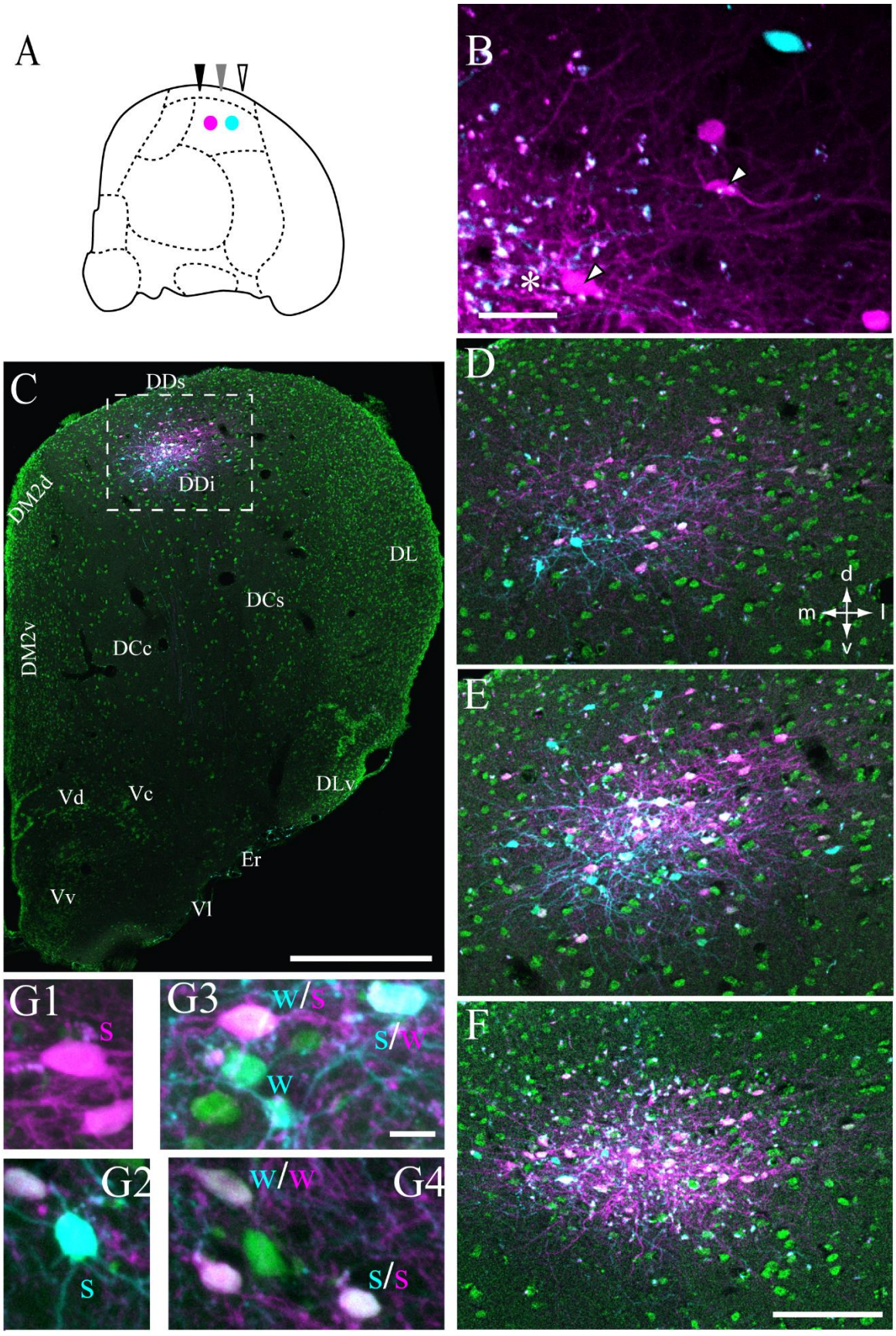
A
B
C
DDs
DDi
DM2d
DL
DCs
DM2v
DCc
Vd
Vc
DLv
Er
Vv
Vl
D
d
m
l
v
E
F
G1
s
G3
w/s
s/w
w
G2
s
w/w
G4
s/s

Figure 3-7: Overlap of DDi connectivity as seen with double injections

A: Schematic in a parasagittal plane illustrating the fluorophore injection sites (Mini-Ruby in magenta and Alexa-647 in cyan). In all subsequent panels, Nissl staining is displayed by green fluorescence. The white arrow shows the position of panel D, the gray arrow that of panel E and the black arrow that of panel F. **B:** DDi at the level of the magenta injection site (magenta dot in A). "*" marks the edge of the injection site. Small white arrows mark cells which show evidence of dendritic labeling; note strong labeling of dendrites extending from the injection site. Note lack of dendritic labeling in the cyan cell. **C:** low magnification of the region (transverse plane) between the injection sites in panel A (gray arrow). The injections were confined to DDi. The dashed box displays the regions illustrated in D-F. **D:** DDi rostral to the injection sites. Overlapping cyan and magenta cells can be identified, while white cells are double stained. Arrows in the right bottom display the orientation in D-F. **E:** High magnification of the box in panel B illustrating DDi between the injection sites. Cells that project to either (cyan or magenta) or both (white) injection sites have overlapping distributions. **F:** DDi caudal to the injection sites. Spatial overlap is again evident. **G:** high magnification of DDi neurons. **G1** and **G2** show cells strongly labeled with a single dye (s). **G3** displays a weakly filled cell (w) and two strongly and weakly double stained cells (s/w). **G4** shows a double weakly labeled cell (w/w), a double strongly labeled cell (s/s) and an unstained cell in green. Scale bar B is 25 µm. Scale bar C is 500 µm; scale bar D-F is 100 µm. Scale bar in G3 applies to G1-G4 and is 10 µm.

CONNECTIVITY ACROSS DD SUBDIVISIONS

The strongest intra-DD connections are between DDi and DDmg. We first describe the relatively minor connections associated with DDs and then turn to a detailed analysis of DDi/DDmg connectivity.

MINOR INTERCONNECTIONS OF DDS WITH DDI AND DDMG

Injections contained within DDs (*in vivo*, N=2) reveal sparse anterograde labeling spread throughout the dorsal parts of both DDi and DDmg (data not shown). We did not observe any retrogradely labeled neurons in either DDmg or DDi. As DDs is a shallow region (about 200 µm thick), injections had to be very small to avoid contamination of DDi or DDmg; thus the sparse anterograde labeling may simply be a consequence of the limited number of neurons taking up

the tracer. We therefore conclude that there does indeed exist uni-directional connectivity from DDs to both DDmg and DDi, but we cannot define the intensity or possible patterning of these projections.

DDI TO DDMG CONNECTIONS.

Injections in DDmg (*in vitro*, N=4; *in vivo*, N=1) label numerous neurons throughout DDi including those caudal to DDmg (Fig. 4) and many more in the main part of DDi, rostral to DDmg (Fig. 8A). For the four cleanest injections there were a total of 286 cells retrogradely filled in DDi. Labeled cells extended rostrally up to ~250 µm into DDi (Fig.8B); this represents approximately 35% of the full DDi rostro-caudal extent. DDi is a roughly cuboidal structure and the DDi neurons projecting to DDmg occupy only a fraction of this volume. This implies that DDi is itself internally differentiated and that not all DDi neurons have direct access to DDmg.

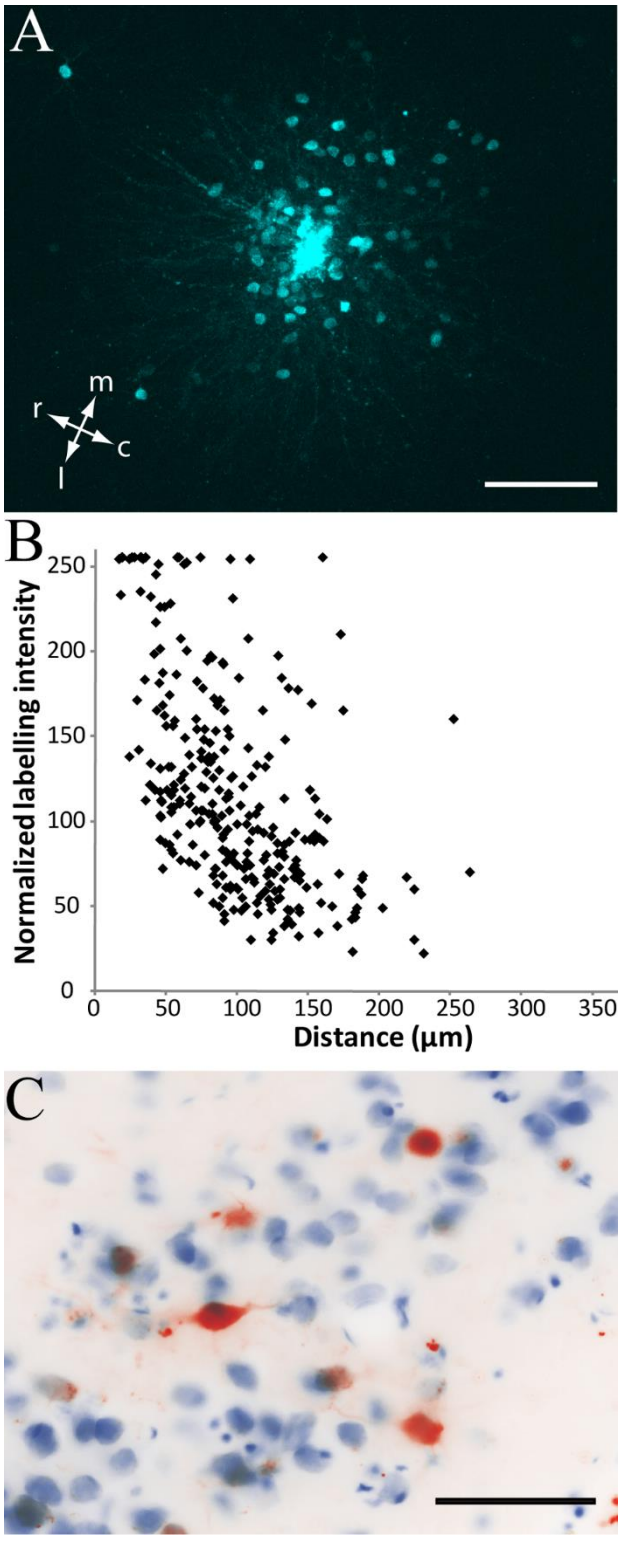

Figure 3-8: Connections between DDi and DDmg

A: Horizontal slice preparation showing a contained injection in DDmg labeling surrounding DDi cells. Orientation arrows are display at the left bottom. **B:** Labeling intensity of DDi neurons as a function of distance (μm) from the injection in DDmg. **C:** Retrograde labeling of a few DDmg neurons after *in vivo* injections contained in DDi. Scale bar A is 100 μm; scale bar C is 50 μm.

In vivo injections contained within DDi (N=7) revealed retrograde labeling of cells in DDmg (Fig 8C). As contamination of a transition zone where we note significant invasion of DDi by dendrites from DDmg cells was a concern, we performed injections in both caudal and rostral regions of DDi. Both revealed similar retrograde staining in DDmg.

We conclude that bidirectional connectivity is present between DDmg and DDi and that the DDi to DDmg projection is stronger than the reverse projection. The connection originating in DDmg and terminating in DDi covers a larger distance with termination spread throughout the length of DDi. That originating in DDi and terminating in DDmg is strong but restricted to parts of DDi in close proximity to DDmg.

EXTRINSIC DD CONNECTIVITY

SUBPALLIAL CONNECTIONS OF DD

Injections contained within DDi (*in vivo*, N=7) and DDmg (*in vivo*, N=1) each respectively labeled both cells and terminals in Er. The distribution of staining was slightly different however. The DDmg injection stained only terminals in the upper cluster of Er cells (Fig. 9 A) while cells were stained along with a very few terminals in the lower cluster of cells (Fig. 9 B). Injections in DDi however stained both cells and terminals throughout Er (Fig. 9 C).

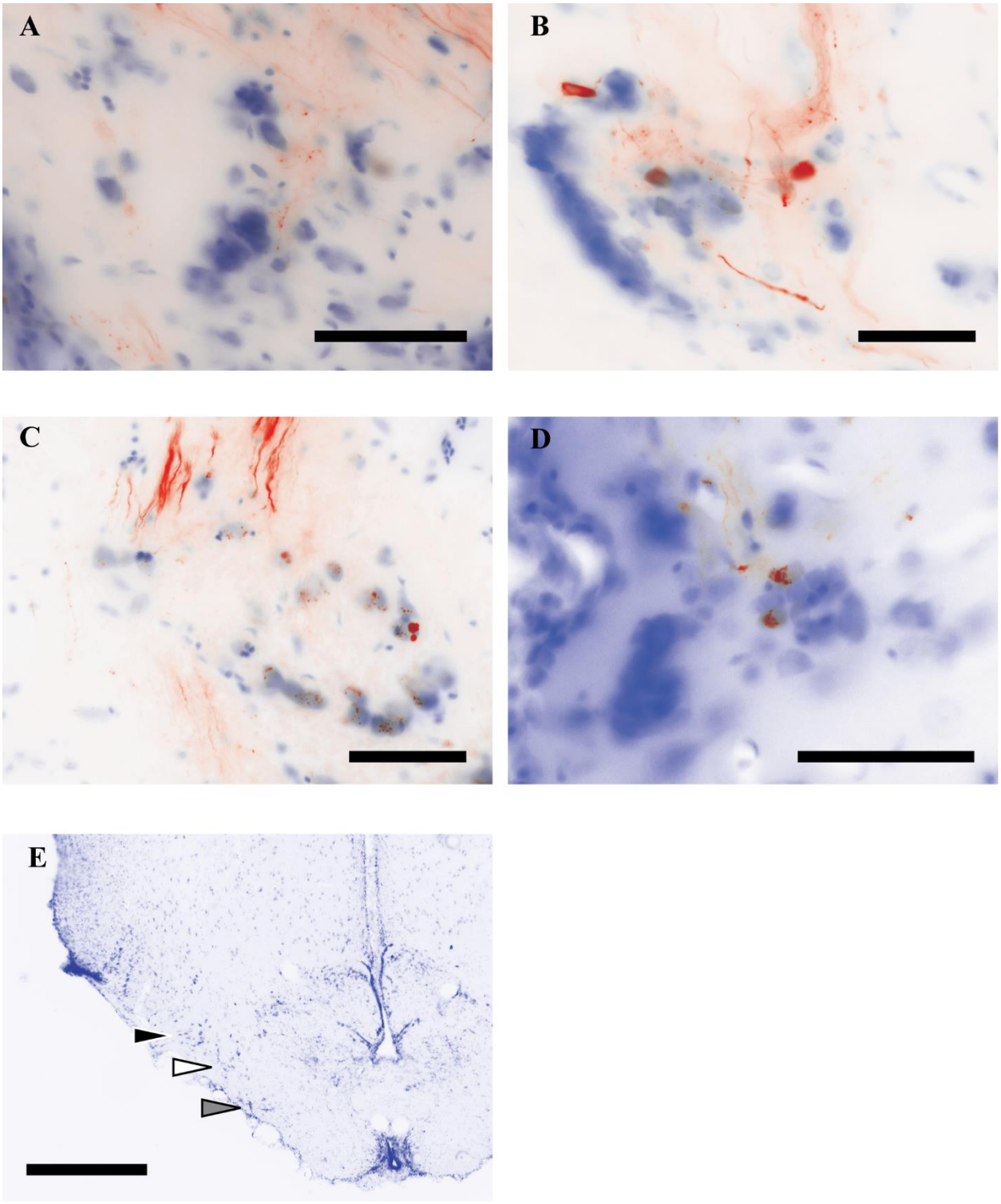

Figure 3-9: Connections between DD and Er or Vl

A: Terminals in the upper grouping of cells in Er (black arrow in panel E) stained following injection in DDmg. **B:** Cells and terminals in the lower grouping of cells in Er (white arrow in

panel E) stained following injection in DDmg. **C:** Cells and terminals faintly stained throughout Er following injection in DDi. **D:** A small number of cells and a few terminal fibers stained in Vl (gray arrow in panel E) following injection in DDs. **E:** The relative positions of these three areas are shown in the transverse plane. The black arrow shows the more dorsally located upper grouping of cells in Er, the white arrow, the slightly more ventral lower grouping of cells in Er, and the grey arrow, the even more ventrally located Vl. Scale bar A-D is 50 µm; Scale bar E is 500µm.

Injections restricted to DDs (*in-vivo*, N= 2) showed minor retrograde and possible anterograde labeling in Vl (Fig. 9 D), but no cells or fibers were labeled in Er. These same injections did reveal both retrograde and anterograde labeling in Vc and Vd (Fig. 10 E). Similar to injections in DDi, labeled cells and terminals appeared spread throughout Vc and Vd.

The same DDi and DDmg injections also labeled both cells and terminals in Vc and Vd (Fig. 10 B-D). Similar to the staining in Er, retrograde and anterograde connections from DDmg appear to be segregated whereas those from DDi are more intermixed. While DDi injections labeled both cells and terminals throughout Vc and Vd (Fig. 10 B), The DDmg injection revealed only terminals in the more laterally located Vc (Fig. 10 C), and primarily cells in the more medially located Vd (Fig. 10 D).

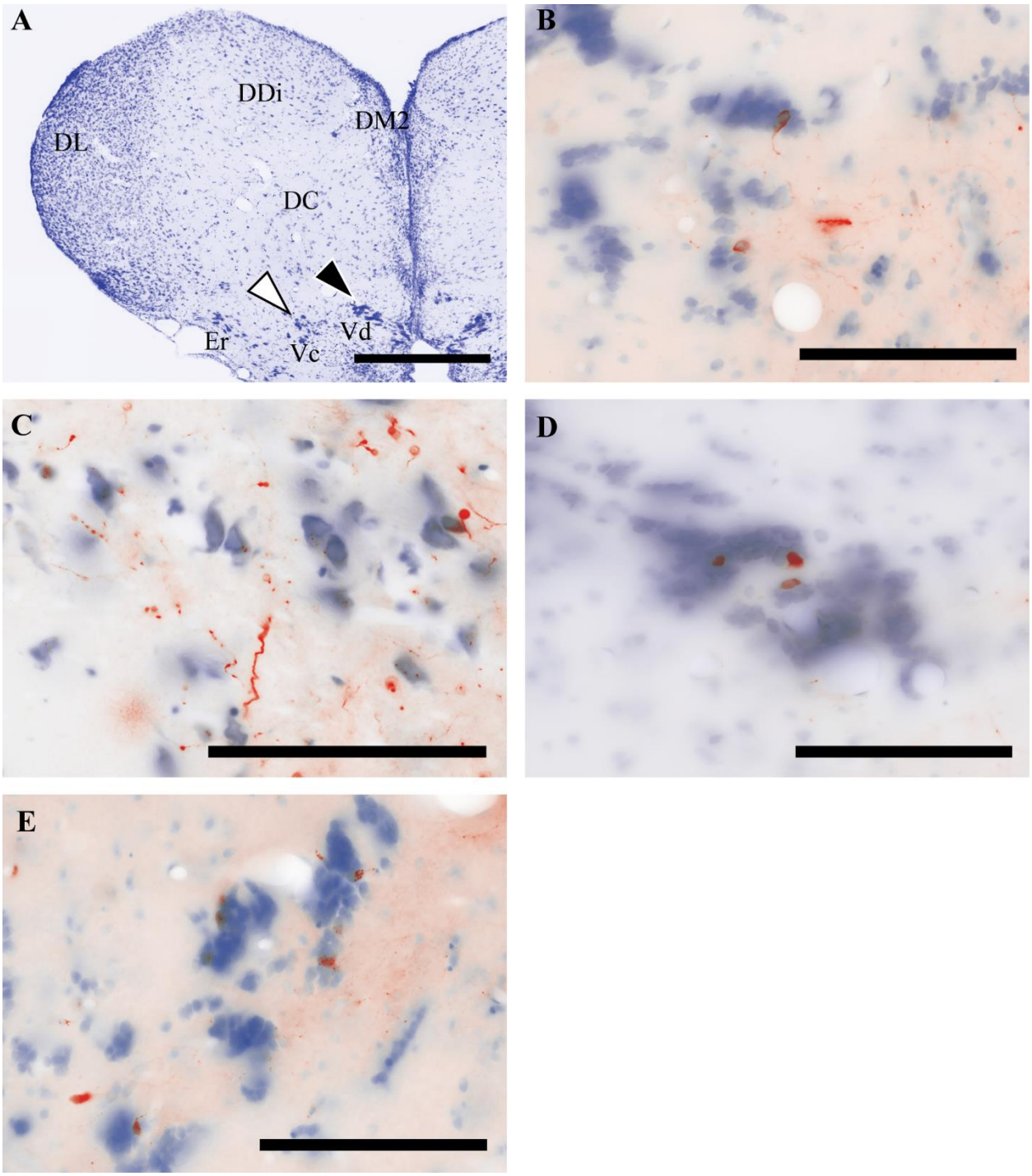

Figure 3-10: Connections between DD and Vc/Vd

A: The relative positions of Vc and Vd are shown in the transverse plane. The black arrow shows the more medially located Vd, the white arrow, the more lateral Vc. **B:** Cells and terminals stained throughout Vc/Vd following injection in DDi. **C:** Terminals in Vc (white arrow in panel A) stained

following injection in DDmg. **D:** Cells and, possibly, a very few terminals stained in Vd (black arrow in panel A) following injection in DDmg. **E:** Cells and terminals stained throughout Vc/Vd following injection in DDs. Close inspection of zoomed in versions of panels D and E (not shown) confirmed that the staining of cells followed precisely the Nissl staining of the cell bodies. Scale bar A is 500 µm; Scale bar B-E is 100 µm.

PALLIAL CONNECTIONS OF DD

Injections contained within DDi (N=7) stained terminals in DC core (DCc) (Harvey-Girard et al., 2013) (Fig. 11 B). An injection in DCc retrogradely labeled two cells in DDi (N=1, data not shown). Injections in DDs (N=2) also stained terminals in DCc but they appear restricted to the dorso-lateral corner (Fig. 11 C). Although the invasion into DCc of terminals from DDs neurons appears far more superficial than those coming from DDi, it must be remembered that DDs injections were by necessity much smaller than those in DDi, and that this might be a result of the difference in injection volume.

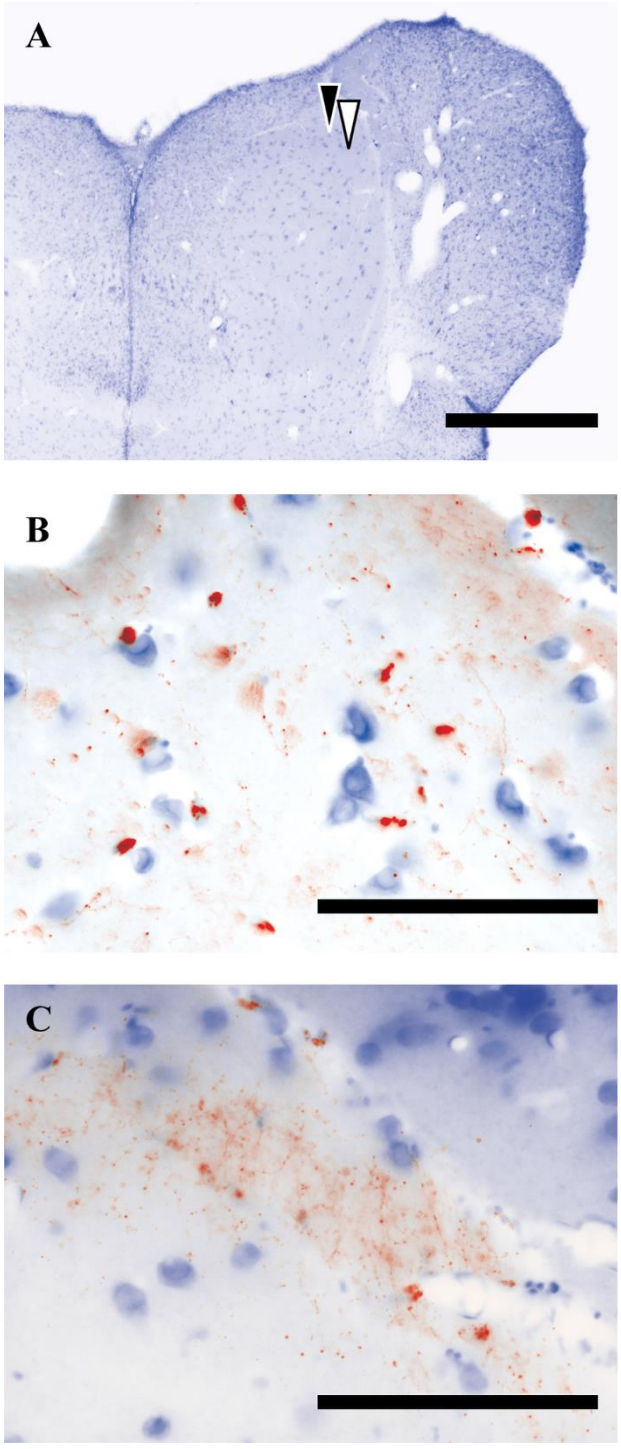

Figure 3-11: Projections of DD to DCcore (DCc)

A: Low magnification image of the pallium of one of the DDi/DDs injected fish. The white arrow indicates the location of the image shown in panel B, the black arrow, that in panel C. **B:** Stained terminals spread through the lateral parts of DCc following injection in DDi. Larger strongly

labeled structures are associated with blood vessels likely due to tracer uptake by the vasculature. **C:** Stained terminals restricted to the dorso-lateral shoulder of DCc following injection in DDs. Scale bar A is 500 μm; Scale bar B-C is 100 μm.

Injections in all regions of DD revealed significant connections with DL. Injections contained in DDi (N=7) stained a large number of cells throughout DL (Fig. 12 A-C), but not in DLc; this confirms Giassi et al (Giassi et al., 2012b) who also noted that DL was the major source of input to DD and, specifically, DDi. The cells were spread through DL, and the exact distribution was sensitive to the precise injection site and, with the same injection, also varied along the rostro-caudal DL axis. At some levels, labeled DL cells were more concentrated near its lateral surface while at other levels they were spread throughout its depth (Fig. 12 A-C). We suspect that there is a complicated spatial organization of the DL to DDi projection, but with our limited sample we were unable to fully characterize its 3-D organization.

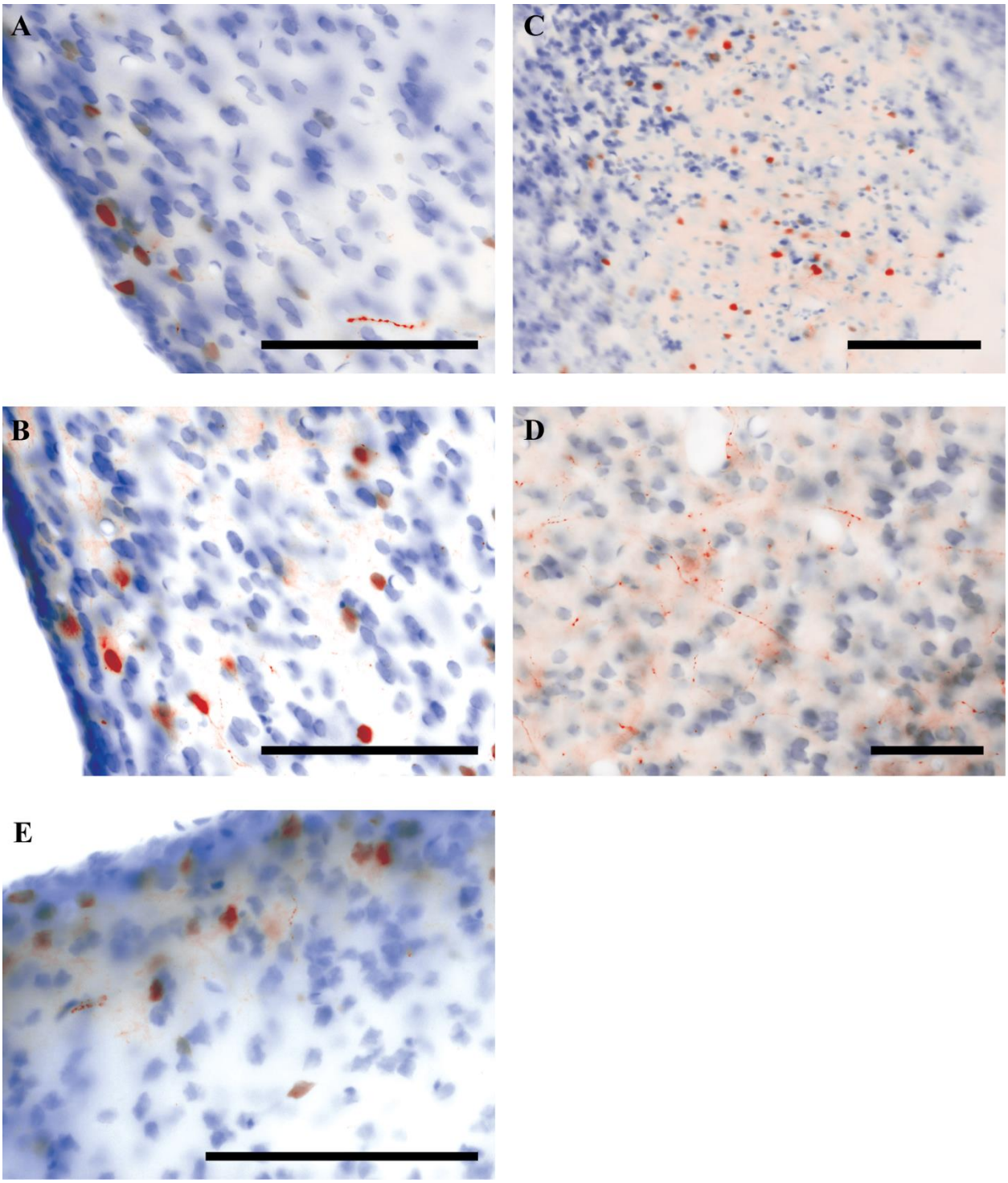

Figure 3-12: Connections between DD and DL

A&B: An injection in DDi labeled cells concentrated at the lateral surface of DL in some areas (A) and extending throughout the depth of DL in others (B). **C:** Cells labeled in DLc following injection

in DDmg. **D:** Labeled terminals sparsely distributed throughout DL following injection in DDmg. **E:** Cells stained in medial DL restricted to its dorso-lateral surface following injection in DDs. Scale bar A-E is 50 µm.

We further quantified the DL neuron projections to DDi. We estimated the injection site volume (~$1.13x10^6$ µm³) in DDi (N=5). By stereology, we previously estimated the cell density in DDi to be 225cells/10^6µm³ (Trinh et al., 2015). The injection site volume and the DDi cell density allowed us to estimate that there were 237.4 ± 62.8 DDi cells in this volume. We then counted all the retrogradely labeled DL neurons in all the transverse sections without any distinction between strongly or weakly labeled cells. On average we counted 3538±834 DL cells per injection. This allowed us to crudely estimate the number of DL neurons projecting to a single DDi neuron at 16.5±4.2 (N=5). Previously, we had estimated that there were 225 DL neurons for each DDi neuron (Trinh et al., 2015). Our analysis suggests that only 7.3% of the DL neurons project to DDi. This is consistent with a previous qualitative analysis (Giassi et al., 2012b) that also concluded that only a fraction of DL neurons project to either DD or DC. We conclude that the majority of DL neurons are likely excitatory interneurons and that they are the ones that generate the cryptic laminar and columnar connectivity. We do not know whether the same DL neurons project to both DDi and DC, or whether they are separate populations (Giassi et al., 2012b; see Concluding remarks) and whether they have local recurrent collaterals (Trinh et al., 2015).

An injection confined to DDmg (N=1) stained retrogradely a large number of cells spread through DLc (Fig. 12 C), but not in DL. Additionally, a large number of terminals were anterogradely stained throughout DL (Fig. 12 D), but not DLc as already expected (Giassi et al.,

2012b). Injections restricted to DDs (N=2) also retrogradely stained cells in DL (Fig. 12 E), although not nearly as many as DDi injections. These cells seemed restricted to the dorso-lateral surface in the parts of DL directly adjacent to the area of DDs where the injection was localized.

Injections restricted to all three regions of DD (DDi, N=7; DDmg, N=1; DDs, N=2) each stained terminals in DM2v (Fig. 13 panels A, B, and C respectively). Injections in DDs (N=2) also labeled a very few cells in DM2v (data not shown), however the stained cells only appear in the more caudal portion of DM2v. Injections restricted to DDs (N=2) also weakly labeled both terminals (Fig. 13, C) and a very few cells (data not shown) in DM2d. Injections in DDmg (N=1) also label a very small, but tightly clustered grouping of cells at the dorso-lateral edge of DM2v (Fig. 13, D). DM2d and DM2v are the small subdivisions of DM, with DM1 and DM2c being much larger (Giassi et al., 2012a; 2012b; 2012c; Harvey-Girard et al., 2013) and the connections of these small regions and DD are not strong. Further, in agreement with Giassi et al (Giassi et al., 2012b), no connections of DD with the dorsal posterior pallium (DP), the main olfactory territory (Sas et al., 1993).

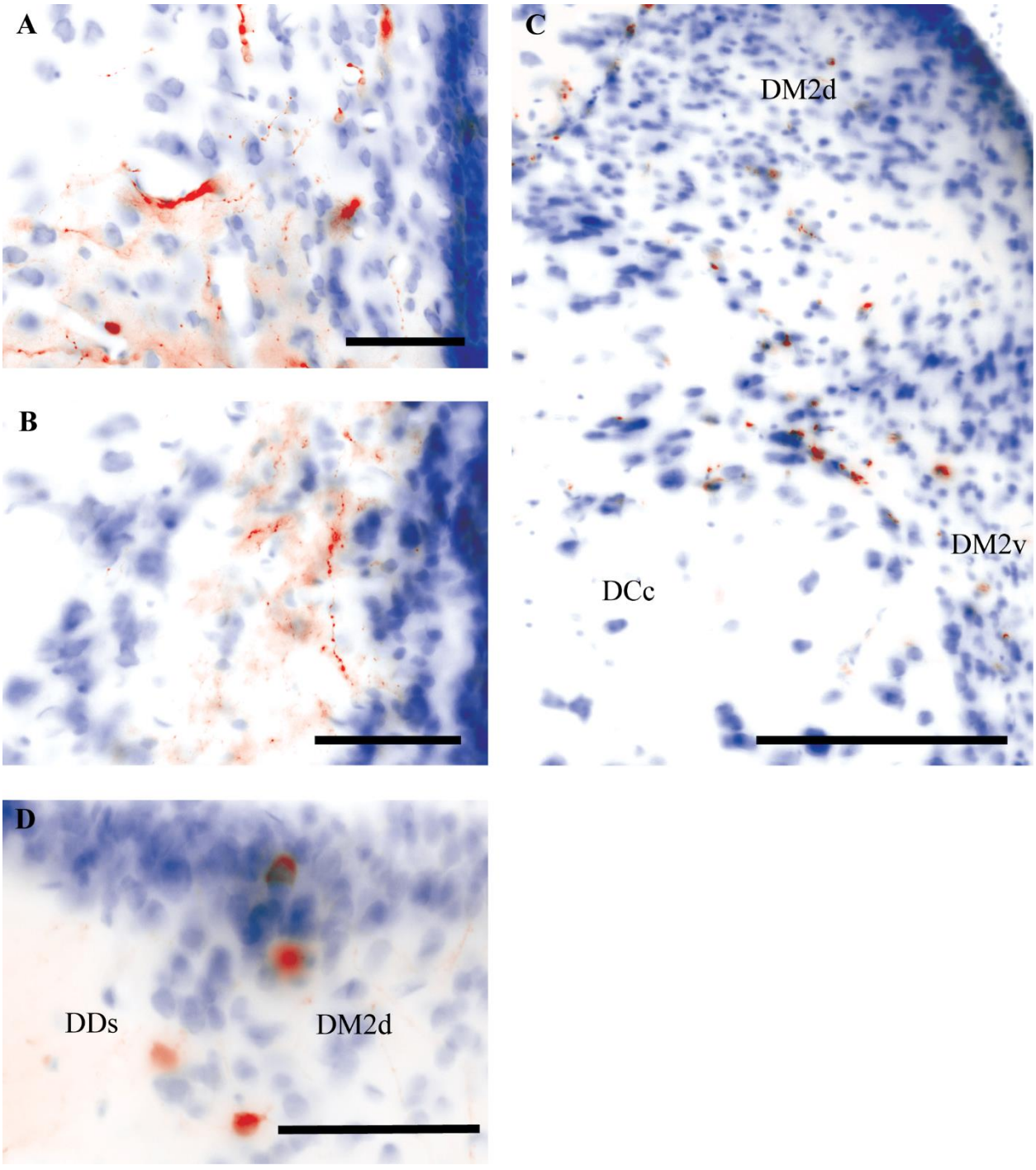

Figure 3-13: Connections between DD and DM2

A: Terminals stained in DM2v following injection in DDi. **B:** Terminals stained in DM2v following injection restricted to DDmg. **C:** Terminals stained in both DM2d and DM2v following injection in DDs. **D:** Cells labeled in the dense grouping of cells at the lateral boundary of DM2d adjacent to

DDs following injection in DDmg. Dorsal and lateral surfaces are top and left respectively for all panels. Scale bar A-D is 50 µm.

LOCALIZATION OF CONNEXIN 35 IN THE SUBPALLIUM

As part of other studies, we cloned *A. leptorhynchus* connexin-35. We briefly describe its localization in the subpallium because of the relevance of this information to our discussion of DD/DL function.

Among the several types of connexin, connexin-35 (the homolog of tetrapod Cx-36 in teleosts) is specific to neurons (Sohl et al., 2005; Harris and Locke, 2009). We performed a degenerate PCR from a whole brain cDNA library using primers targeting conserved regions of connexin-35 (Cx35) which resulted in a cDNA fragment 899 base pairs in length. After cloning we randomly selected and sequenced three of these clones, which presented identical sequences. The predicted amino acid sequence of AptCx35 was aligned with similar regions of its vertebrate orthologs which included amino acid sequences from zebrafish Cx35 and from Cx36 of five tetrapods (Fig. 14 A). The partial AptCx35 amino acid sequence is 75.2% similar to the zebrafish Cx35 sequence and 70.6% similar to its human Cx36 homolog. The four transmembrane segments, displayed by a black bar, show a high level of conservation, between 90 to 100%, with zebrafish and human homologs. The N-terminal helix segment forming the pore region (shaded bar) and the Cx signature 1 segment (pale gray bar) are perfectly conserved among all homologs. The Cx signature 2 segment (dark gray bar) is conserved at 88% between AptCx35 sequence and its zebrafish and human homologs, while the calcium binding domain (white bar) is identical at 80% in amino acid identity. Furthermore, a PKA site involved in perch Cx35 PKA modulation is

conserved at S-110 in AptCx35 (Mitropoulou and Bruzzone, 2003). This high conservation level in functional sites strongly suggests similar functionality of neuronal connexins in *A. leptorhynchus*.

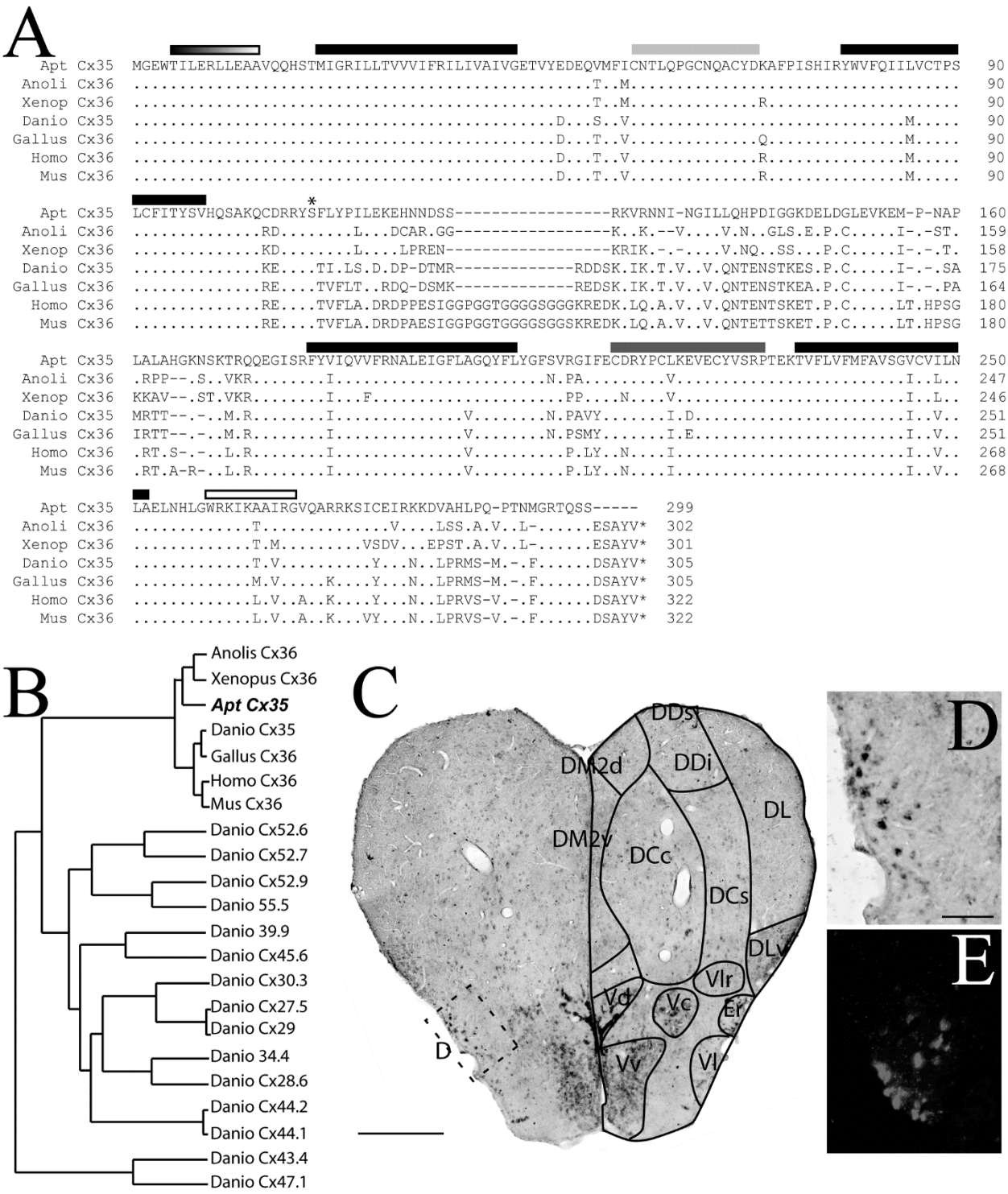

Figure 3-14: Sequence analysis of Apteronotid Cx35 and *in situ* hybridization in *A. leptorhynchus* telencephalon

A: Predicted amino acid sequence alignment of AptCx35 with zebrafish Cx35 and five Cx36 homologs from tetrapods (a lizard *Anolis carolensis*, an amphibian *Xenopus leavis*, a bird *Gallus gallus*, and two mammals *Mus musculus* and *Homo sapiens*). Shaded bar: N-terminal helix; black bars: transmembrane segments; pale gray bar: sequence of connexin signature 1; dark gray bar: sequence of connexin signature 2; white bar: calcium-binding domain; * : PKA phosphorylation site (Mitropoulou and Bruzzone, 2003; Harris and Locke, 2009). **B**: Phylogeny tree made using PHYLIP (Felsenstein, 1989; RRID: SCR_006244) of AptCx35 and the connexins-35/36 used in panel A and 15 paralog connexin amino acid sequences from zebrafish expressed in the whole body. AptCx35 was aligned against orthologs of Cx35/36 from different vertebrates which included anole (*Anolis carolinensis*; XM_003229683.2), chicken (*Gallus* gallus; NM_204582.1), human (*Homo sapiens*; NM_020660.2), mouse (*Mus musculus*; NM_010290.2), African clawed frog (*Xenopus laevis*; XM_002939244.3) and 16 connexin paralogs from zebrafish (*Danio rerio*; Cx47.1 - XM_005163657.2, Cx43.4 - NM_131069.2, Cx44.1 - NM_131809.2, Cx44.2 - AF304050, Cx27.5 - AF304049, Cx28.6 - BC162878.1, Cx29 - NM_131811.2, Cx30.3 - NM_212825.2, Cx34.4 - XM_005158501.2, Cx35 - BC162926.1, Cx39.9 - NM_212826.1, Cx45.6 - GU363508.1, Cx52.6 - XM_005160517.2, Cx52.7 - NM_001113502.1, Cx52.9 - EU190985.1, Cx55.5 - AF304048.2. **C**: Low magnification of a telencephalic section rostral to the anterior commissure showing antisense AptCx35 RNA probe labeling made by *in situ* hybridization. AptCx35 is expressed in Er but not in Vl. The dashed rectangle area is displayed in panel D at a higher magnification. **D**: High magnification image displaying a high level of mRNA transcript expression of AptCx35 in Er. **E**: High magnification of the Er nucleus showing immunostaining of GABA as done previously by Giassi et al. (2012c). Scale Bar C is 500 µm; Scale bar D-E is 50 µm.

As the connexin gene family is quite large, we did a phylogenetic comparison of AptCx35 with 21 connexin amino acid sequences (Fig. 14 B); the previous zebrafish Cx35 and the five tetrapod Cx36 orthologs (Fig. 14 A), and also 15 different connexin sequence paralogs from zebrafish. Overall, our phylogeny analysis shows that AptCx35 is closely related to the subgroup of Cx-35/36 (Fig. 14 B).

We performed *in situ* hybridization in order to localize AptCx35 in *A. leptorhynchus* adult telencephalon as we did previously with several RNA probes (Harvey-Girard et al., 2007; 2010;

2013). Figure 14 C displays a low magnification of a telencephalic section rostral to the anterior commissure labeled with the antisense AptCx35 RNA probe (the sense probe did not show any labeling, data not shown). The AptCx35 RNA probe strongly labeled several subpallium structures. Vd, Vc and Vv are strongly labeled by the AptCx35 RNA probe. Most relevant to this work, the neurons of Er express high level of AptCx35, which becomes more evident at high magnification (Fig. 14 D). These large neurons of Er also express high level of GABA as previously indicated (Giassi et al., 2012b) (Fig. 14, E).

DISCUSSION

Our analysis of DD circuitry is consistent with and greatly extends our previously reported studies on the interconnectivity of DD with DL, DC and the subpallium (Giassi et al., 2012b). While our earlier studies relied on large DD injections that encompassed all three DD subdivisions - DDi, DDs and DDmg – we now report on tracer injections confined to a single subdivision. This has allowed us to analyze the intrinsic connections of DD, and to clarify the complex relations of DD with DL, DC, and subpallium. It is clear that not only is DD a very distinct component of the gymnotiform pallium but that, despite its small size, it is differentiated into three very distinct subdivisions, each of which has very different intrinsic and extrinsic connectivities. In addition to the differences in connectivity, the DD subdivisions are also functionally distinct: cells in DDs are spontaneously active *in vivo* while DDi/DDmg cells are silent but can be switched into activity ('Up states') by electrosensory or acoustic stimuli (Elliott and Maler, 2015).

This discussion is composed of five parts. We first briefly summarize overall DD connectivity. Second, because of its comparative and functional importance, we discuss in more

detail the intrinsic connectivity of DDi and the connections between DDi and DDmg. Third, we turn to possible homologies between DD of *Apteronotus* and a similarly situated region in the pallium of cichlid, goldfish, and zebrafish. This is especially important because of recent functional studies of this region in the zebrafish pallium (Aoki et al., 2013). Fourth, we show that our connectivity and immunohistochemical data implies very precise analogies with the circuitry of the mammalian hippocampus. We discuss whether these analogies indicate homologous circuitry. Last, we use the parallels between the DD/DL circuitry and hippocampal circuitry to draw concrete conclusions as to the function of DD. In all cases, we strive to make testable predictions that flow from our hypotheses.

In this Discussion we refer to five species of teleosts. Four of these species are grouped in the otophala clade: *A. leptorhynchus* and *Gymnotus carapo*, are further classified in the order of gymnotiforms, while *Danio rerio* (zebrafish) and Carassius auratus (goldfish) are in the order of cypriniforms. The last species is a cichlidae, *A. burtoni*, and is therefore more distant from the other species as it is part of the clade of euteleostei.

SUMMARY OF OVERALL DD CONNECTIONS (SEE FIG. 15)

CONNECTIONS WITHIN AND ACROSS DD SUBDIVISIONS (FIG. 15A).

DDi and DDs have strong intrinsic connections while those within DDmg are minor. We have shown that DDi is a strongly connected random network and is very likely a small world network. DDi has a strong projection to DDmg while the reciprocal DDmg to DDi projection is minor. Finally, DDs has small unidirectional projections to both DDi and DDmg.

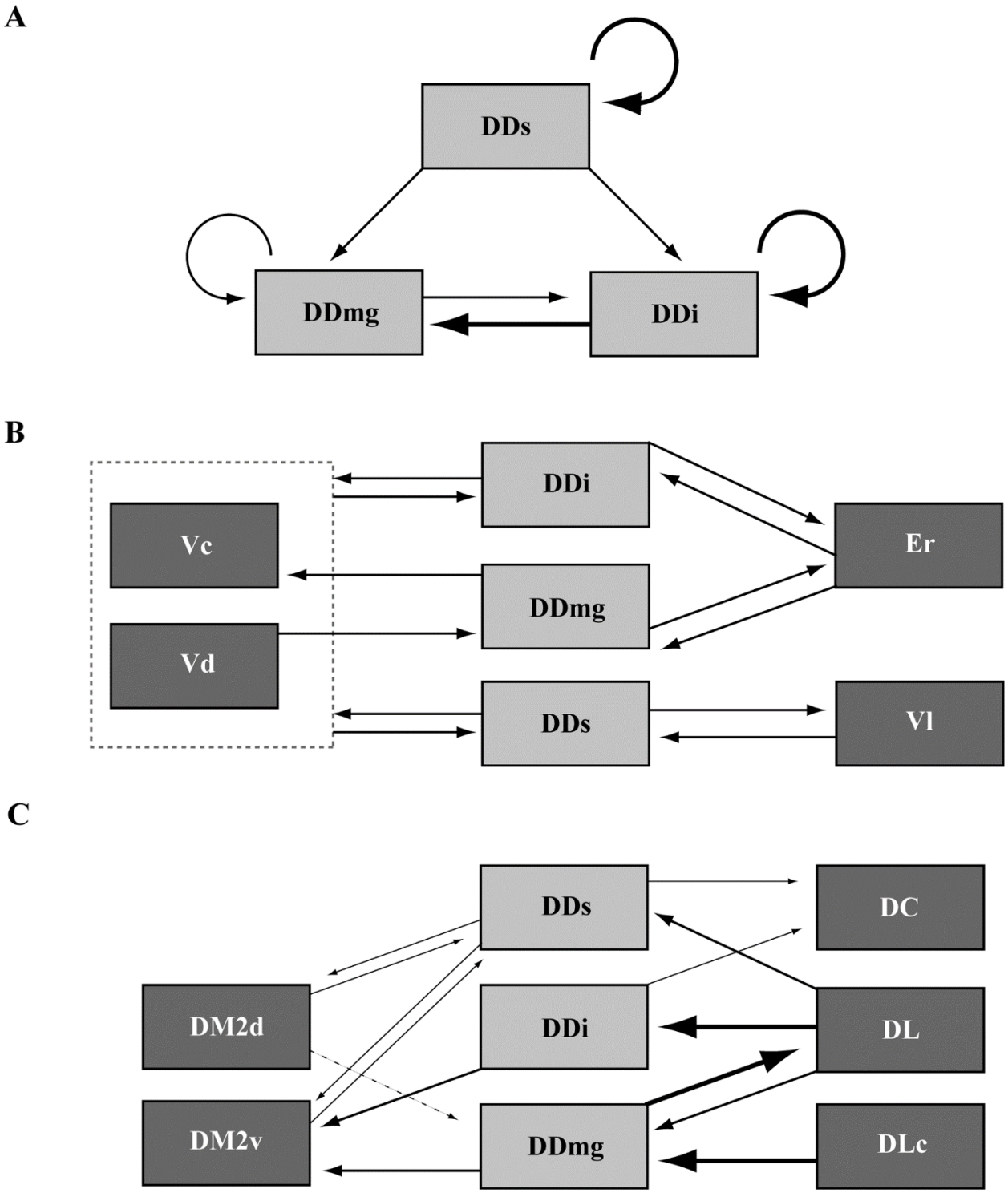

Figure 3-15: Summary of DD connections

The thickness of the arrows represents our estimate of the strength of the connections with dashed lines indicating the weakest of projections considered. The direction of the arrows

represent the direction of the projections. **A:** Intrinsic connections of DD. Recurrent connections are indicated by the curved arrows. **B:** DD connections wih the subpallium. **C:** Connections of DD with the pallium.

CONNECTIONS OF DD WITH SUBPALLIUM (FIG. 15B)

DDi and DDs have reciprocal connections with Vc and Vd; in contrast, DDmg projects to Vc and receives input from Vd. As previously discussed (Harvey-Girard et al., 2013) we have identified Vc/Vd as part of the gymnotiform striatum and the pallial projections as likely arising from dopaminergic neurons. Below we discuss the implications of the DDi projections to Vc/Vd.

DDi and DDmg both have reciprocal connections with Er; below we discuss the implications of these connections. Lastly, DDs has very minor reciprocal connections with Vl.

CONNECTIONS OF DD WITH OTHER AREAS OF PALLIUM (FIG. 15C)

As previously proposed (Giassi et al., 2012b), the strongest DD connections are the DL to DDi projection, the DLc to DDmg and the DDmg to DL projection. There are additional projections of DL to DDmg dendrites and DL to DDs. There are therefore three loops connecting DL to itself via DD emphasizing the importance of DD and DL interactions. The strongest loop is DL->DDi->DDmg->DL; the other two loops are a short loop: DLc/DL->DDmg->DL; and a long loop: DL->DDs->DDi->DDmg->DL. In all cases, DDmg is the final common source of DL input.

DL projects massively upon DC (Giassi et al., 2012b). There are also small indirect pathways from DL to DDi and DDs and DDi/DDs to DC. These appear to have a relatively restricted terminal zone within dorsal DC. Lastly there are minor connections between DD and DM2d and DM2v.

ANALYSIS OF DDI INTRINSIC CONNECTIVITY

In a previous report, we analyzed intra-DL connectivity and found that it was highly local and organized into cryptic layers and columns (Trinh et al., 2015). We therefore carefully examined connectivity with each DD subdivision for any hint of spatially organized connectivity. DDmg has very sparse intrinsic connectivity and we were not able to discern any spatial preference. DDs has strong intrinsic connectivity. This subdivision is narrow in the dorsal-ventral direction (Fig. 2A-D) and, again, no spatial preference was observed. Our sample size for DDs was insufficient for a more quantitative analysis using graph theory.

DDi intrinsic connectivity is strong and, given our large sample size, we were able to analyze it in detail. Simple observation did not indicate any laminar, columnar, or any other spatial organization of this connectivity. In order to be completely certain, we re-plotted the labeled cells (from confocal stacks) in spherical coordinates – the retrogradely labeled cells were isotropically distributed (not shown). We conclude that the intrinsic connectivity of each pallial subdivision is specific to that region and, presumably, linked to its function (see below).

Our graph theoretic analysis showed that DDi is likely strongly connected for spherical diameters greater than 130 µm; this is just slightly larger than the ~100 µm diameter estimated for strong connectivity in DL (Trinh et al., 2015). However, further analysis shows that the pattern of recurrent connectivity is entirely different in DDi as compared with that found in DL. DL is approximately 2000 µm in its rostro-caudal dimension and the maximal distance of recurrent connections is ~150 µm. It therefore takes at least 13 synaptic steps to go from end to end in DL. In contrast, DDi is ~680 µm and the maximally distant recurrent connection is ~400 µm. It

therefore takes less than two synaptic steps to traverse the full extent of DDi. We conclude that DL is a local recurrent network (LRN) while DDi is a global recurrent network (GRN) and this distinction has important implications as to their respective functions (see below).

The striking differences in the staining intensity across retrogradely labeled DDi cells (Figs. 5, 6,7) suggests a much stronger hypothesis: that DDi is a small world network (SWN). A SWN has two characteristic features (Durrett, 2007; Bullmore and Sporns, 2009; Newman, 2010; Bullmore and Sporns, 2012) which we crudely describe here. First, a SWN is clustered, i.e. two nodes (neurons) that connect to a third node are likely to be connected to each other. Second, only a few intermediate nodes are required to connect any two nodes in the network. This second attribute is typically demonstrated by showing that the fall-off in probability of connectivity is a long-tailed distribution, i.e. that it decays much more slowly than expected from an exponential distribution. We were able to successfully fit an exponential curve to the spatial decay in connection probability (Fig. 6A). The exponential fit was not, however, very good at accounting for the most distant connections (Fig. 6D) and this difficulty would have been greater had we been able to correctly model the spatial decay. It is notoriously difficult to fit long tailed distributions to data simply because there are few data points in the tails of the distribution. We do not consider our exponential fit as ruling out a long tailed distribution and therefore not ruling out the possibility of DDi being a SWN.

The combination of clustering and a long-tailed distribution of connection probability endow a SWN with the ability to do both efficient local computations and rapidly convey these computations to every other node in the network.

How do we interpret the different intensities of retrograde labeling in DDi? We hypothesize that the reason that some cells are strongly labeled is because they make more synaptic contacts on the cells within the tracer injection site; that is, that strong labeling indicates strong synaptic connectivity and therefore that weak labeling indicates weaker synaptic connectivity. We note that cells can be 'strongly' connected out to a radius of ~130 µm (Fig. 6A,C) and that this encompasses the region of strong connectivity; in contrast, 'weak' connectivity is almost entirely associated with the longer range connections (Fig. 6C,D,E,F). We therefore further hypothesize that the 'strongly' connected DDi cells form local clusters over a radius of ~130 µm while the 'weakly' connected cells permit rapid transfer of the 'cluster' computations to other, more distant, clusters. Remarkably, a similar architecture exists in cortex where the neurons with the most input and output connections are also connected strongly with each other (Bullmore and Sporns, 2012; Nigam et al., 2016). There is even evidence that cortical neurons with the same signal specificity (i.e. orientation tuning) are preferentially connected by strong synapses (Cossell et al., 2015). This result is consistent with a theoretical analysis performed by Siri et al. (Siri et al., 2007). They suggest that small world networks will automatically form when the synapses of a random neural network are endowed with Hebbian synaptic plasticity. In this case, an input pattern will cause the connections between neurons with correlated activity to strengthen so that the network becomes maximally sensitive to the "learned" pattern. This further implies that the DDi network may be capable of performing pattern completion (see below).

DDi to DDmg projections are very strong but the cells of origin are confined to approximately the caudal third of DDi. This has two interesting implications. First, there is possibly further differentiation of DDi with respect to its DL input. Second, the recurrent activity

in DDi will have to spread to its caudal third before it can influence DDmg and its feedback projections to DL. The consequences of these arrangements are currently not known.

DOES DD EXIST IN OTHER TELEOSTS AND, IF SO, WHAT IS ITS FUNCTION?

Here we discuss the possible identity of DD in three teleost fish where there is sufficient published material to make a tentative comparison: a cichlid fish (Burmeister et al., 2009), the goldfish (Northcutt, 2006), and the zebrafish (Aoki et al., 2013). There are no detailed studies of DD circuitry in any of these fish but there are important behavioral and physiological studies that we discuss below.

Detailed ethological analyses by Fernald and colleagues (Fernald, 1977; Fernald and Hirata, 1977) have revealed intricate communication and social interactions of the African cichlid fish, *Astatotilapia (Haplochromis) burtoni*, including dramatic changes of body color patterns that indicate male social status. The pallium of *A. burtoni* is highly differentiated (Burmeister et al., 2009). Close examination of Fig. 2 of this paper suggests that a DD with similar location and cytoarchitectonics is also present in these fish. The region labeled 'DC2' is located between DM and DL and delimited by clear sulci. DC2 cell organization in panel A is similar to that of DDi while, in panel B, it is very similar to DDmg. We propose that DC2 of *A. burtoni* is homologous to DD of gymnotiform fish. A very large putative DD with a more lateral location is identified in Fig. 4 of Burmeister et al. but, based on its location, it may be a subdivision of DL. Due to the poor quality of the Nissl staining in this paper however we acknowledge a plausible alternate interpretation with DC2 homologous to DDmg and Dd-d homologous to DDs/DDi. A clarification of these issues, and thus the possibility of correct comparison with gymnotiform and other teleost fish will

require detailed immunohistochemical and connectivity studies of the *A. burtoni* pallium (see below). This is important because extensive studies have shown that the expression of the immediate early gene Egr-1, which has been linked to long-term social memory in *Apteronotus* (Harvey-Girard et al., 2011), is highly conserved in this species (Burmeister et al., 2005). Fernald and colleagues have shown that social interactions can induce Egr-1 expression in various brain regions, including DL and DM (Burmeister et al., 2005; Maruska et al., 2013a; 2013b; Desjardins et al., 2015). These studies were done using micro-dissected brain regions and did not evaluate Egr-1 mRNA expression in DC2 (DD?). Based on our work we predict that, when the fish receives social stimulation, the DC2 (DD?) region will show very strong increases in Egr-1 mRNA expression (Harvey-Girard et al., 2011) as well as a specific electrophysiological response – induction of Up states (Elliott and Maler, 2015). We believe that *A. burtoni* is an outstanding system to investigate the neural bases of social learning and, in particular, the interactions of DD and DL in such learning.

Northcutt (2006) has identified DD in the goldfish pallium; its location and wedge shape are similar to that of gymnotiform fish and it also projects to DL and possibly DM. On this basis, we assume that DD in gymnotiform and gold fish are homologous. Detailed behavioral studies have shown that, in the goldfish, spatial learning is impaired or eliminated following DL lesions whereas simple 'emotional learning' such as fear conditioning remains intact (Broglio et al., 2005). These authors reported the opposite result following DM lesions: 'emotional learning' is greatly impaired while spatial learning is not affected. An important result concerns avoidance conditioning because it allows us to connect DD function in goldfish and zebrafish. In this paradigm the fish is in one chamber but has access to a second chamber. A cue (conditioned

stimulus, e.g. light) is presented in the test chamber followed by an aversive unconditioned stimulus (e.g. an electric shock). The fish then has to learn that, upon presentation of the light stimulus, it has to escape to the second chamber and thus avoid the shock. An important distinction in this paradigm is in the relative timing of the cue and shock. If the shock is delayed but still overlaps the cue, then this is termed 'delay avoidance conditioning'. When a short time (e.g. 5 s) intervenes between the end of the cue stimulus and shock, it is termed 'trace avoidance conditioning' since there must be a memory trace of the cue to associate with the subsequent non-overlapping shock. Lesions of DM disrupt delay avoidance conditioning while DL lesions have no effect. In contrast, trace avoidance conditioning is disrupted by lesions of either DM or DL (Broglio et al., 2005); similar results are reported for hippocampal lesions in rodents – they disrupt trace but not delay conditioning – and this has led these authors to support the putative homology of DL and hippocampus. Most importantly, DD lesions also disrupt trace but not delay conditioned avoidance memory retrieval. It is important to note that the initial acquisition of the trace avoidance response is not affected by these lesions (Vargas et al., 2009). These results are critical for our interpretation of the experiments on zebrafish presented below. Based on our anatomical results, we hypothesize that the 'trace' of the cue stimulus must be maintained in the reciprocal connections of the DD and DL recurrent networks.

A DD region is difficult to discern in zebrafish and it has been suggested (Mueller et al., 2011) that it may not be a valid subdivision of the teleost pallium. Instead, these authors have suggested that DC extends to the surface of the pallium and intervenes between DM and DL. This issue becomes critical in the light of an important recent paper (Aoki et al., 2013). Aoki and colleagues used an active avoidance conditioning paradigm and emphasized that it is a form of

reinforcement learning where, after the cue (light) and aversive stimulus (shock) are associated, the cue initiates an escape response before the shock is delivered. This paradigm was not explicitly presented as either delay or trace avoidance conditioning. The light cue was presented for 15 s and, if the fish had not avoided the shock (by swimming to a connected compartment) it was then shocked. There was never any overlap of cue and shock and so this is not delay conditioning, but there was also no time interval between cue and shock and so it might be considered 0 interval trace conditioning; this subtle distinction is important for the discussion below. The key result of this paper is that, 24 hours (but not 30 minutes) after learning, the cue evoked a Ca^{2+} signal in cells within a circumscribed superficial pallial region. Aoki et al reasoned that this region is an essential component of memory retrieval. When Aoki et al. lesioned this region, cue avoidance acquisition was normal but there was no memory of cue-shock pairing 24 hours later; again, they reasoned that this region is important for long-term storage and/or retrieval of such memories. We note the similarity of this result with those reported in the Vargas et al paper (2009; DD lesion) described above. There is no question as to the validity and importance of these results and conclusions. The key question for this Discussion is the identity of the region identified by Aoki et al. (2013); we argue that it is, in fact, DD.

The 'memory' region illustrated in all the Figures of Aoki et al. (2013) is clearly located between DM and DL. The authors, following Mueller et al. (2011), suggested that DC reaches the dorsal edge of pallium without an intervening DD. However, the connections of this region are consistent with those of the apteronotid DD and not DC (nor with those of DL or DM). Aoki et al. (2013) reported that injections into this region resulted in strong labeling of fibers in the anterior commissure, and anterograde labeling within the ventral dorsal (Vd) region. In addition, there

was both anterograde and retrograde labeling within a nucleus containing GABAergic neurons and described as the dorsal entopeduncular nucleus (dEP). We hypothesize that dEP is identical to Er (see below). There was no efferent projection to the midbrain torus semicircularis or tectum. This entire connectivity pattern is consistent with that of the gymnotiform DD and not DC, DL or DM as shown in this paper and our previous work (Giassi et al., 2012a; 2012b). In addition, although not reported explicitly, Fig. 4H illustrates labeled fibers in DL following a DD tracer injection; again this is consistent with the connections of DD and not DC. Further support for this idea is found in Supplementary Fig. S4I. This image illustrates the distribution of cannabinoid receptors (CB1R) in pallium. A comparison to the distribution of CB1R mRNA in *Apteronotus* (Harvey-Girard et al., 2013) suggests close agreement with the apteronotid pattern: a medial region (DM) has strong CB1R expression as does the rostral DL. In between these CB1R positive regions lies a region devoid of CB1R label consistent with our demonstration that DD lacks these receptors in *Apteronotus*. As noted above, lesions of DD in goldfish block retrieval, but not acquisition, of trace avoidance conditioning memories (Vargas et al., 2009); again this is entirely consistent with the results reported in Aoki et al. (2013). There remains one important difficulty – avoidance conditioning uses a fear inducing stimulus (shock) and, as described by (Broglio et al., 2005), involves DM in both the delay and trace training conditions. In gymnotiform fish, DD connects strongly to DL and minimally to DM and this would seem to contradict our hypothesis. A clue that may explain this apparent contradiction is seen in the movies within the Supplementary Information of Aoki et al. (2013). When presented with the light cue, the trained zebrafish successfully avoids the shock by immediately turning and heading toward the entrance to the neutral compartment. In other words, we suspect that the fish is performing spatial as well

as trace avoidance learning. Given the importance of DL for spatial learning (see above), this may be one reason why DD, with its extensive connections to DL, is critically involved. We also note that this confound was likely present in our earlier paper on induction of Egr1 expression by social signals, since the fish swam toward the dipoles emitting the electric communication signal (Harvey-Girard et al., 2010).

We hypothesize that DD is present in all teleosts and, as already suggested by Aoki et al. (2013), is critical for the formation and retrieval of many forms of memory, including those generated by spatial, reinforcement, and possibly social learning. In all cases, we hypothesize that this requires sustained activity in a loop comprising the recurrent networks of DD and DL. This hypothesis requires strong evidence for the homology of the gymnotiform DD with that of at least goldfish, cichlid fish and zebrafish. Here we present the most salient predictions by which our hypothesis can be judged. DD in goldfish, DC2 in *A. burtoni* and the 'retrieval' region in zebrafish should be negative for CaMKIIα (Giassi et al., 2012c) and this should contrast with the strong expression of this second messenger enzyme in the adjacent DL, DM and DC. The putative DD should have strong reciprocal connections with ipsilateral DL as well as connections to the subpallium and contralateral DD and DL as described here and previously reported (Giassi et al., 2012b). DD should have very strong intrinsic recurrent connections (see Results). Neurons in DD should go into Up state activity when the fish is presented with appropriate stimuli (Elliott and Maler, 2015); the stimuli may well be species-specific, e.g. social signals in *A. burtoni* and cues for trace conditioning in goldfish and zebrafish. Such stimuli should also induce the strong expression of Egr-1 mRNA. On a more speculative note, we propose that Egr-1 activation may be

a necessary intermediate step between the initial learning and the subsequent (24 hours) Ca^{2+} signal seen by Aoki et al. (2013) in zebrafish pallium (DD?).

ANALOGOUS DD/DL AND HIPPOCAMPAL CIRCUITRY

PRELIMINARY BACKGROUND.

CONSERVED ORIGIN OF TELENCEPHALIC GABAERGIC NEURONS.

In mammals telencephalic GABAergic neurons are derived from the subpallial ventricular zone and mainly from its medial ganglionic eminence; these include the neurons of the basal ganglia, as well as GABAergic interneurons of the hippocampus and cortex (Pleasure et al., 2000; Marin and Rubenstein, 2001; 2003). Detailed analyses have revealed the genetic mechanisms that determine the final targets of the migrations to the basal ganglia versus the tangential migrations to cortex (Marin and Rubenstein, 2001; 2003). Studies in the zebrafish indicate that these are highly conserved genetic pathways which specify the fate of telencephalic GABAergic neurons (MacDonald et al., 2010; Yu et al., 2011). In addition, the distribution of these genes in the developing zebrafish subpallium is also consistent with their role in the specification of the basal ganglia as well as the dorsally migrating neurons that reach the pallium (Mueller et al., 2008).

CONSERVED ORGANIZATION OF VERTEBRATE BASAL GANGLIA.

The organization of the mammalian basal ganglia has been extensively documented and reviewed; here we use a comprehensive review (Gerfen and Bolam, 2010). In brief, GABAergic striatal neurons project to the external and internal divisions of the globus pallidus (GPe and GPi, respectively); in primates, GPe and GPi are directly contiguous while, in rodents, GPi is separated

from GPe and is referred to as the entopeduncular nucleus. The striatal GABAergic neurons express either Substance P (SP) or encephalin (Enk). The SP containing GABA cells preferentially innervate the GPi (entopeduncular nucleus), while the Enk GABA cells preferentially project to the GPe. GPe projects to the entopeduncular nucleus and it, in turn, is the main output pathway of the basal ganglia; a key target of the entopeduncular nucleus is the lateral habenula (Herkenham and Nauta, 1977). The striatum receives a dopaminergic (DA) input from the midbrain substantia nigra. A remarkable new discovery has revealed that the individual entopeduncular cells that project to the lateral habenula can release both GABA and glutamate and transmit aversive (anti-reward) signals (Shabel et al., 2012; Shabel et al., 2014).

The organization of the basal ganglia appears to be highly conserved in at least reptiles and birds (Reiner, 2010). The globus pallidus, however, does not appear to be separated into external and internal divisions since the SP and Enk containing striatal efferents are intermingled within it.

While the details of basal ganglia structure in elasmobranchs have not been entirely clarified (Reiner, 2010), recent studies have shown that the entire basal ganglia circuitry may be conserved even in lampreys (Stephenson-Jones et al., 2012).

WHAT ARE ER AND VL?

Extensive early studies already identified the dorsal portion of the ventral division of the subpallium (Vd) as the teleost striatum (Reiner, 2010). This conclusion has been completely vindicated in a recent study of the adult zebrafish that used the combinatorial expression pattern of many genes found in pallium and subpallium of mammals (Ganz et al.,

2012). In gymnotiform fish, the striatal region is slightly more elaborate and, on the basis of the presence of DA innervation, SP+ cells and cannabinoid receptors (AptCB1R), also includes central (Vc) and intermediate (Vi) regions (Harvey-Girard et al., 2013).

The identity of the teleost pallidum has remained more elusive although numerous studies had suggested that the ventral part of the ventral division of the subpallium (Vv) might be the pallidum (Reiner, 2010). An important clarification was provided by Ganz et al (2102) who suggested that the dorsal part of Vv was homologous to the GPe while its ventral part corresponded to the septum; this hypothesis was strengthened when we showed that the distribution of AptCb1R was entirely consistent with this interpretation (Harvey-Girard et al., 2013).

Based strictly on its location and previous literature, we labeled two laterally located subpallial cells groups as the rostral entopeduncular nucleus (Er) and the ventral lateral subpallium (Vl) (Maler et al., 1991). The Er consisted of mostly large cells located at the edge of the subpallium and dorsal to the anterior commissure (AC); Vl consisted of smaller cells and was located ventral to the AC. Mueller and Guo (Mueller and Guo, 2009) described two GABAergic cell groups that appear identical to the Er and Vl of Maler et al. (1991); the GABAergic character of these cells in *Apteronotus* was confirmed in Giassi et al. (Giassi et al., 2012c). Based on cell size, Mueller and Guo (2009) suggested that the dorsal group was homologous to the mammalian entopeduncular nucleus and therefore labeled it EN (formerly, ENd, Vl was formerly named ENv). Ganz et al (2012) examined the expression pattern of dlx and nk2 genes and concluded that, in agreement with Mueller and Guo (2009), the zebrafish EN (Er, ENd) was homologous to the

mammalian entopeduncular nucleus. The nature of Vl (ENv) was not clarified in either of these papers.

Okamoto and colleagues have made remarkable progress to clarify this issue – to summarize, they have proposed that ENv (Vl) is homologous to the entopeduncular nucleus. Amo et al. (2010) first identified the zebrafish lateral habenula (LH) and located it ventral to the medial habenula. Subsequently, Amo et al. (2014) demonstrated that the zebrafish LH projected to the raphe and received input from ENv exactly as expected from the LH connections in mammals. Most remarkably, they also demonstrated that ENv cells expressed the vesicular glutamate transporter (vglut2a) and that their target LH cells responded to aversive stimulation. Therefore, these authors demonstrated that ENv (Vl) has the connectivity, dual GABA/glutamate transmitters, and function corresponding to the entopeduncular nucleus of mammals. We consider this to be very strong evidence of homology and here provide supporting evidence from the literature on gymnotiform fish. (A) Vv and Vl are innervated by SP (Weld and Maler, 1992) and Enk (Richards and Maler, 1996) immunoreactive fibers as would be expected for GPe and GPi (entopeduncular nucleus); these peptides are not found in Er (ENd?). From the location of SP and Enk cell bodies and the fiber trajectories, we hypothesize that this peptidergic innervation of Vv and Vl arises from cells within Vd, Vc, Vi (gymnotiform striatum), although this remains to be rigorously proven. (B) Vv appears to project to Vl but not Er (Wong, 1997); this presumably corresponds to the projection of GPe to the entopeduncular nucleus (GPi). (C) Finally, Vl neurons are somatostatin positive (Sas and Maler, 1991) as are many entopeduncular neurons (Vincent and Brown, 1986). The somatostatin positive entopeduncular neurons project to LH (Vincent and Brown, 1986). Correspondingly, Sas and Maler (1991) illustrate a very dense somatostatin

innervation in a small region immediately ventral and lateral to the medial habenula of *Apteronotus*; this region is presumably homologous to the LH of zebrafish. The conserved expression of somatostatin in neurons of the entopeduncular nucleus suggests an important and unexplored role for this peptide in the basal ganglia regulation of aversive behaviors.

We propose that the terminology be simplified and Vl (ENv) be simply designated the entopeduncular nucleus (EN); here we will refer to it as EN(Vl) so as to remain consistent with the Figure designation (Vl). The full characterization possible in zebrafish may not be necessary for the identification of EN(Vl) in other teleosts; merely the location of a somatostatin positive cell cluster at the lateral edge of the subpallium and ventral to the AC may be sufficient.

Er (ENd) has, as discussed above, none of the key properties of an entopeduncular nucleus. We now propose that Er (ENd) neurons are pallial GABAergic interneurons that have failed to make a complete migration from the subpallial ventricular zone to the pallium (DL and DD), but instead have accumulated at the edge of the subpallium ventral to DL and dorsal to the AC. In particular, we propose that Er (ENd) is homologous to the somatostatin expressing GABAergic interneurons of the pallium and we therefore now suggest that it be abbreviated as P-intSS; in the following we use P-intSS (Er) so as to remain consistent with the Figures. P-intSS (Er) can be recognized in other teleosts by: (A) its strong reciprocal connections with DL and DD; (B) its expression of glutamic acid decarboxylase (GAD), GABA, and somatostatin; (C) its expression of Cx35 and therefore likely gap junction connectivity of its neurons; (D) its afferent input from DD. It is not known whether P-intSS (Er) has any other inputs.

WHAT ARE DL AND DD? TWO ALTERNATIVE HYPOTHESES.

Our first hypothesis was originally proposed by Ito and Yamamoto (2009) and reinforced by Harvey-Girard et al. (2012) and Trinh et al. (2015) and is illustrated in Figure 16. This theory ignores DD and emphasizes the similarity of DL to the input layers of cortex and DC to its deep output layers. The diencephalic preglomerular nucleus (PG) receives sensory input from midbrain regions - tectum and torus semicircularis (TS) - related to object motion and communication signals (Giassi et al., 2012a; Wallach and Maler, 2016). Although not conclusive, a study of the development of the teleost diencephalon has suggested that PG may be homologous to the dorsal thalamus of amniotes (Ishikawa et al., 2007). DL, a major PG target, could then be considered as equivalent, and perhaps homologous to, a cortical input layer; this idea is further reinforced by the laminar and columnar organization of the intrinsic connectivity of DL (Trinh et al., 2015). DL then projects to DC (Giassi et al., 2012b). Based on the projections of DC to tectum and TS, Ito and Yamamoto (2009) suggested that DC was homologous to the deep projection layers of cortex. This idea was reinforced by Harvey-Girard et al's demonstration that DC neurons expressed FoxP2 and Otx1, both markers of cortical deep layers (Harvey-Girard et al., 2012). We assume that the tectum of teleosts and amniotes are homologous and, with less assurance, that DC is homologous to the deep layers of cortex. The parallel between the intermediate connectivity via PG and DL is then also suggestive of a homology between DL and the cortical input layers.

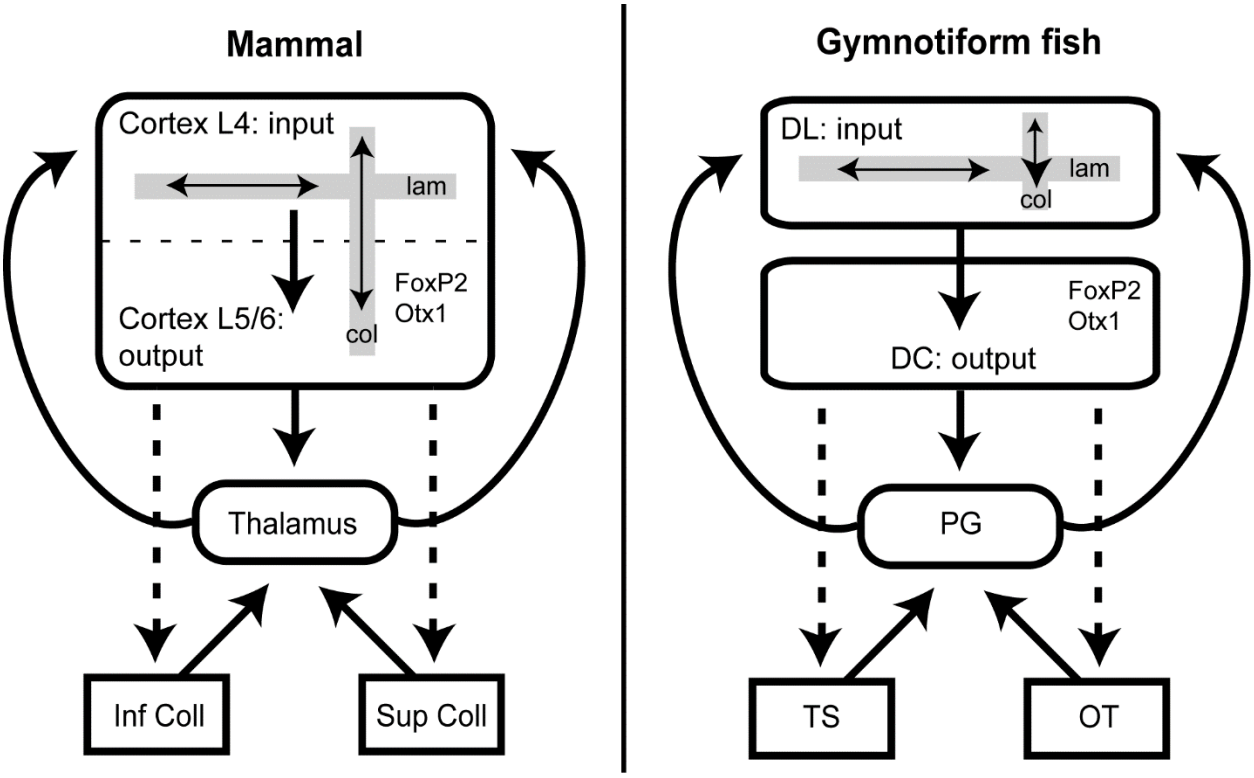

Figure 3-16: A comparison of the connections of mammalian cortex and thalamus with the connections of teleost DL and the preglomerular complex (PG)

We restrict our comparison to the auditory/electrosensory and visual/electrosensory systems where we have the most information for gymnotiform fish. In mammals the inferior and superior colliculi (Inf Coll and Sup Coll respectively) convey auditory and visual input to different nuclei in the thalamus. These thalamic nuclei then project to different cortical regions. These cortical regions in turn provide feedback to the source of their input in thalamus and midbrain. Connectivity in cortex is organized in a laminar (lam) and columnar (col) manner (gray bars and arrows); neurons in the deep (output) layers of cortex express FoxP2 and Otx1.

In gymnotiform fish, the torus semicircularis (TS, electrosensory) and optic tectum (visual, electrosensory; OT) project to PG. Recordings from PG suggest that there is functional segregation of these inputs (Wallach and Maler, 2016). PG in turn projects to DL; there is order in the PG to DL projection (Giassi et al., 2012a) but it cannot be directly linked to the functional segregation of PG input. Connectivity in DL is organized in a laminar and columnar manner (gray bars and arrows). DL in turn projects to DC. DC neurons express FoxP2 and Otx1 (Harvey-Girard et al., 2012). DC projects back to TS, OT and PG (Giassi et al., 2012a). It has been hypothesized that the DC to TS and OT respect function (Giassi et al., 2012a), e.g. the DC cells projecting to OT receive input from OT (via PG and DL) but this is not confirmed. It is also not known whether the

DC to PG projection respects functional boundaries. Overall, however, the parallels of mammalian and gymnotiform ascending sensory pathways to pallium and back to midbrain do show striking similarities.

Our second hypothesis concentrates on the connections between DD, DL, and the subpallium and ignores the connectivity pattern that drove our first hypothesis; this hypothesis is summarized in Fig. 17. The fundamental idea is that DL is homologous to the dentate gyrus (DG), DDmg cells to dentate hilar mossy cells, P-intSS (Er) to the somatostatin expressing hilar GABAergic interneurons and DDi to the CA3 hippocampal field. Here, and in Fig. 17, we present the supporting and contradictory evidence in detail. We do not attempt to incorporate all our data on DD/DL or DG connectivity but emphasize the strongest connections and have selected the comparisons pertinent to our hypothesis.

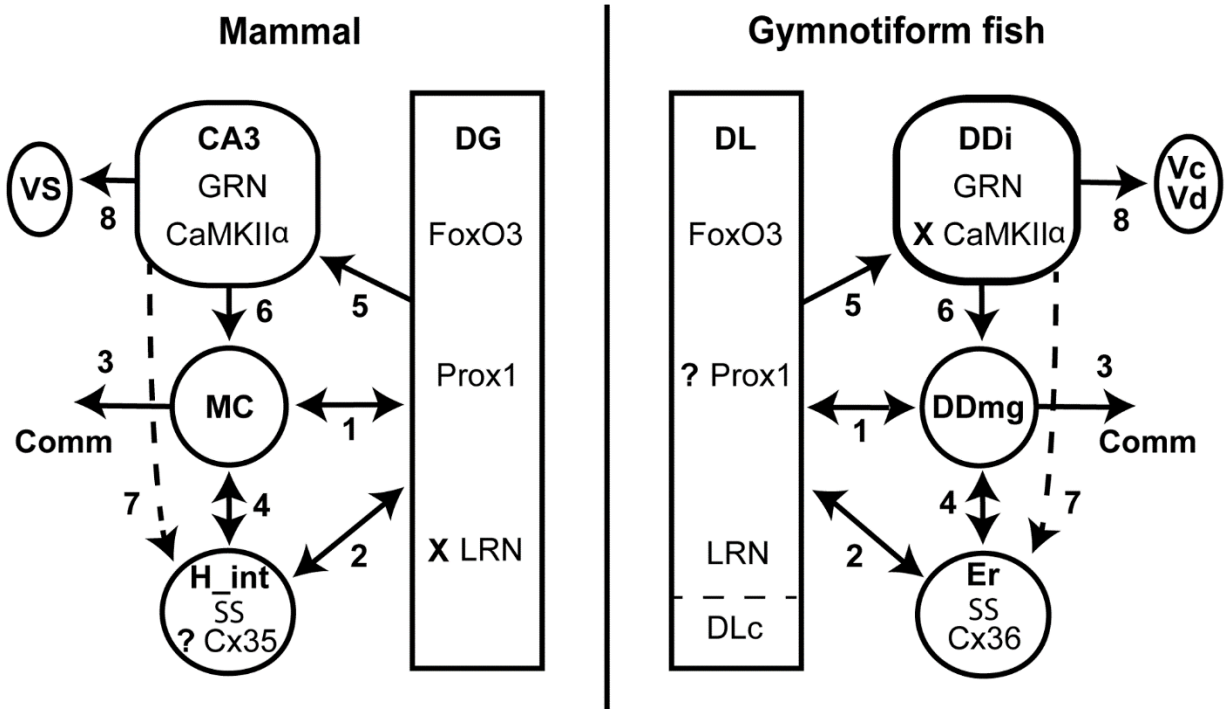

Figure 3-17: A comparison of the mammalian hippocampus and DL/DD

'**X**' indicates absence of a feature and '**?**' unknown. **1.** Dentate gyrus (DG) granule cells/DL connect reciprocally to mossy cells (MC)/DDmg. **2.** DG/DL connects reciprocally with GABAergic hilar interneurons (H_int)/Er. Er neurons are somatostatin (SS) positive as are a subset of hilar interneurons. **3.** MC/DDmg cells have strong commissural connections. **4.** MC/DDmg cells connect reciprocally with H_int/Er neurons. **5.** DG/DL projects to CA3/DDi. **6.** CA3/DDi both have strong global recurrent networks (GRN); they both project to MC/DDmg. This projection in mammals is referred to as the "backprojecting pathway". **7.** CA3/DDi project to H_int/Er. **8.** CA3/DDi project to striatal regions, nucleus accumbens (ventral striatum, VS), and Vc/Vd respectively. The strong parallels of connectivity patterns are evident.

Ganz et al (2014), based on the expression of the Prox1 protein in zebrafish pallium, suggested that DL was, at least in part, homologous to the DG. Prox1 is a precise marker of the adult mammalian DG (Lavado and Oliver, 2007; Lavado et al., 2010; Iwano et al., 2012) and also appears to be a reliable marker for the homologous region of the avian hippocampus (Abellan et al., 2014); the Ganz et al. (2014) hypothesis therefore appears to be solidly based. We tried to replicate this result in the gymnotiform pallium. In our Western blots (data not shown) we did find that the same antibody did label rat brain tissue band at the correct molecular weight. A band at the same location, albeit not as strongly labeled, was found in the gymnotiform telencephalon lane. However, we also found two equally dense lower molecular weight bands for the fish, but not rat, tissue (the Western blots were repeated with many variations and always gave the same result). The Prox1 antibody used by Ganz et al. (2014) is therefore not useful for immunohistochemistry in the gymnotiform fish. We therefore cannot confirm the Ganz et al. (2014) conclusion and this is a weak point of our hypothesis. We do note the DL, DDi, and DDmg cells express FoxO3 (Harvey-Girard et al., 2012). FoxO3 is a molecular marker for hippocampal

neurons including pyramidal cells of CA1/3 and DG granule cells (Hoekman et al., 2006). Therefore, the homology of DL to DG is at least consistent with the expression pattern of this gene.

Under the assumption that DL, including DLc, is homologous to DG, we next hypothesize that its projection to DDmg is equivalent to the DG projection to the hilar mossy cells (Amaral et al., 2007; Scharfman and Myers, 2012). The mossy cells make few recurrent connections amongst themselves (Buckmaster et al., 1996) as is also the case for DDmg cells. DDmg neurons send diffuse feedback to DL as do mossy cells to DG (Buckmaster et al., 1996; Amaral et al., 2007; Scharfman and Myers, 2012); in addition, there is a very large convergence ratio of the DG/DL to the mossy/DDmg cells and, conversely, a large divergence ratio in the feedback projection (Jinde et al., 2013). A strong point in support of this hypothesis is the strong commissural connections of both DDmg, seen in our results and in our previous publication (Giassi et al., 2012b), and the mossy cells (Amaral et al., 2007; Scharfman and Myers, 2012).

In parallel, the DL projection to Er (Giassi et al., 2012b) is equivalent to the DG projection to hilar interneurons including those expressing somatostatin (Scharfman and Myers, 2012). DDmg cells project to local interneurons P-intSS (Er) cells just as mossy cell collaterals project to GABAergic hilar interneurons (Amaral et al., 2007; Scharfman and Myers, 2012) including those expressing somatostatin (Esclapez and Houser, 1995). The hilar interneurons then also project diffusely to DG (Amaral et al., 2007; Scharfman and Myers, 2012) as P-intSS (Er) projects diffusely to DL (Giassi et al., 2012b). DG projects massively to CA3, a global recurrent network (Amaral and Lavenex, 2007; Amaral et al., 2007) and, likewise, DL projects to DDi which is also a global

recurrent network; there is a major discrepancy here in that CA3 pyramidal cells strongly express CaMKIIα (Erondu and Kennedy, 1985) while this kinase is completely absent from DDi (Giassi et al., 2012d). CA3 projects back to mossy cells (the 'backpropagating' pathway in this literature) and the hilar GABAergic interneurons (Scharfman, 2007); likewise, DDi projects strongly to DDmg as well as to Er. CA3 projects to the nucleus accumbens, part of the ventral striatum (Friedman et al., 2002). DDi projects to Vd and Vc, components of the striatum (Harvey-Girard et al., 2013) and we have previously argued (Sas et al., 1993) that this region can also be considered as ventral striatum. There is also a functional parallel in that both hilar (Williams et al., 2007; Larimer and Strowbridge, 2010) and DDmg/DDi (Elliott and Maler, 2015) neurons exhibit Up states.

There may be an additional partial resemblance of mossy and DDmg neurons. A subset of mouse and primate mossy cells contain calretinin; this is not a universal characteristic because rat mossy cells do not express calretinin (Scharfman and Myers, 2012). Remarkably, a subset of neurons within DD of zebrafish are also calretinin positive (Castro et al., 2006). The appearance of these cells and their location at the caudal end of DD (Figs. 3, 5 in Castro et al. 2006) suggests that they may be homologous to gymnotiform DDmg cells. Castro et al. (2006) also note that, although calretinin immunoreactive cells may be present in DD of other teleosts (e.g. trout), they appear to be in a different location. Further studies of the distribution and connectivity of calretinin positive DD cells across a wider range of teleosts, including gymnotiform fish, would be an important exercise. In particular, it would be important to establish whether the zebrafish DD calretinin positive cells had connectivity similar to DDmg (e.g. commissural connections) and whether they were the cells functionally identified by Aoki et al. (2013).

There is clearly a very strong parallel between mammalian DG/mossy cell and gymnotiform DL/DDmg circuitry but minimal support for homology from the few available molecular markers (Fig. 17). Is this evidence for homology or for convergent evolution of circuitry that supports the same computations (Clarke et al., 2015)? This problem has been intensively discussed with respect to possible homologies between nuclear groups within the avian pallium and mammalian laminar cortex. There are three dominant approaches that use different criteria for homology. The first approach emphasizes comparisons of gene expression – i.e., localizing the adult pallial transcriptome, and has led to contradictory conclusions. The most exhaustive of these studies compared the pallial expression pattern (chicken and mice) of over 5000 genes (Belgard et al., 2013). The authors concluded that, with the exception of the striatum and hippocampus, there are "traces of both molecular homoplasy and homology" and that "homology is not a dominant factor in their adult gene expression patterns". A second approach (Puelles et al., 2016) emphasizes the developmental trajectory of pallium and cortex, e.g., "gene expression, neurogenetic timing, stratification patterns, invariant topology, radial vs. tangential migration" as a critical determinant of homology. Lastly, homology has been inferred from patterns of adult connectivity and function as elegantly summarized by Karten (2015) and Faunes et al. (2015). The last approach reached very different conclusions from those of the first two approaches. Based on striking similarities in the connectivity (laminar and columnar) and function of regions within the avian pallium and mammalian cortex, both authors concluded that, although their macroscopic organization is markedly different, there are precise homologies across avian pallium and mammalian cortex. Clearly, our comparison is primarily based on the pattern of connectivity and our hypothesis of homology between the DL/DDmg/ P-intSS /DDi and

DG/mossy cells/hilar SS cells/CA3 circuits is dependent on the same arguments (though with less data) as presented by Karten (2015) and Faunes et al. (2015). A remarkable recent book (Wagner, 2014) offers a fresh look at this difficult problem based on *in silico* experiments on evolution; here we present a highly simplified summary of the author's complicated arguments. Wagner (2014) concludes that many different developmental gene regulatory networks can, because of their redundant control mechanisms, code for the same phenotype. Wagner (2014) summarizes evidence that gene regulatory networks are robust: both *in silico* and real gene knockout experiments reveal that removing single genes from a regulatory phenotype need not change the resulting phenotype, though it may do so. Importantly, these networks are all related in that one can "travel" from any one to another via single mutational changes or knockouts. In addition, small changes in these gene regulatory networks can generate different genotypes; Wagner (2014) suggests that this is the basis for innovation in evolution. In other words, differences in gene expression in neuronal circuits and variation in their final macroscopic appearance do not preclude them arising from a common ancestor, i.e. being homologous. From this perspective, it is entirely possible that the gene regulatory network generating the DL/DDmg/ P-intSS /DDi circuit is homologous to the network generating the DG/mossy cells/hilar SS cells/CA3 circuit. We must also note that, while homology of these circuits is consistent with Wagner's arguments, it is certainly not proven by our data.

The hypothesis that these circuits are homologous makes one very strong prediction. If a mammal (e.g. mouse) is trained in the Aoki et al. (2013) protocol (trace avoidance conditioning, see above) then we predict that, 24 hours after training, mossy (DDmg?) and/or CA3 (DDi?) cells will show a strong Ca^{2+} signal upon presentation of the training cue.

We have provided two interpretations of the relationship of the gymnotiform pallium to that of amniotes and these are apparently mutually exclusive. In the final section of the Discussion we suggest a possible resolution of these seemingly contradictory schemes.

FUNCTIONS OF DD/DL CIRCUITRY: PATTERN SEPARATION AND COMPLETION? (FIG. 18)

In this section we assume that, as per the second hypothesis presented above, that DL/DDmg/DDi are at least functionally similar, and possibly homologous, to DG/mossy cells/CA3.

The mammalian hippocampus is generally believed to be responsible for episodic and, in particular, spatial memory – it associates and initially stores objects, events and locations (Eichenbaum, 2004; Burgess, 2007; O'Keefe, 2007; Eichenbaum and Cohen, 2014). There are two computations that are believed to be essential for episodic memory: pattern separation and pattern completion (auto-association, Rolls, 2013). Pattern separation takes patterns that share many features (e.g. similar faces) and represents them with different neural ensembles – hence it separates the patterns (faces) so that they can be independently recalled. Sensory input is often brief and corrupted by noise so that the entire spatial pattern representing, e.g., a face, is not available. Pattern completion refers to the process whereby such incomplete sensory input is completed, i.e. retrieved as a specific object (e.g. a particular face). Initial theoretical studies assigned pattern separation to the large number of cells in DG (Derrick, 2007) and, in particular, noted the importance of DG for spatial pattern separation (Kesner, 2007). Based on its strong global recurrent connections, theoreticians have proposed that CA3 is the locus for pattern completion (Rolls, 2013). A key requirement for pattern separation in DG is strong competitive inhibition implementing a “winner take all” (WTA) mechanism by which the activation of DG cells

representing one input pattern can suppress activity in DG cells representing different patterns (Rolls, 2016). Hilar inhibitory interneurons may fulfill this role in the mammalian DG. A recent article (Stefanelli et al., 2016) demonstrates that specifically the somatostatin-expressing GABAergic interneurons of the dentate hilus limit the size the neuronal assembly encoding an engram. The authors note that the engram size limit was likely implemented by lateral inhibition enforcing a "competitive distribution of the memory trace." This hypothesis appears to be equivalent to the WTA mechanism discussed by Rolls (2016). We have hypothesized that the gap junction coupled somatostatin-expressing GABAergic neurons of P-intSS (Er) with their diffuse projection to DL implement the same WTA mechanism (Figs. 17, 18). The Stefanelli et al. study and our results suggest deep functional parallels between the mnemonic circuits of mammalian dentate gyrus and of the teleost DL/DD/P-intSS circuitry.CA3 supposedly acts as an attractor network: DG input activates part of one attractor and the reverberatory activity of the recurrent network activates the entire attractor (Rolls, 2007; 2013). This entire theory is supported by a great deal of indirect evidence (Guzowski et al., 2004; Yassa and Stark, 2011; Santoro, 2013) and, most recently, by direct single unit recordings from DG and CA3 (Neunuebel and Knierim, 2014; Lee et al., 2015). A schematic view of memory retrieval runs as follows: a highly processed (cortex) and imperfect sensory input reaches DG where it activates a small subset of neurons (separation). The DG cells activated are only a fraction of all that might be activated by that input; CA3 then completes the pattern and the input is correctly identified.

This elegant theory is purely feedforward : cortical input reaches DG where it is separated into different partial object representations; it then proceeds to CA3 where the partially identified objects are completed; finally, the identified objects are passed back to cortex. This

theory simply ignores the anatomically identified and strong CA3 (DDi?) -> mossy cell (DDmg?) -> DG (DL?) pathway. We propose to extend the theory to incorporate this pathway. This implies a recursive process for pattern completion/separation : the first attempt at pattern completion (CA3, DDi?) is essentially a “guess” as to the identity of the input and this guess is fed back to DG (DL?) via mossy (DDmg?) cells; a winner-take-all inhibitory loop (hilar interneurons; Er? - see above) would then implement feedback specificity. In other words, retrieving memories based on incomplete sensory input is a recursive process and must be iterated until a stable memory is generated. There is some support for this notion in that loss of hilar mossy cells results in deficits of pattern separation (Jinde et al., 2012; Wang et al., 2014).

There is abundant evidence that teleost fish are capable of both pattern separation and completion computations with most studies having been done in the visual system (Wyzisk and Neumeyer, 2007; Sovrano and Bisazza, 2008; Siebeck et al., 2009; Sovrano and Bisazza, 2009; Darmaillacq et al., 2011; Schluessel et al., 2012; Schluessel et al., 2014). Equivalent results have been reported for the electrosense in mormyrid (Graff et al., 2004; von der Emde et al., 2010) and gymnotiform (Graff et al., 2004) fish.

Given that DL is essential for spatial learning in goldfish (see above) we propose that DL and DD are involved in pattern separation/completion. We have shown that DDi/DDmg found neurons that could enter a sustained Up state after repeated stimulus presentations; these Up states appeared to be driven by synaptic input (Elliott and Maler, 2015). We hypothesize that the Up state is due to reverberatory activity within the multiple loops of the DDi recurrent network and the slow NMDA receptor EPSPs (Harvey-Girard et al., 2007) which last longer than the

maximum loop delay time (50 ms). This is consistent with the notion that DDi could support pattern completion via multiple loops within its recurrent connections and a Hebbian learning rule (Siri et al., 2007).

Our own studies in a pulse gymnotiform fish (Jun et al., In press) have monitored the fish's active sensing via discrete sampling events (electric organ discharge rate and body movements) as the fish used its electrosense to learn the location of food with respect to landmark cues. The results of this study indicated that the landmarks are discriminated and that the change in active sampling with learning is consistent with an early phase of pattern separation (intense sampling) that permits each pattern to be identified, followed by pattern completion (minimal sampling) after learning. In the Jun et al study, the fish (*Gymnotus sp*.) appeared to discriminate cylindrical versus square columnar shapes via its electrosensory system in order to locate food. In this context, pattern separation refers to the square and cylindrical shapes activating different, non-overlapping sets of DL neurons. Pattern completion implies that the fish will recognize the square 'pattern' even if it only electrosenses one corner (Fig. 18).

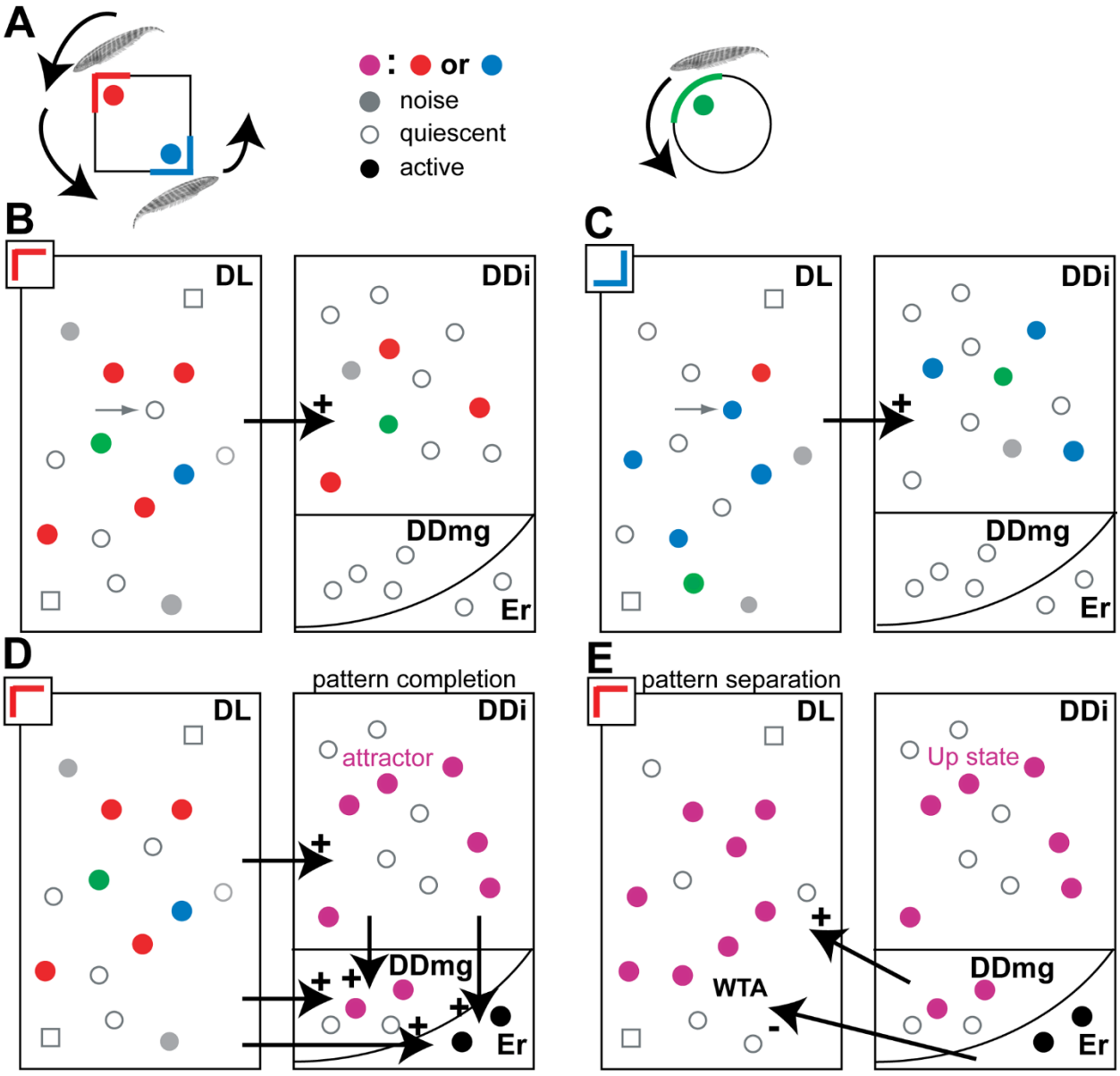

Figure 3-18: Graphic illustration of our hypotheses on the function of DD/DL.

Connecting DDi/DDmg/DL/Er circuitry to electrosensory spatial learning in a pulse electric fish (Jun et al., In press). **A**: The fish swims near and electrically 'scans' square columnar and cylindrical landmarks. It will sample features of a specific landmark (e.g. red and blue corners of the square prism) in temporal contiguity; different landmarks (e.g. the cylinder) will be sampled at non-contiguous times. The short range of the electrosensory system implies that it will only sense small portions of an entire landmark. Here we ask what it would take to recognize the square pattern from any electrosensory viewpoint (pattern completion) and to distinguish it from the circular shape (pattern separation). The majority of DL and DDi neurons are, we assume,

quiescent and symbolically indicated by the open squares at the corners of DL in B-E. The same group of potentially active cells are shown as circles in each panel and their changeable activity level is indicated by its colour, e.g., the thin arrows in DL (**B** and **C**) points to a cell that is inactive as the fish swims by the red corner (**B**) but is activated when the fish swims past the blue corner (**C**). **B**: We assume that, when the fish encounters the upper left corner of the square (red) it induces discharge in a subset of DL neurons (via OT->PG->DL); these in turn activate a subset of DDi neurons. At this point, there is no specificity in this response so that there is overlap with neurons that would also respond to an arc of the cylinder (green) as well as neurons randomly discharging (grey circles, noise). We assume that the 'red corner' responsive neurons predominate. **C**: The same situation applies when the fish encounters the lower left corner of the square (blue). Synaptic plasticity (Hebbian) is assumed to be acting throughout these encounters and strengthening the response of neurons (DDi) to correlated (temporally contiguous) input (Siri et al., 2007). Operations illustrated in **D** and **E** overlap but are presented separately for clarity of exposition; we illustrate using the 'red corner' but the same scenario would occur with the 'blue corner' input. Based on Aoki et al (2012) we assume that the operations suggested in panels D/E are delayed with respect to panels B/C. **D**: The red and blue corner inputs have become associated (Giassi et al., 2012b) in a subset of DDi recurrently connected cells. This subset constitutes the red corner 'attractor' within the DDi attractor network. The same noisy DL input neurons (red), however, now activate the entire 'square' attractor circuit within DDi (purple) and only these cells; this subset would also be activated by the blue corner. The activation of the DDi attractor by either the red or blue corner input is pattern completion. The active DL cells and the DDi attractor both project to DDmg and Er. They activate a subset of DDmg cells (purple) now linked to the DDi attractor. They also activate a large fraction of the gap junction coupled Er cells (black). **E**. The DDi cells enter long lasting Up states (Elliott and Maler, 2015), a signature of the active attractor. The activated DDmg cells (purple) feedback to DL and activate all cells that are activated by either red or blue corners (purple) even though the PG input only activated the fraction indicated in **D**. The active Er cells provide a synchronous, diffuse and non-specific inhibitory input to DL; this inhibition is a 'winner take all' (WTA) mechanism and supresses any weak response of the DL cells to e.g. the cylinder shape or 'noise' (now open circles). The active DL cells now represent strictly the square shape and no longer respond to any other shape. This is therefore pattern separation. The output of the active DL cells to a subset of DC cells (Fig. 16) and their projection to OT now evoke an appropriate response, e.g. swimming towards the food.

In Figure 18, we use the DD circuitry described above to interpret the behavioral studies in terms of pattern association/completion. We note that the final connection to successful food

capture would be the DL->DC->OT-> motor behavior circuit was omitted from this Figure but is illustrated in Figure 16. Further, this theory would require synaptic plasticity throughout the connections of DD, DL, and DC; the presence of a high density of NMDA receptors and high levels of expression of many proteins known to be involved in synaptic plasticity support this assumption (Maler, 1999a; 1999b; Harvey-Girard et al., 2007; 2010; 2013; Giassi et al., 2012c).

Behavioral studies using pattern separation/completion specific tasks combined with detailed electrophysiology and imaging along the lines of the Aoki et al paper may contribute to a deeper understanding of how the common network motifs of teleost and amniote pallium (Figs. 16, 17) contribute to fundamental mnemonic computations.

CONCLUDING REMARKS

We have characterized in detail the intrinsic and extrinsic connections of DD. Several major overall conclusions can be drawn from our results. Firstly, DD, DL and DC core are all intimately interconnected but there are minimal connections of these regions with DM and no obvious connections with DP. This reinforces the view that DL/DD/DC are required for spatial and episodic memory, DM for other, perhaps “emotional”, types of memory, and DP strictly for olfaction, and that these functions are segregated in the teleost pallium. Secondly, the DD region also appears to be present in at least goldfish, cichlid fish and zebrafish and may have similar functions in these teleosts. Thirdly, DD/DL/P-intSS (Er) may implement pattern separation/completion operations in much the same way as the equivalent mammalian hippocampal circuits; this would be the basis for efficient memory storage in DL/DC. Lastly, DD/DL/DC circuitry resembles that of both hippocampal and cortical circuitries. We propose that

this distinction may be artificial and that, in teleosts, the processing functions of cortex via its laminar and columnar connectivity and the mnemonic functions of hippocampus may be combined. If this is correct, then DL might be homologous, in whole or in part, to both cortex and dentate gyrus as previously suggested (Yamamoto et al., 2007). Most importantly, this implies that we may have identified the core memnonic circuit of the vertebrate brain. One approach to this problem might be to determine whether the same or different populations of DL cells project to DD and DC, and to examine the gene expression patterns in these populations. Our hypotheses lead to very specific predictions in this regard. There may be a population of Prox1 expressing DL neurons that projects selectively to DD (mnemonic hippocampal circuit) and a separate population of DL neurons that project selectively to DCcore (cortical-like processing circuit) and that expresses some of the gene markers that identify the superficial, thalamic input recipient layers of the mammalian cortex (Molyneaux, 2007; Rowell, 2010).

OTHER ACKNOWLEDGEMENTS

Special thanks to William Ellis for his technical support and expertise.

CONFLICT OF INTEREST STATEMENT

The authors are not aware of any known or potential personal or financial conflicts of interest.

ROLE OF AUTHORS

All authors had full access to all the data in the study and take responsibility for the integrity of the data and the accuracy of the data analysis. Study concept and design: SBE, EHG, LM. Acquisition of data: SBE, EHG, ACC. Analysis and interpretation of data: SBE, EHG, ACC, LM. Drafting of the manuscript: SBE, EHG, LM. Critical revision of the manuscript for important

intellectual content: SBE, EHG, ACC, LM. Statistical analysis: EHG, LM. Obtained funding: LM. Administrative, technical, and material support: ACC, LM. Study Supervision: LM.

DATA ACCESSIBILITY

GenBank (http://www.ncbi.nlm.nih.gov/genbank/)

Chapter 4 DISCUSSION

In this Discussion I attempt to accomplish four objectives. Firstly I will definitively link persistent activity and corresponding up-states to an evoking naturalistic stimuli in a behaving animal; I will localize the up-states to the DDi subregion of the dorsal pallium, an area involved with memory. Secondly, I will discuss the circuitry of this region as elucidated by the results presented in Chapter 3. This will be followed by an attempt to place these results, and the network they describe, within the theoretical framework of recurrent network models. Lastly I propose a model of homology of teleost pallial circuitry to the more familiar mammalian hippocampal memory circuitry and establish the weakly electric fish and zebrafish as excellent model systems for further investigations into the network mechanisms behind learning and memory.

LINKING UP-STATES, PERSISTENT ACTIVITY, AND THE NATURAL WORLD

In the Introduction, I outlined the research identifying persistent activity and connecting it with up-states, recurrent networks, and an animal's natural environment by presenting characteristic examples of each idea. There remains little question that up-states occur in natural (sleep; Mahon et al., 2006) and artificial (urethane anesthesia; Li et al., 2009) behavioral states, and even in slice preparations with or without stimulation (McCormick et al., 2003). It is also well established that persistent activity occurs in animals during the performance of short-delay memory tasks (Colombo and Gross, 1994), and that persistent activity has been associated in some other cases with up-states. There has been difficulty however in demonstrating that naturalistic stimuli drive persistent activity that is associated with up-states in an awake animal. In Chapter 2 we present evidence of exactly this association in the dorsal subdivision of the pallium of *A. leptorhynchus*.

The presentation of a simulated EOD in the form of a sinusoidal wave in the frequency range of 600 – 1000 Hz represents a common and natural stimulus for apteronotid fish (Marsat et al., 2012; Fotowat et al., 2013). Although immobilized, this fish continues to behave electrically as though it were freely moving and does not demonstrate the significant physiological signs of stress shown when handled or deprived of oxygen (Hitschfeld et al., 2009). These fish have been shown to respond to mimic EODs as though they were naturally occurring EODs in many studies, even attempting to communicate with or showing typical aggressive or territorial behavior toward the source of the mimic (eg., Zupanc et al., 2006). Thus our experimental scenario, presenting EOD mimics to an immobilized, but otherwise aware and behaving fish, represents an excellent protocol for examining the neural responses of *Apteronotus* under conditions it would be expected to encounter naturally.

I demonstrate that, similar to work done in primates, presentation of naturalistic stimuli evoked barrages of spiking activity in ensembles of otherwise quiescent cells. Extracellular recordings in DDi (and possibly DDmg) cells, which otherwise did not spike, produced these barrages in response to the presentation of mimic EODs of a variety of frequencies simulating different types of encounters with conspecifics which might occur naturally. This included simulation of male-female, female-female, and male-male encounters. Mimics that were close and more distant, higher and lower in frequency than the subject fish were presented, as relative EOD frequency has been associated with dominance (Zakon et al., 2002). These periods of spiking began 137-1170 s (mean: 592.7 ± 232.8 s) following the onset of stimulus presentation, lasted 10-2428 s, and contained 6-1135 spikes. Similar barrages resulted from the presentation of acoustic stimuli (pure tones) showing that the response was sensitive to multiple sensory

modalities. This, combined with the varied EOD mimics show that the response was not tied to a specific type of social encounter but suggest rather that they are related to the fish's sensory environment. As each stimulus was presented from a specific source, we must acknowledge that a potential spatial component exists with each stimulus. These responses showed no correlation to the state of stimulation once initiated; spiking began just as readily during periodic stimulus presentations as in between. The spiking also often continued after stimulus cessation. Thus, similar to what has been seen in mammals and primates, persistent activity could be initiated in DDi with the presentation of naturalistic stimuli and this persistent activity took the form of barrages of spiking in otherwise quiescent cells.

Unlike the primate work however, we were able to perform whole cell patch clamp recordings in the same area as our extracellular recordings and associate the results with this same naturalistic stimulation. These intracellular recordings showed that spiking, which followed the same time course and variability as the spike trains recorded using extracellular techniques, was always associated with a sustained depolarization of the membrane potential (mean V_m shift: 26.8 ± 5.6 mV) resembling closely the up-states recorded in mammals (Chapter 2, Figure 3). This shows compellingly that up-states are not an artificial phenomenon or only seen spontaneously, but can be evoked during the normal behavior of the animal and underlie the spiking barrages recorded extracellularly.

The fact that the spiking, or up-state, activity did not preferentially occur during or between stimulus presentations, and often persisted beyond stimulus presentation seems to corroborate the idea put forward by MacLean et al. (2005) that up-state activity can be caused

by local network dynamics, but initiated or gated by thalamic input. Sensory information in the fish would arrive at the dorsal pallium from the preglomerular nucleus (PG) – a diencephalic structure analogous or perhaps homologous to the tetrapod dorsal thalamus (Giassi et al., 2012a). The highly variable onset latency, spike rate, and response duration we see in our spiking responses would suggest that the stimulus, although necessary to initiate the response, is not directly correlated with the spike timing.

CIRCUITRY OF THE DD REGION

Curious to understand the neural substrate capable of producing persistent firing and up-states, I performed microinjections of neural tracer, restricted to the individual subdivisions of DD. The connectivity had been roughly mapped out in previous work by Giassi et al. (2012a, b), but not with a fine enough resolution to appreciate the intricacies such a network might reveal. This connectivity is outlined in Figure 15 of Chapter 3, but I will outline the relevant connections here. As was seen in Giassi et al.'s work, significant bi-directional connectivity was shown between DD and DL. Our smaller injections revealed that this connectivity is not however evenly distributed throughout DD. Rather we showed that DL projects to DDi, but receives input from DDmg. DDs also receives input from DL and is connected to other telencephalic structures, but as my electrophysiological recordings centered on DDi and DDmg, I will focus my discussion here on these areas. Both DDi and DDmg also connect bi-directionally to Vc/Vd (homologous to tetrapod striatum), and Er (whose function is discussed at some length in the Discussion of Chapter 3). DDi and DDmg send fibres to DM2 (homologous to tetrapod amygdala) and may receive input back via DDs, but this connection is minor.

The second thing that these smaller injections allowed, in addition to clarifying precise targets of connections with telencephalic nuclei, was an analysis of the circuitry intrinsic to each DD subregion. DDmg was found to have some intrinsic, but relatively sparse, interconnectivity and significant commissural connections. Most interestingly, DDi was revealed to contain highly recurrent circuitry. Numerical analysis presented in Chapter 3 (Figure 3-6) shows that DDi is likely a globally recurrent network and a small world network. The implications of this conclusion will be discussed below. It is also important to note that DDi is highly enriched for NMDA receptors (Giassi et al., 2012c), although interestingly lacking in CAMKIIα (Giassi et al., 2012c).

THEORETICAL MODELS OF PERSISTENT ACTIVITY IN LEARNING AND MEMORY

Wang (2001) proposes that persistent activity is likely achieved by either recurrent network structure or by bi-stability within a single neuron, with network recurrent connectivity being the more likely candidate for that related to memory. He describes a general network structure whereby reverberant excitation via recurrent collaterals can lead to sustained activity which can persist beyond the removal of the outside stimulation which initiated the response. In his analysis, Wang refers to several specific models including one by Amit and Brunel (1997) where a recurrent excitatory network, paired with an inhibitory network produces persistent activity in a subpopulation of nodes (model neurons) in response to stimulation. Interestingly, the spontaneous activity appears abruptly and occurs in an ensemble of nodes specific to the unique stimulus, and this only if the stimulus was previously encountered (known). This is a perfect example of how recurrent network structure with plasticity can both store

representations of stimuli, but also present them in stable states of persistent activity in select neuronal ensembles. One of the hallmarks of attractor networks is that the attractor states are relatively stable to external perturbations. This appears to be facilitated by self-governing persistent activity, triggered by external stimuli, but once initiated, maintained by the recurrent dynamics of the network itself.

The inhibitory parts of the network serve both to regulate and stabilize the recurrent excitation, and to supress adjacent activity, emphasizing the active ensemble and supressing external perturbations to the active state. Wang further describes the need for regulation of network state by a balancing of inhibition and excitation. He speaks of some of the likely mechanisms which, when modelled, add such stability to the model networks, mentioning feedback inhibition and the regulatory capacity of excitation mediated by NMDA receptors with slow responses. Several properties of NMDA receptor mediated excitation make it an excellent candidate. The slow decay of NMDA mediated currents would allow the integration of recurrent activity as long as the delay along recurrent fibres is faster that the decay of the NMDA current. NMDA receptors also have unique voltage-gating properties mediated by their magnesium blockade which make them excellent candidates for participating in sustaining activity in already depolarized cells. Their slow release of bound glutamate might further act as a stabilizing mechanism, as once saturated, they could effectively limit any possible positive feedback from the recurrent excitation needed to generate and sustain an up-state. Experiments have shown that blockade of NMDA receptors is more effective than blockade of AMPA receptors in abolishing memory-related persistent activity (Shima and Tanji, 1998)

Wang (2008), in a later paper, reviewed how recurrent attractor networks, capable of storing memory representations in the sustained firing state of groups of neurons, are involved in decision making relative to working memory tasks. Most of this work is considered in relation to the delay period activity observed between cue and test stimulus presentations during a delayed match to sample test. He simulated a recurrent network wherein different (in this case two) pools (representing neural ensembles) represent different choices (in this case right vs. left saccade). Recurrent excitation would begin to excite both pools, but once one attractor was activated, it was sustained and the other supressed by winner-take-all inhibition. The now active attractor represents a decision by the network. Fecteau and Munoz (2006) put forward the concept of a salience map whereby the most distinct object might be selected as a target for attention by a similar decision making process. They propose that, rather than a conscious, considered decision, this evaluation of salience occurs as sensory representations of different features compete and win on the basis of relative distinctness. If we generalize this concept to features of an episode, or memory-encoded event, rather that objects competing for attention, it fits well with the concept of pattern separation where the representation of different features of a memory element must be sparsified and orthogonalized to separate them from those of similar elements. Such a process might work in a way very similar to that proposed by Wang (2008) where these features compete to define the memory representation of an element and win on the basis of relative distinctiveness or salience. A similar structure could serve for pattern completion, where similar, partially activated, attractors compete for full activation. The ensemble which best corresponds in the more salient details of the representation will "win" and suppress the competing alternatives. These competitive processes would likely, by Wang's

reasoning, make use of competitive structures, like winner-take-all networks, implemented in a recurrent network with multi-modal sensory input.

FITTING DDI WITHIN THIS THEORETICAL FRAMEWORK

In Chapter 2 we describe activity very similar to that observed in simulations of some of the implementations of such an architecture mentioned by Wang. In Chapter 3, we demonstrate that the architecture of the DD region incorporates both global recurrence in DDi and local recurrence in DL; DL, as we have already described in the Introduction, is linked to spatial memory by lesion experiments. We show in our numerical analysis of DDi interconnectivity in Chapter 3 that it is very likely that the global recurrent connections in DDi would allow the integration of recurrent activity within the decay time of NMDA currents. Additionally, in Giassi et al. (2012c) the DD region, and specifically DDi are shown to have an abundance of local interneurons which are a likely source of the feedback inhibition and that the principal cells are highly enriched for NMDA receptors (Giassi et al., 2012c), both requirements of the Wang theory. Additional sources of feedback inhibition which might produce similar regulation or stabilization of recurrent excitation are found in the DD network. In chapter 3 I show that an inhibitory feedback pathway exists in the bi-directional connections between DD and Er. DL is also highly interconnected with Er allowing further control of this inhibitory pathway. Ellis et al. (2008) also show that DD cells are enriched for SK2 channels whose large AHPs could provide a similar regulatory inhibitory feedback. In Chapter 2 I show that DDi cells exhibit persistent activity in the form of up-states in response to multiple modalities of sensory stimulation, sometimes in the same cell. Both the presence of up-states, which might further stabilize attractor states, and the evidence of multi-modal integration, which would be necessary for representation of the environment and

experience, are important here. These evidences further reinforce the suitability of the DD - DL network for the storage and retrieval of content-addressable memory related to the sensory representation of the animal's experience.

Most of the animal evidence for persistent activity mentioned by Wang is in relation to the delay period activity observed between cue and test stimulus presentations during a delayed match to sample test. Although in this task the delays are very short, with very little extension we might apply these same concepts to our own network and the larger and more varied delays we see in our Chapter 2 results. Consider the idea of an iterative process of pattern separation and completion proposed in the Discussion of Chapter 3. We might consider that memory representations are being iteratively orthogonalized and sparsified (separated) and then linked or associated (completed) in a process of internalizing the representation of, for example, the environment and the relationship of its salient details (we will discuss such a scenario in the following section of this Discussion). This would lead to the memory representation being refined, having new elements added, or old ones removed as necessary. Assuming that the ensemble of active neurons in a network represents either a memory, or a representative address, this would mean that the exact arrangement of active neurons would change during this process. This would be especially true if we consider pattern separation to involve the competitive evaluation of detail salience as mentioned earlier. Differing slightly from the delayed match to sample task mentioned earlier, we know that, for mammals, spatial details are retained for a long period of time extending over days (Thompson and Best, 1990). Therefore, it is not surprising that response onset latencies and durations of persistent activity in DD neurons activated by spatially relevant stimuli are highly variable.

THEORIES OF PATTERN SEPARATION AND PATTERN COMPLETION

Traditional thought on the localization of pattern separation and pattern completion places the two processes in different fields of the mammalian hippocampal formation. Pattern separation is associated with the Dentate Gyrus, while pattern completion is believed to occur in CA3. The reasoning for this is discussed in the Introduction to this thesis, but I will briefly mention some details again here. As increasing experimental evidence demonstrated a clear role for the hippocampus in certain types of memory, and seeing that a process akin to what we now call pattern completion must be taking place (as evidenced by the stability of functional memory and place field firing despite perturbations of environmental cues) it was concluded that pattern completion was likely occurring within this structure. Experimental evidence corroborated this theory when Nakazawa et al. (2002) found that a CA3 restricted NMDA receptor knockout prevented mice from maintaining stable place fields and from remembering the location of a goal when presented with an incomplete set of familiar cues, but not with a complete set. Additionally, the impressive recurrence of the CA3 field collaterals fit the theoretical demands of attractor network models capable of recalling a memory (activation of an entire attractor) in response to a partial set of inputs. This made CA3 a perfect candidate as the locus of pattern completion. The idea that pattern separation was localized in the DG stems from the idea that this process would have to occur upstream of the pattern completing CA3 and that the sparse, but powerful mossy fiber synapses onto CA3 cells would be perfect candidates for training representations in CA3. Experimental evidence presented by Neunuebel and Knierim (2014) seems to corroborate this theory of localization. They recorded simultaneously from populations of DG and CA3 place cells during a local-global cue mismatch paradigm. DG cells showed

decreased coherence caused by the mismatch, whereas CA3 cells did not. This was interpreted to suggest that CA3 fields are able to remain stable via pattern completion and DG fields change due to their involvement in pattern separation.

More recent work has begun to question this separation of function. Lee et al. (2015) point out that the connectivity of CA3 differs along its longitudinal axis. Recurrent collaterals in the area proximal to DG send collaterals back to the hilus and not to more distal regions of CA3. These proximal cells, in turn, receive recurrent input from more distal parts of CA3. Further, when this group tested population responses in the same local-global cue mismatch paradigm Neunuebel and Knierim (2014) used, they found the responses in proximal CA3 resembled those recorded in DG rather than those in distal CA3. They conclude that rather than a distinct separation, there may exist a gradient of functional transition moving from DG to distal CA3. Another point to note is that under either architecture, the standard feedforward model of DG to CA3 may not be adequate and pattern completion circuitry could potentially affect pattern separation circuitry.

The presence of circuitry necessary for non-sequential pattern separation and completion also supports the iterative model I proposed earlier. Further support for this idea comes from Leutgeb and Leutgeb (2007) who describe how CA1 and CA3 place cells remap immediately upon a mouse's entering a new environment. CA1 cells solidify their place fields after several minutes while, although they also begin firing very quickly, CA3 fields change for 10-20 minutes following. The facts that CA3 fields are established almost immediately, and that CA1 fields remain stable from this point on suggest that more time is not needed to encode a representation of the

environment as a place map. The changing of these fields is rather consistent with an ongoing, or iterative refinement process to the representation.

Further evidence against the clean dissociation of pattern separation and completion is presented by Nakashiba et al. (2012). This group generated a transgenic mouse whereby they were able to selectively repress the output of either old DG granule cells or new (adult-born) DG granule cells. They then tested these mice in either a partial cue water maze to test pattern completion, or a near-identical pair of mazes, where in one the mouse would receive a shock and not in the other, to test pattern separation. Pattern separation was impaired only by repression of young granule cells and pattern completion only by repression of the output of old granule cells.

These evidences together suggest that the localization and sequence of pattern separation and pattern completion may not be as simple as previously supposed. If homology of circuitry can be established between the dorsal pallium of the teleost and that of the mammalian cortico-hippocampal network, the first steps of which I present in this thesis, the teleost would provide an excellent experimental model in which to directly measure the neural activity in the involved networks. This would be a significant step in answering some of the questions presented here.

A MODEL FOR SPATIAL MEMORY IN THE DORSAL PALLIUM OF A WEAKLY ELECTRIC FISH

I will now look at how these concepts might work together within the DD network structure elucidated in Chapter 3 and using ideas of decision-making attractor networks

suggested by the persistent activity seen in Chapter 2. I will use the scenario presented by Jun et al. (2016). They trained a pulse-type gymnotiform to perform a spatial memory task in order to find food. The fish exhibited evidence of EOD scanning (transient increase in EOD rate) near landmarks while learning, but not once having learned the environment. Presumably this reflected both the attention of the fish to the landmarks and the learning processes which allowed the fish to navigate more quickly using the now familiar landmarks as spatial reference points. We describe how the processes of both pattern separation and pattern completion might be involved in such an experiment in Chapter 3 and in figure 3-18. In Jun et al.'s experiment, it is important to note that different groups of fish were trained with or without landmarks. Those trained with landmarks performed better and showed tighter patterns of exploration as training progressed, suggesting that the fish were using the landmarks to facilitate spatial mapping. The EOD scanning rate increased while learning the environment (early trials), but not once learned (late and probe trials), further suggesting that this learning of landmarks was what facilitated spatial mapping. Looking carefully at the exploration density maps (figure 3, Jun et al., 2016) we note that after learning, the fish passed by landmarks, but did not explore or swim around them. Evidence is presented in this paper that the environmental mapping was performed primarily using electrolocation. This implies that the fish only "see" or more accurately, sense, a small portion of a landmark while passing by and navigating toward the goal. In order for this to be an effective navigation strategy, it would require that the fish, only sampling a small portion of a single, unique landmark, is able to determine its identity and by extension its own spatial location. The implication is that sampling a small portion of the landmark allows the fish to generalize its location in a broader context encompassing perhaps the rest of the landmark, and certainly the

landmark's position in the environment. This would involve pattern completion. Additionally, the fact that the navigating fish in late trials does not, after encountering one landmark, scan the remaining landmarks before navigating to the goal, suggests that the fish is able to, after sensing only a small portion of one landmark, identify the unique landmark from similar others. This would involve pattern separation. Thus, presumably by means of these two memory processes, the fish is able to quickly establish its own spatial position and the relative location of the goal.

According to our model of circuit homologies proposed in the discussion of Chapter 3, the pallial network, being presented with a partial representation of a landmark (electrosensory image) will stimulate DDi. Reverberatory activity in DDi (due to local recurrent circuitry) will settle on the network state (subset of active neurons) which represents the memory of the landmark in the relevant spatial context (experimental tank). This is illustrated in Chapter 3, figure 3-18, panel D. The mechanism by which it would settle on this state would likely be similar to those proposed by Hopfield (1982), Rolls (2013), and Wang (2001, 2008) for attractor networks in working memory, or those putatively implemented in the mammalian CA3. The stability of this attractor state would be reinforced by both the intrinsic up-state dynamics, as well as inhibitory suppression of perturbations and competing attractors by interneurons and/or via reciprocal connections with Er. This would, in turn, activate both DDmg and Er. These would provide DL with both the excitatory (from DDmg) and inhibitory (from Er) input needed to othogonalize the representation, thereby differentiating it from that of the other landmarks in the tank. In further support, preliminary data recorded from the DD region of free swimming Gymnotus carapo, has revealed place-related neural activity (Fotowat, personal communication). Once this has been

more solidly established, it would further strengthen the argument that these networks are operating in ways parallel to the hippocampal formation in mammals.

PREDICTIONS FOR FUTURE WORK

This interpretation of the results presented in this thesis makes several predictions. Firstly, I would expect that recording from large numbers of cells in DDi during the performance of spatial learning (or other learning with a spatial component) would result in the sustained activation of distinct neural ensembles. I further predict that the set of neurons composing the activated ensemble would be distinct for distinct memory events. Secondly, I would expect that a similar phenomenon would occur in DL, and would not be surprised if persistent activity in the form of up-states was found there as well. Thirdly, I predict that, as mentioned in the Discussion of Chapter 3, distinct populations of cells in DL will project to DD and to DCc respectively, each expressing distinct markers setting them apart as hippocampal-like in the first, and cortex-like in the second case.

Chapter 5 REFERENCES

Abellan A, Desfilis E, Medina L (2014). Combinatorial expression of Lef1, Lhx2, Lhx5, Lhx9, Lmo3, Lmo4, and Prox1 helps to identify comparable subdivisions in the developing hippocampal formation of mouse and chicken. *Front Neuroanat* **8**, 59.

Abrahams S, Pickering A, Polkey CE, Morris RG (1997). Spatial memory deficits in patients with unilateral damage to the right hippocampal formation. *Neuropsychologia* **35**(1), 11-24.

Aimone JB, Deng W, Gage FH (2011). Resolving new memories: a critical look at the dentate gyrus, adult neurogenesis, and pattern separation. *Neuron* **70**, 589-596.

Amaral DG, Ishizuka N, Claiborne B (1990). Neurons, numbers and the hippocampal network. *Prog Brain Res* **83**, 1-11.

Amaral D, Lavenex P (2007). Hippocampal neuroanatomy. In: Anderson P, Morris R, Amaral D, Bliss T, O'Keefe J, eds. The Hippocampus Book. Oxford: Oxford University Press. p 37-114.

Amaral DG, Scharfman HE, Lavenex P (2007). The dentate gyrus: fundamental neuroanatomical organization (dentate gyrus for dummies). *Prog Brain Res* **163**, 3-22.

Amit DJ, Brunel N (1997). Model of global spontaneous activity and local structured activity during delay periods in the cerebral cortex. *Cereb Cortex* **7**, 237-252.

Amo R, Aizawa H, Takahoko M, Kobayashi M, Takahashi R, Aoki T, Okamoto H (2010). Identification of the zebrafish ventral habenula as a homolog of the mammalian lateral habenula. *J Neurosci* **30**, 1566-1574.

Amo R, Fredes F, Kinoshita M, Aoki R, Aizawa H, Agetsuma M, Aoki T, Shiraki T, Kakinuma H, Matsuda M, Yamazaki M, Takahoko M, Tsuboi T, Higashijima S, Miyasaka N, Koide T, Yabuki Y, Yoshihara Y, Fukai T, Okamoto H (2014). The habenulo-raphe serotonergic circuit encodes an aversive expectation value essential for adaptive active avoidance of danger. *Neuron* **84**, 1034-1048.

Andersen, P., Morris, R., Amaral, D., Bliss, T., & OKeefe, J. (Eds.). (2006).*The hippocampus book*. Oxford University Press.

Aoki T, Kinoshita M, Aoki R, Agetsuma M, Aizawa H, Yamazaki M, Takahoko M, Amo R, Arata A, Higashijima S, Tsuboi T, Okamoto H (2013). Imaging of neural ensemble for the retrieval of a learned behavioral program. *Neuron* **78**(5), 881-894.

Belgard TG, Montiel JF, Wang WZ, Garcia-Moreno F, Margulies EH, Ponting CP, Molnar Z (2013). Adult pallium transcriptomes surprise in not reflecting predicted homologies across diverse chicken and mouse pallial sectors. *Proc Natl Acad Sci U S A* **110**, 13150-13155.

Benda J, Longtin A, Maler, L (2006). A synchronization-desynchronization code for natural communication signals. *Neuron* **52**, 347-358.

Blaser N, Dell'omo G, Dell'ariccia G, Wolfer DP, Lipp HP (2013). Testing cognitive navigation in unknown territories: homing pigeons choose different targets. *J Exp Biol* **216**, 3123-3131.

Broglio C, Gomez A, Duran E, Ocana FM, Jimenez-Moya F, Rodriguez F, Salas C (2005). Hallmarks of a common forebrain vertebrate plan: specialized pallial areas for spatial, temporal and emotional memory in actinopterygian fish. *Brain Res Bull* **66**(4-6), 277-281.

Bshary R, Brown C (2014). Fish cognition. *Curr Biol* **24**(19), R947-R950.

Bshary R, Gingins S, Vail AL (2014). Social cognition in fishes. *Trends Cogn Sci* **18**, 465-471.

Buckmaster PS, Wenzel HJ, Kunkel DD, Schwartzkroin PA (1996). Axon arbors and synaptic connections of hippocampal mossy cells in the rat in vivo. *J Comp Neurol* **366**, 271-292.

Bullmore E, Sporns O (2009). Complex brain networks: graph theoretical analysis of structural and functional systems. *Nat Rev Neurosci* **10**, 186-198.

Bullmore E, Sporns O (2012). The economy of brain network organization. *Nat Rev Neurosci* **13**, 336-349.

Burgess N (2007). Computational Models of the Spatial and Mnemonic Functions of the hippocampus. In: Anderson P, Morris R, Amaral D, Bliss T, O'Keefe J, eds. The hippocampus book. P 714-749.

Burmeister SS, Jarvis ED, Fernald RD (2005). Rapid behavioral and genomic responses to social opportunity. *PLoS Biol* **3**, e363.

Burmeister SS, Munshi RG, Fernald RD (2009). Cytoarchitecture of a cichlid fish telencephalon. *Brain Behav Evol* **74**, 110-120.

Castro A, Becerra M, Manso MJ, Anadon R (2006). Calretinin immunoreactivity in the brain of the zebrafish, *Danio rerio*: distribution and comparison with some neuropeptides and neurotransmitter-synthesizing enzymes. I. Olfactory organ and forebrain. *J Comp Neurol* **494**, 435-459.

Carr CE, Maler L (1986). Electroreception in Gymnotiform fish. In T.H. Bullock and W. Heiligenberg (eds): Electroreception. New York John Wiley and Sons. 319-373.

Catania K (2014). The shocking predatory strike of the electric eel. *Science* **346**(6214), 1231-1234.

Chacron MJ, Longtin A, Maler L (2011). Efficient computation via sparse coding in electrosensory neural networks. *Curr opin neurobiol* **21**(5), 752-760.

Clarke SE, Longtin A, Maler L (2015). Contrast coding in the electrosensory system: parallels with visual computation. *Nat Rev Neurosci* **16**, 733-744.

Clayton NS (2015). Ways of thinking: from crows to children and back again. *Q J Exp Psychol* **68**, 209-241.

Clayton NS, Bussey TJ, Dickinson A (2003). Can animals recall the past and plan for the future? *Nat Rev Neurosci* **4**, 685-691.

Collin SP, Whitehead D (2004). The functional roles of passive electroreception in non-electric fishes. *Anim Biol*, **54**(1), 1-25.

Colombo M, Gross CG (1994). Responses of inferior temporal cortex and hippocampal neurons during delayed matching to sample in monkeys (Macaca fascicularis). *Behav Neurosci* **108**(3), 443-455.

Cossell L, Iacaruso MF, Muir DR, Houlton R, Sader EN, Ko H, Hofer SB, Mrsic-Flogel TD (2015). Functional organization of excitatory synaptic strength in primary visual cortex. *Nature* **518**, 399-403.

Darmaillacq AS, Dickel L, Rahmani N, Shashar N (2011). Do reef fish, Variola louti and Scarus niger, perform amodal completion? Evidence from a field study. *J Comp Psychol* **125**, 273-277.

Derrick BE (2007). Plastic processes in the dentate gyrus: a computational perspective. *Prog Brain Res* **163**, 417-451.

Desjardins JK, Becker L, Fernald RD (2015). The effect of observers on behavior and the brain during aggressive encounters. *Behav Brain Res* **292**, 174-183.

Dowben RM, Rose JE (1953). A metal-filled microelectrode. *Science* **118**, 22-24.

Durrett R (2007). Random graph dynamics. New York: Cambridge University Press.

Eichenbaum H (2004). Hippocampus; cognitive processes and neural representations that underlie declarative memory. *Neuron* **44**, 109-120.

Eichenbaum H, Cohen NJ (2014). Can we reconcile the declarative memory and spatial navigation views on hippocampal function? *Neuron* **83**, 764-770.

Ekstrom A, Kahana M, Caplan J, Fields T, Isham E, Newman E, Fried I (2003). Cellular networks underlying human spatial navigation. *Nature* **425**, 184-187.

Elliott SB, Maler L (2015). Stimulus induced up states in the dorsal pallium of a weakly electric fish. *J Neurophysiol* **114**, 2071-2076.

Ellis LD, Maler L, Dunn RJ (2008). Differential distribution of SK channel subtypes in the brain of the weakly electric fish Apteronotus leptorhynchus. *J Comp Neurol*, ***507***(6), 1964-1978.

Engler G, Zupanc GKH (2001). Differential production of chirping behavior evoked by electrical stimulation of the weakly electric fish, Apteronotus leptorhynchus. *J Comp Physiol A* **187**, 747-756.

Erondu NE, Kennedy MB (1985). Regional distribution of type II Ca^{2+}/calmodulin-dependent protein kinase in rat brain. *J Neurosci* **5**, 3270-3277.

Esclapez M, Houser CR (1995). Somatostatin neurons are a subpopulation of GABA neurons in the rat dentate gyrus: evidence from colocalization of pre-prosomatostatin and glutamate decarboxylase messenger RNAs. *Neuroscience* **64**, 339-355.

Faunes M, Francisco Botelho J, Ahumada Galleguillos P, Mpodozis J (2015). On the hodological criterion for homology. *Front Neurosci* **9**, 223.

Fecteau JH, Munoz DP (2006). Salience, relevance, and firing: a priority map for target selection. *Trends Cogn Sci* **10**(8), 382-390.

Felsenstein J (1989). PHYLIP: Phylogeny inference package (version 3.2). *Cladistics* **5**, 164-166.

Fernald RD (1977). Quantitative behavioural observations of *Haplochromis burtoni* under semi-natural conditions. *Anim Behav* **25**, 643-653.

Fernald RD, Hirata NR (1977). Field study of *Haplochromis burtoni*: quantitative behavioural observations. *Anim Behav* **25**, 964-975.

Folgueira M, Bayley P, Navratilova P, Becker TS, Wilson SW, Clarke JD. 2012. Morphogenesis underlying the development of the everted teleost telencephalon. *Neural dev* **7**, 32.

Fortin NJ, Agster KL, Eichenbaum HB (2002). Critical role of the hippocampus in memory for sequences of events. *Nat Neurosci* **5**, 458-462.

Fotowat H, Harrison RR, Krahe R (2013). Statistics of the electrosensory input in the freely swimming weakly electric fish Apteronotus leptorhynchus. *J Neurosci,* **33**(34), 13758-13772.

Friedman DP, Aggleton JP, Saunders RC (2002). Comparison of hippocampal, amygdala, and perirhinal projections to the nucleus accumbens: combined anterograde and retrograde tracing study in the Macaque brain. *J Comp Neurol* **450**, 345-365.

Fritzsch B (1993). Fast axonal diffusion of 3000 molecular weight dextran amines. *J Neurosci Meth* **50**, 95-103.

Fugère V, Krahe R (2010).Electric signals and species recognition in the wve-type gymnotiform fish *Apteronotus leptorhynchus*. *J Exp Biol* **213**, 225-236.

Ganz J, Kaslin J, Freudenreich D, Machate A, Geffarth M, Brand M (2012). Subdivisions of the adult zebrafish subpallium by molecular marker analysis. *J Comp Neurol* **520**, 633-655.

Ganz J, Kroehne V, Freudenreich D, Machate A, Geffarth M, Braasch I, Kaslin J, Brand M (2014). Subdivisions of the adult zebrafish pallium based on molecular marker analysis. *F1000Research* **3**, 308.

Gebhardt K, Bohme M, Von der Emde G (2012). Electrocommunication behavior during social interactions in two species of pulse-type weakly electric fish (Mormyridae). *J Fish Biol* **81**(7), 2235-2254.

Gentner TQ, Fenn KM, Margoliash D, Nusbaum HC (2006). Recursive syntactic pattern learning by songbirds. *Nature* **440**, 1204-1207.

Gerfen CR, Bolam JP (2010). The Neuroanatomical Organization of the Basal Ganglia. In: Steiner H, Tseng K, eds. Handbook of basal ganglia structure and function. Cambridge, Mass.: Academic Press. p 3-28.

Giassi AC, Duarte TT, Ellis W, Maler L (2012a). The Organization of the Gymnotiform Fish Pallium in Relation to Learning and Memory: II. Extrinsic connections. *J Comp Neurol* **520**, 3338–3368.

Giassi AC, Ellis W, Maler L (2012b). The Organization of the Gymnotiform Fish Pallium in Relation to Learning and Memory: III. Intrinsic connections. *J Comp Neurol* **520**, 3369–3394.

Giassi AC, Harvey-Girard E, Valsamis B, Maler L (2012c). Organization of the gymnotiform fish pallium in relation to learning and memory: I. Cytoarchitectonics and cellular morphology. *J Comp Neurol* **520**(15), 3314-3337.

Gonçalves DM, Oliveira RF (2010). Hormones and sexual behavior of teleost fishes. In Norris D, Lopez K (Eds.) *Hormones and reproduction on vertebrates, volume 1 – fishes,* 119-147.

Graff C, Kaminski G, Gresty M, Ohlmann T (2004). Fish perform spatial pattern recognition and abstraction by exclusive use of active electrolocation. *Curr Biol* **14**, 818-823.

Guzowski JF, Knierim JJ, Moser EI (2004). Ensemble dynamics of hippocampal regions CA3 and CA1. *Neuron* **44**, 581-584.

Hagedorn M, Heiligenberg W (1985). Court and spark: electric signals in the courtship and mating of gymnotoid fish. *Anim Behav* **33**, 254-265.

Harris AL, Locke D (2009). Connexins, a guide. New York: Humana Press, Springer.

Harvey-Girard E, Dunn RJ, Maler L (2007). Regulated expression of N-methyl-D-aspartate receptors and associated proteins in teleost electrosensory system and telencephalon. *J Comp Neurol* **505**, 644-668.

Harvey-Girard E, Giassi AC, Ellis W, Maler L (2012). The organization of the gymnotiform fish pallium in relation to learning and memory: IV. Expression of conserved transcription factors and implications for the evolution of dorsal telencephalon. *J Comp Neurol* **520**, 3395-3413.

Harvey-Girard E, Giassi AC, Ellis W, Maler L (2013). Expression of the cannabinoid CB1 receptor in the gymnotiform fish brain and its implications for the organization of the teleost pallium. *J Comp Neurol* **521**, 949-975.

Harvey-Girard E, Maler L (2013). Dendritic SK channels convert NMDA-R-dependent LTD to burst timing-dependent plasticity. *J Neurophysiol* **110**, 2689-2703.

Harvey-Girard E, Tweedle J, Ironstone J, Cuddy M, Ellis W, Maler L (2010). Long-term recognition memory of individual conspecifics is associated with telencephalic expression of Egr-1 in the electric fish *Apteronotus leptorhynchus*. *J Comp Neurol* **518**(14), 2666-2692.

Hebb DO (1949). *The organization of behavior*. New York, Wiley.

Heiligenberg W (1991). Neural nets in electric fish. The MIT Press.

Heiligenberg W (1980). The jamming avoidance response in the weakly electric fish *Eigenmannia*. A behavior controlled by distributed evaluation of electroreceptor afferences. *Naturwissenschaften* **67**, 499-507.

Heiligenberg W, Bastian J (1984). The electric sense of weakly electric fish. *Ann Rev Physiol* **46**, 561-583.

Herkenham M, Nauta WJ (1977). Afferent connections of the habenular nuclei in the rat. A horseradish peroxidase study, with a note on the fiber-of-passage problem. *J Comp Neurol* **173**, 123-146.

Hill AJ, Best PJ (1981). Effects of deafness and blindness on the spatial correlates of hippocampal unit activity in the rat. *Exp Neurol* **74**, 204-217.

Hitschfeld EM, Stamper SA, Vonderschen K, Fortune ES, Chacron MJ (2009). Effects of restraint and immobilization on electrosensory behaviors of weakly electric fish. *ILAR J*, **50**(4), 361-372.

Hoekman MF, Jacobs FM, Smidt MP, Burbach JP (2006). Spatial and temporal expression of FoxO transcription factors in the developing and adult murine brain. *Gene Expr Patterns* **6**, 134-140.

Hopfield JJ (1982). Neural networks and physical systems with emergent collective computational abilities. *Proc Natl Acad Sci* **79**, 2554-2558.

Hopkins CD (1981). On the diversity of electric signals in a community of mormyrid electric fish in West Africa. *Amer Zool* **21**(1), 211-222.

Hopkins CD (1976). Stimulus filtering and electroreception: tuberous electroreceptors in three species of gymnotoid fish. *J Comp Physiol* **111**, 171-207.

Hori E, Nishio Y, Kazuki K, Umeno K, Tabuchi E, Sasaki K, Endo S, Ono T, Nishijo H (2005). Place-related neural responses in the monkey hippocampal formation in a virtual space. *Hippocampus* **15**, 991-996.

Hupe GL, Lewis JE (2008). Electrocommunication in free swimming brown ghost knifefish, *Apteronotus leptorhynchus*. *J Exp Biol* **211**, 1657-1667.

Ishikawa Y, Yamamoto N, Yoshimoto M, Yasuda T, Maruyama K, Kage T, Takeda H, Ito H (2007). Developmental origin of diencephalic sensory relay nuclei in teleosts. Brain Behav Evol **69**, 87-95.

Ito H, Yamamoto N (2009). Non-laminar cerebral cortex in teleost fishes? *Biol Lett* **5**, 117-121.

Iwano T, Masuda A, Kiyonari H, Enomoto H, Matsuzaki F (2012). Prox1 postmitotically defines dentate gyrus cells by specifying granule cell identity over CA3 pyramidal cell fate in the hippocampus. *Development* **139**, 3051-3062.

Jeanne JM, Thompson JV, Sharpee TO, Gentner TQ (2011). Emergence of learned categorical representations within an auditory forebrain circuit. *J Neurosci* **31**, 2595-2606.

Jinde S, Zsiros V, Jiang Z, Nakao K, Pickel J, Kohno K, Belforte JE, Nakazawa K (2012). Hilar mossy cell degeneration causes transient dentate granule cell hyperexcitability and impaired pattern separation. *Neuron* **76**, 1189-1200.

Jinde S, Zsiros V, Nakazawa K (2013). Hilar mossy cell circuitry controlling dentate granule cell excitability. *Front Neural Circuits* **7**, 14.

Jones MW, Errington ML, French PJ, Fine A, Bliss TV, Garel S, Charnay P, Bozon B, Laroche S, Davis S (2001). A requirement for the immediate early gene Zif268 in the expression of late LTP and long-term memories. *Nat Neurosci* **4**(3), 289-296.

Jun JJ, Longtin A, Maler L (2016). Active sensing associated with spatial learning reveals memory-based attention in an electric fish. *J Neurophys*, In Press.

Karten HJ (2015). Vertebrate brains and evolutionary connectomics: on the origins of the mammalian 'neocortex'. *Philos Trans R Soc Lond B Biol Sci* **370**.

Ke MT, Fujimoto S, Imai T (2013). SeeDB: a simple and morphology-preserving optical clearing agent for neuronal circuit reconstruction. *Nat Neurosci* **16**, 1154-1161.

Kesner RP (2007). A behavioral analysis of dentate gyrus function. *Prog Brain Res* **163**, 567-576.

Krahe R, Gabbiani F (2004). Burst firing in sensory systems. *Nat Rev Neurosci* **5**, 13-23.

Krahe R, Maler L (2014). Neural maps in the electrosensory system of weakly electric fish. *Curr opin neurobiol* **24**, 13-21.

Lanciago JL, Wouterlood FG (2011). A half century of experimental neuroanatomical tracing. *J Chem Neuroanat* **42**, 157-183.

Larimer P, Strowbridge BW (2010). Representing information in cell assemblies: persistent activity mediated by semilunar granule cells. *Nat Neurosci* **13**(2), 213-222.

Lavado A, Lagutin OV, Chow LM, Baker SJ, Oliver G (2010). Prox1 is required for granule cell maturation and intermediate progenitor maintenance during brain neurogenesis. *PLoS Biol* **8**.

Lavado A, Oliver G (2007). Prox1 expression patterns in the developing and adult murine brain. *Dev Dyn* **236**, 518-524.

Lavenex P, Amaral DG (2000). Hippocampal-neocortical interaction: a hierarchy of associativity. *Hippocampus* **10**, 420-430.

Lee H, Wang C, Deshmukh SS, Knierim JJ (2015). Neural population evidence of functional heterogeneity along the CA3 transverse axis: pattern completion versus pattern separation. *Neuron* **87**, 1093-1105.

Leutgeb S, Leutgeb JK (2007). Pattern separation, pattern completion, and new neuronal codes within a continuous CA3 map. *Learn Mem* **14**, 745-757.

Lewis BL, O'Donnell P (2000). Ventral tegmental area afferents to the prefrontal cortex maintain membrane potential 'up' states in pyramidal neurons via D_1 dopamine receptors. *Cereb Cortex* **10**, 1168-1175.

Li CT, Poo M, Dan Y (2009). Burst spiking of a single cortical neuron modifies global brain state. *Science* **324**(5927), 643-646.

Mahon S, Vautrelle N, Pezard L, Slaght SJ, Deniau J-M, Chouvet G, Charpier S (2006). Distinct patterns of striatal medium spiny neuron activity during the natural sleep-wake cycle. *J Neurosci*, **26**, 12587–12595.

MacDonald RB, Debiais-Thibaud M, Talbot JC, Ekker M (2010). The relationship between dlx and gad1 expression indicates highly conserved genetic pathways in the zebrafish forebrain. *Dev Dyn* **239**, 2298-2306.

Maclean JN, Watson BO, Aaron GB, Yuste R (2005). Internal dynamics determine the cortical response to thalamic stimulation. *Neuron* **48**, 811-823.

Malamut BL, Saunders RC, Mishkin M (1984). Monkeys with combined amygdalo-hippocampal lesions succeed in object discrimination learning despite 24-hour intertrial intervals. *Behav Neurosci* **98**, 759-769.

Maler L (1999a). The distribution of adenylate cyclase in the brain of *Apteronotus leptorhynchus* as revealed by forskolin binding. *J Comp Neurol* **408**, 170-176.

Maler L (1999b). The distribution of protein kinase C in the brain of *Apteronotus leptorhynchus* as revealed by phorbol ester binding. *J Comp Neurol* **408**, 161-169.

Maler L (2007). Neural strategies for optimal processing of sensory signals. *Prog Brain Res* 165, 135-154.

Maler L, Sas E, Johnston S, Ellis W (1991). An atlas of the brain of the electric fish Apteronotus leptorhynchus. *J Chem Neuroanat* **4**, 1-38.

Mann EO, Kohl MM, Paulsen O (2009). Distinct roles of $GABA_A$ and $GABA_B$ receptors in balancing and terminating persistent cortical activity. *J Neurosci* **29**(23), 7513-7518.

Marin O, Rubenstein JL (2001). A long, remarkable journey: tangential migration in the telencephalon. *Nat Rev Neurosci* **2**, 780-790.

Marin O, Rubenstein JL (2003). Cell migration in the forebrain. *Annu Rev Neurosci* **26**, 441-483.

Marsat G, Longtin A, Maler L (2012). Cellular and circuit properties supporting different sensory coding strategies in electric fish and other systems. *Curr Opin Neurobiol* 22(4), 686-92.

Maruska KP, Becker L, Neboori A, Fernald RD (2013a). Social descent with territory loss causes rapid behavioral, endocrine and transcriptional changes in the brain. J Exp Biol **216**, 3656-3666.

Maruska KP, Zhang A, Neboori A, Fernald RD (2013b). Social opportunity causes rapid transcriptional changes in the social behaviour network of the brain in an African cichlid fish. J Neuroendocrinol **25**, 145-157.

McClean JN, Watson BO, Aaron GB, Yuste R (2005). Internal dynamics determine the cortical response to thalamic stimulation. *Neuron* **48**, 811-823.

McCormick DA, Shu Y, Hasenstaub A, Sanchez-Vives M, Badoual M, Bal T (2003). Persistent cortical activity: mechanisms of generation and effects on neuronal excitability. *Cereb Cortex* **13**, 1219-1231.

Metzner W, Heiligenberg W (1991). The coding of signals in the electric communication of the gymnotiform fish *Eigenmania*: from electroreceptors to neurons in the Taurus semicircularis of the midbrain. *J Comp Neurol* **169**, 135-150.

Mitropoulou G, Bruzzone R (2003). Modulation of perch connexin35 hemi-channels by cyclic AMP requires a protein kinase A phosphorylation site. *J Neurosci Res* **72**, 147-157.

Modrell MS, Bemis WE, Northcutt RG, Davis MC, Baker CVH (2011). Electrosensory ampullary organs are lateral line placode-derived in bony fishes. *Nat Commun* **2**.

Molyneaux BJ, Arlotta P, Menezes JRL, Macklis JD (2007). Neuronal subtype specification in the cerebral cortex. *Nat Rev Neurosci* **8**, 427-437.

Moortgat KT Keller CH Bullock TH Sejnowski TJ (1998). Submicrosecond pacemaker precision is behaviorally modulated: the gymnotiform electromotor pathway. *Proc Natl Acad Sci* **95**, 4684–4689.

Mueller T, Dong Z, Berberoglu MA, Guo S (2011). The dorsal pallium in zebrafish, Danio rerio (Cyprinidae, Teleostei). *Brain research* 1381, 95-105.

Mueller T, Guo S (2009). The distribution of GAD67-mRNA in the adult zebrafish (teleost) forebrain reveals a prosomeric pattern and suggests previously unidentified homologies to tetrapods. *J Comp Neurol* 516, 553-568.

Mueller T, Wullimann MF, Guo S (2008). Early teleostean basal ganglia development visualized by zebrafish Dlx2a, Lhx6, Lhx7, Tbr2 (eomesa), and GAD67 gene expression. *J Comp Neurol* 507, 1245-1257.

Muller RU, Kubie JL (1989). The firing of hippocampal place cells predicts the future position of freely moving rats. *J Neurosci* **9**(12), 4101-4110.

Nakashiba T, Cushman JD, Pelkey KA, Renaudineau S, Buhl DL, McHugh TJ, Barrera VR, Chittajallu R, Iwamoto KS, McBain CJ, Fanselow MS, Tonegawa S (2012). Young dentate granule cells mediate pattern separation whereas old granule cells contribute to pattern completion. *Cell* **149**(1), 188-201.

Nakazawa K, Quirk MC, Chitwood RA, Watanabe M, Yeckel MF, Sun LD, Kato A, Carr CA, Johnston D, Wilson MA, Tonegawa S (2002). Requirement for hippocampal CA3 NMDA receptors in associative memory recall. *Science* **297**(5579), 211-218.

Neunuebel JP, Knierim JJ (2014). CA3 retrieves coherent representations from degraded input: direct evidence for CA3 pattern separation and dentate gyrus pattern separation. *Neuron* **81**, 416-427.

New JG (2007). The evolution of vertebrate electrosensory systems, *Brain Behav Evol* **50**(4), 244-252.

Newman MEJ (2010). Networks: an introduction. New York: Oxford University Press.

Nigam S, Shimono M, Ito S, Yeh FC, Timme N, Myroshnychenko M, Lapish CC, Tosi Z, Hottowy P, Smith WC, Masmanidis SC, Litke AM, Sporns O, Beggs JM (2016). Rich-club organization in effective connectivity among cortical neurons. *J Neurosci* **36**, 670-684.

Northcutt RG (2006). Connections of the lateral and medial divisions of the goldfish telencephalic pallium. *J Comp Neurol* **494**, 903-943.

Northcutt RG (2008). Forebrain evolution in bony fishes. *Brain Res Bull* **75**, 191-205.
O'Keefe J (1976). Place units in the hippocampus of the freely moving rat. *Exp Neurol* **51**, 78-109.

Perrone R, Macadar O, Silva A (2009). Social electric signals of freely moving dyads of Brachyhypopomus pinnicaudatus. *J Comp Physiol A*, **195**, 501-514.

O'Keefe J (2007). Hippocampal physiology in the behaving animal. In: Anderson P, Morris R, Amaral D, Bliss T, O'Keefe J, eds. The Hippocampus Book. Oxford: Oxford University Press. p 475-548.

Pleasure SJ, Anderson S, Hevner R, Bagri A, Marin O, Lowenstein DH, Rubenstein JL (2000). Cell migration from the ganglionic eminences is required for the development of hippocampal GABAergic interneurons. *Neuron* **28**, 727-740.

Popper AN, Fay RR (1973). Sound detection and processing by teleost fishes: a critical review. *J Acoust Soc Am* **53**, 1515-1529.

Puelles L, Ayad A, Alonso A, Sandoval JE, MartInez-de-la-Torre M, Medina L, Ferran JL (2016). Selective early expression of the orphan nuclear receptor Nr4a2 identifies the claustrum homolog in the avian mesopallium: Impact on sauropsidian/mammalian pallium comparisons. *J Comp Neurol* **524**, 665-703.

Ramón Y Cajal S (1901-1902). Estudios sobre la corteza cerebral humana. *Trab Inst Cajal Invest Biol* **1**, 1-227.

Reiner A, Veenman CL, Medina L, Jiao Y, Del Mar N, Honig MG (2000). Pathway tracing using biotinylated dextran amines. *J Neurosci Meth* **103**, 27-37.

Reiner A (2010). The conservative evolution of the vertebrate basal ganglia. In: Steiner H, Tseng K, eds. Handbook of Basal Ganglia Structure and Function. Cambridge, Mass.: Academic Press. p 30-62.

Richards S, Maler L (1996). The distribution of met-enkephalin like immunoreactivity in the brain of *Apteronotus leptorhynchus*, with emphasis on the electrosensory system. *J Chem Neuroanat* **11**, 173-190.

Rodríguez F, López JC, Vargas JP, Gómez Y, Broglio C, Salas C (2002). Conservation of spatial memory function in the pallial forebrain of reptiles and ray-finned fishes. *The Journal of neuroscience*, **22**(7), 2894-2903.

Rolls ET (2007). An attractor network in the hippocampus: theory and neurophysiology. *Learn Mem* **14**, 714-731.

Rolls ET (2013). The mechanisms for pattern completion and pattern separation in the hippocampus. *Front Sys Neuro* **7**, 74.

Rolls ET (2015). Pattern separation, completion, and categorisation in the hippocampus and neocortex. *Neurobiol Learn Mem*, In Press.

Roth G (2015). Convergent evolution of complex brains and high intelligence. *Philos Trans R Soc Lond B Biol Sci* **370**.

Rowell JJ, Mallik AK, Dugas-Ford J, Ragsdale CW (2010). Molecular analysis of neocortical layer structure in the ferret. *J Comp Neurol* **518**, 3272-3289.

Salas C, Rodriguez F, Vargas JP, Duran E, Torres B (1996). Spatial learning and memory deficits after telencephalic ablation in goldfish trained in place and turn maze procedures. *Behav Neurosci* **110**, 965-980.

Santoro A (2013). Reassessing pattern separation in the dentate gyrus. Front Behav Neurosci **7**, 96.

Sas E, Maler L (1991). Somatostatin-like immunoreactivity in the brain of an electric fish (*Apteronotus leptorhynchus*) identified with monoclonal antibodies. *J Chem Neuroanat* **4**, 155-186.

Sas E, Maler L, Weld M (1993). Connections of the olfactory bulb in the gymnotiform fish, *Apteronotus leptorhynchus*. *J Comp Neurol* **335**, 486-507.

Scharfman HE (2007). The CA3 "backprojection" to the dentate gyrus. *Prog Brain Res* **163**, 627-637.

Scharfman HE, Myers CE (2012). Hilar mossy cells of the dentate gyrus: a historical perspective. *Front Neural Circuits* **6**, 106.

Schluessel V, Fricke G, Bleckmann H (2012). Visual discrimination and object categorization in the cichlid Pseudotropheus sp. *Anim Cogn* **15**, 525-537.

Schluessel V, Kraniotakes H, Bleckmann H (2014). Visual discrimination of rotated 3D objects in Malawi cichlids (Pseudotropheus sp.): a first indication for form constancy in fishes. *Anim Cogn* **17**, 359-371.

Scoville WB, Milber B (1957). Loss of recent memory after bilateral hippocampal lesions. *J Neurol Neurosurg Psychiatry* **20**, 11-21.

Shabel SJ, Proulx CD, Piriz J, Malinow R (2014). Mood regulation. GABA/glutamate co-release controls habenula output and is modified by antidepressant treatment. *Science* **345**, 1494-1498.

Shabel SJ, Proulx CD, Trias A, Murphy RT, Malinow R (2012). Input to the lateral habenula from the Basal Ganglia is excitatory, aversive, and suppressed by serotonin. *Neuron* **74**, 475-481.

Shima K, Tanji J (1998). Involvement of NMDA and non-NMDA receptors in the neuronal responses of the primary motor cortex to input from the supplementary motor area and somatosensory cortex: studies of task-performing monkeys. *Jpn J Physiol* **48**, 275-290.

Siebeck UE, Litherland L, Wallis GM (2009). Shape learning and discrimination in reef fish. *J Exp Biol* **212**, 2113-2119

Siri B, Quoy M, Delord B, Cessac B, Berry H (2007). Effects of Hebbian learning on the dynamics and structure of random networks with inhibitory and excitatory neurons. *J Physiol Paris* **101**, 136-148.

Skaggs WE, McNaughton BL (1996). Replay of neuronal firing sequences in rat hippocampus during sleep following spatial experience. *Science* **271**, 1870-1873.

Sohl G, Maxeiner S, Willecke K (2005). Expression and functions of neuronal gap junctions. *Nat Rev Neurosci* **6**, 191-200.

Sovrano VA, Bisazza A (2008). Recognition of partly occluded objects by fish. *Anim Cogn* **11**, 161-166.

Sovrano VA, Bisazza A (2009). Perception of subjective contours in fish. *Perception* **38**, 579-590.

Spiers HJ, Burgess N, Hartley T, Vargha-Khadem F, O'Keefe J (2001). Bilateral hippocampal pathology impairs topographical and episodic but not recognition memory. *Hippocampus* **11**, 715-725.

Stabentheiner A (1988). Correlations between hearing and sound production in piranhas. *J Comp Physiol* **162**, 67-76.

Stark CEL, Squire LR (2000). Recognition memory and familiarity judgements in severe amnesia: no evidence for a contribution of repetitive priming. *Behav Neurosci* **114**, 459-467.

Stefanelli T, Bertolini C, Luscher C, Muller D, Mendez P (2016). Hippocampal somatostatin interneurons control the size of neuronal memory ensembles. *Neuron* **89**: 1074–1085.

Stephenson-Jones M, Ericsson J, Robertson B, Grillner S (2012). Evolution of the basal ganglia; Dual output pathways conserved throughout vertebrate phylogeny. *J Comp Neurol.*

Squire LR (1992). Memory and the hippocampus: a synthesis from findings with rats, monkeys and humans. *Psychol Rev* **99**, 195-231.

Squire LR, Zola-Morgan S (1991). The medial temporal lobe system. *Science* **253**, 1380-1386.

Thompson LT, Best PJ (1990). Long-term stability of the place-field activity of single units recorded from the dorsal hippocampus of freely behaving rats. *Brain Res* **509**, 299-308.

Trinh AT, Harvey-Girard E, Teixeira F, Maler L (2015). Cryptic laminar and columnar organization in the dorsolateral pallium of a weakly electric fish. *J Comp Neurol* **524**, 408-428.

Vargas JP, Lopez JC, Portavella M (2009). What are the functions of fish brain pallium? *Brain Res Bull* **79**(6), 436-440.

Vincent SR, Brown JC (1986). Somatostatin immunoreactivity in the entopeduncular projection to the lateral habenula in the rat. *Neurosci Lett* **68**(2), 160-164.

Von der Emde G (1999). Active electrolocation of objects in weakly electric fish. *J Exp Biol* **202**, 1205-1215.

Von der Emde G, Behr K, Bouton B, Engelmann J, Fetz S, Folde C (2010). 3-Dimensional Scene Perception during Active Electrolocation in a Weakly Electric Pulse Fish. *Front Behav Neurosci* **4**, 26.

Wagner A (2014). Arrival of the fittest. New York: Current.

Wallach A, Maler L. Representation of electrolocation related stimuli in the thalamus analog of weakly electric fish. 2016; Montevideo, Uruguay. International Society of Neuroethology.

Wang, XJ (2001). Synaptic reverberation underlying mnemonic persistent activity. *Trends Neurosci* **24**(8), 455-463.

Wang XJ (2008). Decision making in recurrent neuronal circuits. *Neuron* **60**(2), 215-234.

Wang H, Yuan Y, Zhang Z, Yan H, Feng Y, Li W (2014). Dysbindin-1C is required for the survival of hilar mossy cells and the maturation of adult newborn neurons in dentate gyrus. *J Biol Chem* **289**, 29060-29072.

Weld MM, Maler L (1992). Substance P-like immunoreactivity in the brain of the gymnotiform fish *Apteronotus leptorhynchus*: presence of sex differences. *J Chem Neuroanat* **5**, 107-129.

Williams PA, Larimer P, Gao Y, Strowbridge BW (2007). Semilunar granule cells: glutamatergic neurons in the rat dentate gyrus with axon collaterals in the inner molecular layer. *J Neurosci* **27**, 13756-13761.

Wilson CJ, Kawaguchi Y (1996). The origins of two-state spontaneous membrane potential fluctuations of neostriatal spiny neurons. *J Neurosci* **16**(7), 2397-2410.

Wong CJH (1997). Connections of the basal forebrain of the weakly electric fish, *Eigenmannia viriscens*. *J Comp Neurol* **389**, 49-64.

Wyzisk K, Neumeyer C (2007). Perception of illusory surfaces and contours in goldfish. *Vis Neurosci* **24**, 291-298.

Yamamoto N, Ishikawa Y, Yoshimoto M, Xue HG, Bahaxar N, Sawai N, Yang CY, Ozawa H, Ito H (2007). A new interpretation on the homology of the teleostean telencephalon based on hodology and a new eversion model. *Brain Behav Evol* **69**, 96-104.

Yassa MA, Stark CE (2011). Pattern separation in the hippocampus. *Trends Neurosci* **34**, 515-525.

Yu M, Xi Y, Pollack J, Debiais-Thibaud M, Macdonald RB, Ekker M (2011). Activity of dlx5a/dlx6a regulatory elements during zebrafish GABAergic neuron development. *Int J Dev Neurosci* **29**, 681-691.

Zakon HH, Dunlap KD (1999). Sex steroids and communication signals in electric fish: a tale of two species. *Brain Behav Evol* **54**, 61-69.

Zakon HH, Meyer JH (1983). Plasticity of electroreceptor tuning in the weakly electric fish, *Sternopygus dariensis*. *J Comp Physiol* **153**(4), 477-87.

Zakon H, Oestreich J, Tallarovic S, Triefenbach F (2002). EOD modulations of brown ghost electric fish : JARs, chirps, rises, and dips. *J Phys Paris* **96**(5-6), 451-458.

Zupanc GK (2002). From oscillators to modulators: behavioral and neural control of modulations of the electric organ discharge in the gymnotiform fish, *Apteronotus leptorhynchus*. *J Physiol Paris* **96**(5–6), 459–472.

Zupanc GK, Sirbulescu RF, Nichols A, Ilies I (2006). Electric interactions through chirping behavior in the weakly electric fish, *Apteronotus leptorhynchus*. *J Comp Physiol A*, **192**(2), 159-173.